The Cholinergic Status differentially alters GABAergic Inhibition in Neocortex

Dissertation

zur Erlangung des Grades eines
Doktors der Naturwissenschaften

der Mathematisch-Naturwissenschaftlichen Fakultät
und
der Medizinischen Fakultät
der Eberhard-Karls-Universität Tübingen

vorgelegt
von

Luise Liebig
aus Bautzen, Deutschland

August 2016

Tag der mündlichen Prüfung: 28. 03. 2017

Dekan der Math.-Nat. Fakultät: Prof. Dr. W. Rosenstiel
Dekan der Medizinischen Fakultät: Prof. Dr. I. B. Autenrieth

1. Berichterstatter: Prof. Dr. B. Antkowiak

2. Berichterstatter: Prof. Dr. C. Schwarz

Prüfungskommission: Prof. Dr. B. Antkowiak

Prof. Dr. C. Schwarz

Prof. Dr. F. Schaeffel

PD Dr. T. Freilinger

Erklärung / Declaration:

Ich erkläre, dass ich die zur Promotion eingereichte Arbeit mit dem Titel:

„The Cholinergic Status differentially alters GABAergic Inhibition in Neocortex"

selbständig verfasst, nur die angegebenen Quellen und Hilfsmittel benutzt und wörtlich oder inhaltlich übernommene Stellen als solche gekennzeichnet habe. Ich versichere an Eides statt, dass diese Angaben wahr sind und dass ich nichts verschwiegen habe. Mir ist bekannt, dass die falsche Abgabe einer Versicherung an Eides statt mit Freiheitsstrafe bis zu drei Jahren oder mit Geldstrafe bestraft wird.

I hereby declare that I have produced the work entitled

*"*The Cholinergic Status differentially alters GABAergic Inhibition in Neocortex*",*

submitted for the award of a doctorate, on my own (without external help), have used only the sources and aids indicated and have marked passages included from other works, whether verbatim or in content, as such. I swear upon oath that these statements are true and that I have not concealed anything. I am aware that making a false declaration under oath is punishable by a term of imprisonment of up to three years or by a fine.

Tübingen, den ....

Datum / Date Unterschrift /Signature

Table of content

A. Abbreviations

ACh		Acetylcholine
	ACh^+	ACh & Neostigmine
	ACh^-	Atropine & Mecamylamine
aCSF		Artificial cerebro-spinal fluid
AHP		Afterhyperpolarization
CCK		Cholecystokinin
CI		Confidence interval
Em		Membrane potential
	Em_{rest}	Resting membrane potential
EPSP		Excitatory postsynaptic potential
GABA		γ-aminobutyric acid
$GABA_AR$		$GABA_A$-receptors
GFP		Green fluorescent protein
ifr		Instantaneous firing rate
IN		Interneuron
IPSC		Inhibitory postsynaptic current
LFP		Local field potential
mAChR		Muscarinic ACh receptor
nAChR		Nicotinic ACh receptor
Neo		Neostigmine
PV+		Parvalbumin-positive
PY		Pyramidal cell
R		Cell resistance
SOM+		Somatostatin-positive
τ		Membrane time constant or IPSC decay time constant
TTX		Tetrodotoxin
VIP+		Vasoactive intestinal polypeptide-positive

B. List of Tables

C. List of Supplementary Material (Tables)

D. List of Figures

1 Introduction

1.1 Summary

This thesis study was designed to investigate the impact of the neuromodulator acetylcholine (ACh) on γ-aminobutyric acid (GABA)-ergic inhibition in neocortex. GABAergic inhibition counterbalances excitatory transmission by glutamatergic pyramidal cells (PY), the dominating neuronal cell type in cortex. Inhibition is provided by a diversity of interneuron (IN) classes which differ in terms of morphology, electrophysiological properties and sensitivity to ACh. Importantly, IN classes establish postsynaptic connections characterized by specific subtype composition of the $GABA_A$ receptors ($GABA_AR$). Thus, the principal hypothesis investigated here is that ACh should modulate the quality and possibly the magnitude of GABAergic inhibition in neocortex by altering the relative inhibitory impact of different $GABA_AR$ subtypes. This hypothesis was investigated on the basis of subtype-specific $GABA_AR$ pharmacology and targeted recordings of somatostatin-positive (SOM^+) INs in mostly spontaneously active *in vitro* preparations of neocortex. Congruent with expectations, ACh excited SOM^+ INs and increased inhibition in the network, as evident in a higher frequency of inhibitory postsynaptic potentials (IPSCs) recorded in voltage-clamp experiments and shorter and smaller spontaneous network bursts in extracellular recordings in organotypic cultures of neocortex. To investigate the involvement of specific $GABA_AR$ subunits, $GABA_AR$ modulators with differing subunit preferences were tested in the presence and absence of ACh. Results revealed that the actions of $GABA_AR$ modulators on burst parameters and correlation of activity were specifically altered by the presence of ACh. Overall, inhibition and decorrelation increased most when the $\alpha_{1,2,3}$ modulator zolpidem was applied in the presence of ACh, while the additional modulation of $GABA_ARs$ containing the α_5 subunit with diazepam suspended the differences between the two ACh conditions. The functional antagonism of α_5 subunit-containing $GABA_AR$ by L-655,708 evoked a difference between the two ACh conditions opposite to the differences seen with zolpidem. Thus, the α_5 subunit is proposed to play an important role in ACh-induced inhibition.

1.2 The role of acetylcholine for cortical processing

Cerebral cortex, the outer shell of the mammalian brain, functions as the main processing and storage center for afferent signals (e.g. sensory input) and relays processed information back to deep brain regions. It is organized into columns and layers, which take on specific functions. Neocortex, the largest part of cerebral cortex, is composed of five to six histologically distinct layers, depending on the area. According to the classic hierarchical model, sensory input from thalamus to sensory neocortex terminates in layers IV and VI, is transmitted to superficial layers II and III and outputted via subcortically projecting neurons in layers V and VI (Schüz and Miller, 2002; Xu and Callaway, 2009). Additionally, layer V pyramidal neurons (PYs) are directly activated by thalamus (Constantinople and Bruno, 2013; Krause et al., 2014). PYs are glutamatergic projection neurons. They are the dominating cell type in cortex, which form excitatory intracortical subnetworks (Otsuka and Kawaguchi, 2008), and transmit the computational outcome to both, other cortical areas and extracortical brain regions .

It has long been recognized that neuromodulators alter and shape cortical activity. Neocortex is the target of a number of neurotransmitter and –modulator systems, e.g. acetylcholine (ACh), 5-hydroxytryptamine (serotonin), dopamine and noradrenaline, which help to fine-tune cortical output by modulating neuronal excitability (Bacci et al., 2005). The neocortex receives cholinergic input mostly from projection neurons located in the nucleus basalis of Meynert within the basal forebrain (Selden et al., 1998; Woolf, 1991). Although the entire depth of neocortex is innervated by cholinergic fibers, layers II-III, V and VI receive the most pronounced innervations, with region-dependent specificities (Eckenstein et al., 1988; Tian et al., 2014; Zaborszky et al., 2013). A question still discussed in the literature is whether ACh fibers form classical synapses onto target neurons (synaptic transmission) or whether they release ACh nonspecifically into the extracellular space, providing a tonic-modulating concentration (volume transmission). In line with the classification of ACh as a neuromodulator (as opposed to a neuro*transmitter*) in the central nervous system (CNS), the volume transmission hypothesis has long been favored (Descarries, 1998; Kimura, 2000; Sarter et al., 2009; Yamamoto et al., 2010). Only recently, more evidence was provided for the co-existence of direct synaptic ACh transmission, which may be essential for specific attention tasks like cue detection (Parikh et al., 2007, 2008; Sarter et al., 2014; Turrini et al., 2001).

On the behavioral level, ACh is involved in – grossly speaking – attention, wakefulness, learning and memory (Broussard et al., 2009; Hasselmo and McGaughy, 2004; Hasselmo and Sarter, 2011; Jiménez-Capdeville and Dykes, 1996). For example, in microdialysis studies it was shown that ACh concentrations were higher during wakefulness in comparison to sleep, especially during periods of

activity (Jiménez-Capdeville and Dykes, 1996; Marrosu et al., 1995). While concentrations of ACh changed state-dependently in somatosensory and visual cortical areas, no changes were measured in motor cortical areas (Jiménez-Capdeville and Dykes, 1996). These findings not only showed that the ACh status seems to play a role for the sleep-wake cycle but also suggested that ACh is necessary for stimulus processing. Another study by Parikh et al. (2007) supported the importance of ACh for attention by demonstrating that cue detection coincided with an increase in ACh concentration, that more cues were missed when cholinergic input to the medial prefrontal cortex (but not to motor cortex) were abolished and that the pre-cue cholinergic concentration was a predictor of cue detection. In line with these observations, cognitive impairment as seen for example in schizophrenic patients is likely related to a dysfunctional cholinergic system (Carruthers et al., 2015; Gould et al., 2015). Patients suffering from different types of dementia are commonly treated with acetylcholinesterase inhibitors increasing the cholinergic level in the brain to improve cognitive performance (Engelhardt et al., 2007).

Focused attention and cue detection involve an enhancement of the signal-to-noise ratio of afferent sensory information in neocortex (Wester and Contreras, 2013). Research has provided evidence that gating attention towards a specific stimulus is achieved by an ACh-induced reduction of ongoing cortico-cortical excitatory signal transmission amongst PYs. At the same time, thalamic afferent input to cortex, which carries information about the newly detected stimulus, remains unaffected, as recently confirmed by a calcium imaging study (Runfeldt et al., 2014). Thus, thalamic signaling is allowed to pass through to cortex, where it can be processed with less intracortical interference before it is relayed back to deeper brain regions (Castro-Alamancos and Gulati, 2014; Gigout et al., 2012; Hasselmo and McGaughy, 2004; Oldford and Castro-Alamancos, 2003; Picciotto et al., 2012). This switch from intracortical communication to afferent input processing has been correlated with network activity in different frequency bands. During resting states (inactivity) and sleep when intracortical communication dominates, detected EEG frequencies mostly fall in the delta frequency band and below (≤ 5Hz), while states of activity, when new stimuli are processed, are associated with higher frequencies in the theta (~ 6-12 Hz) to gamma (~ 30-80 Hz) range (Cape et al., 2000; Manns et al., 2000). It has been shown that the presence of ACh leads to a decrease of the delta power and below, while power in the theta and gamma frequency bands increases, again supporting the role of ACh for attention (Buhl et al., 1998; Kalmbach and Waters, 2014; Tateno et al., 2005). The shift from low to high frequencies in the power spectrum caused by an increase in ACh concentrations has been termed *desynchronization* (Metherate et al., 1992). Another characteristic of the presence of ACh is reduced firing synchrony between cortical neurons termed *decorrelation* and thought to improve stimulus coding and perception (Goard and Dan, 2009).

Subnetwork- and cell type-specific modulation of excitation and inhibition seem to underlie the switch from inactivity or sleep to a state of attentiveness. Undoubtedly, ACh changes the state of excitability of neuronal groups in preparation for subsequent stimulus processing (Picciotto et al., 2012). While tonic ACh concentrations can elicit depolarization in neocortical PYs of layer V via muscarinic and nicotinic receptors (Hedrick and Waters, 2015; Pafundo et al., 2013; Vidal and Changeux, 1993), ACh also has a strong inhibitory component mediated by multiple mechanisms (Arroyo et al., 2012; Gulledge and Stuart, 2005; Gulledge et al., 2007, 2009). Not only does phasically applied ACh inhibit layer V PYs directly via M_1 muscarinic receptors located on these neurons (Gulledge and Stuart, 2005) and decreases glutamatergic excitatory postsynaptic potentials (EPSPs) via muscarinic M4 receptors (Gigout et al., 2012), but additionally some types of inhibitory γ-aminobutyric acid (GABA) interneurons (INs) are excited by ACh and thus, inhibition mediated via these INs is strengthened by ACh (Amar et al., 2010; Blatow et al., 2003; Gulledge et al., 2007; Kawaguchi, 1997; Lucas-Meunier et al., 2009; Porter et al., 1999). Generally, different cortical IN classes respond in quite distinct ways to ACh application. Therefore, the effect of ACh on cortical GABAergic INs presumably plays a central role for the transition of the neocortical modus operandi from spontaneous intracortical activity towards thalamic input enhancement. Before effects of ACh on specific IN types are described in more detail, the GABAergic IN system will be introduced next.

1.3 GABAergic INs in neocortex

If neocortex were designed as a purely excitatory network, its computational capacity would be limited greatly and information transmission would eventually become unstable (Kepecs and Fishell, 2014). Thus, modulation of PY activity by INs, which release the inhibitory neurotransmitter GABA, is indispensable. Even though INs only make up about 10 – 20% of the total neuronal population in neocortex, they powerfully counteract runaway excitation and allow for the execution of specific computational goals, promoting a dynamically adjustable network (Fino et al., 2013; Kepecs and Fishell, 2014; Rudy et al., 2011; Schüz and Miller, 2002). The proper balance between excitation and inhibition in the brain, which can be understood as the constant adjustment of inhibitory power in relation to excitation present in the network, is essential for normal functioning (Isaacson and Scanziani, 2011; Okun and Lampl, 2008). An insufficient amount of GABAergic inhibition – in combination with environmental factors – increases the susceptibility to numerous neurological disorders, e.g. epilepsy, schizophrenia, anxiety disorder and autisms (Gonzalez-Burgos and Lewis, 2008; Jiang et al., 2012; Levitt et al., 2004; Rudolph and Möhler, 2014; Tai et al., 2014). By contrast, a controlled pharmacological increase in inhibition is a major molecular mechanism of anesthesia (Rudolph and Antkowiak, 2004).

The IN population is heterogeneous and the classification of IN types is in the center of an ongoing debate in the scientific literature (DeFelipe et al., 2013). INs can be grouped in terms of morphological, molecular and physiological features (Ascoli et al., 2008; Hu et al., 2014). On the basis of the coexpression of molecular markers, three main IN groups were identified by Rudy et al. (2011): Ca^{2+}-binding protein parvalbumin-positive neurons (PV^+), neuropeptide somatostatin-positive neurons (SOM^+), and ionotropic serotonin receptor 5-HT_{3a}-expressing neurons. These groups can be further subdivided by morphological and electrophysiological features. Briefly, the PV^+ IN group has been split up into fast-spiking and multipolar bursting cells. Named after their morphological appearance, basket and chandelier cells both belong to the fast-spiking class (Figure 1). The SOM^+ group is made up of Martinotti cells located in layers II/III to VI, some of which coexpress the Ca^{2+}-binding proteins calretinin (CR), calbindin (CB), the neuropeptide Y (NPY) or cholecystokinin (CCK). They can be fast-spiking, regular-spiking, or irregular-spiking with classic or bursting onset responses (Wang et al., 2004). Furthermore, a transgenic mouse line termed X94 revealed at least one further group of SOM^+ cells located in layer IV and V and innervating layer IV, unlike Martinotti cells (Ma et al., 2006). The main group expressing the 5-HT_{3a} receptor contains INs coexpressing the neuropeptide vasoactive intestinal polypeptide (VIP). Basket cells expressing CCK and innervating the soma of PYs belong to the VIP^+ group. The rest of 5-HT_{3a} INs are VIP-negative, but mostly $reelin^+$. In this thesis, PV^+ basket cells and SOM^+ Martinotti cells will be in focus, although other IN groups will also be discussed.

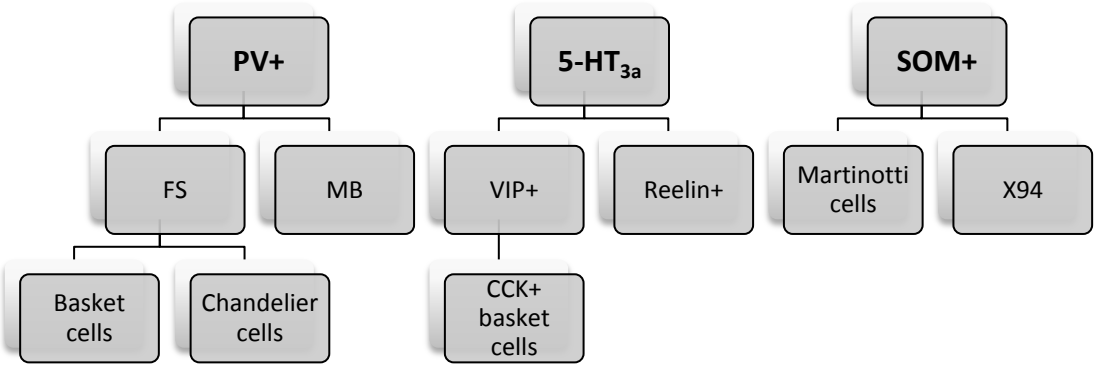

FIGURE 1: CLASSIFICATION OF GABAERGIC CORTICAL INS BY MORPHOLOGICAL, MOLECULAR AND PHYSIOLOGICAL FEATURES (modified from Rudy et al. (2011)).

1.3.1 PV+ basket cells

About 50% of INs are PV^+ multipolar basket cells; they make up the largest IN population and are likely the central building block of neocortical inhibition and essential for the excitation/inhibition

balance (Beierlein et al., 2003; Hu et al., 2014; Markram et al., 2004; Rudy et al., 2011; Xue et al., 2014). Electrophysiologically, PV^+ basket cells belong to the fast-spiking group, which is characterized by short action potential duration, a particularly low input resistance, a fast membrane time constant, and non-adapting firing patterns upon constant current injection. These characteristics endow the cells with the ability to discharge brief, high-frequency bursts of action potentials in response to synaptic excitation (Ascoli et al., 2008; Hu et al., 2014; Kawaguchi, 1995; Kawaguchi and Kubota, 1998; Klostermann and Wahle, 1999; McCormick et al., 1985). Additionally, molecular features including a high density of dendritic voltage-gated K^+ channels and axonic Na^+ channels, and the prevalence of fast P/Q-type Ca^{2+} channels and synaptotagmin 2 in presynaptic terminals set PV^+ basket cells apart from other IN types (Hu et al., 2014; Kruglikov and Rudy, 2008; Rossignol et al., 2013; Zaitsev et al., 2007). Their morphology is characterized by dense axonal arborizations near or just above their soma with horizontal branching (Kawaguchi, 1993, 1995). These basket-like structures are draped around somata, axon initial segments and proximal dendrites of PYs, where they establish synapses with $GABA_A$ receptors ($GABA_AR$) in which the α_1 subunit dominates (Hu et al., 2014; Kawaguchi and Kubota, 1998; Thomson et al., 2000; Wafford et al., 1993). Further description of $GABA_A$Rs will follow later on.

Taken together, PV^+ basket cells are equipped to promote fast temporal signal integration and precise action potential propagation. They are involved in feedback and feedforward inhibition, but due to their non-adapting action potential firing and fast kinetics, they are especially suited for the latter type. Feedforward inhibition occurs if INs and their postsynaptically connected PYs simultaneously receive excitatory input. Briefly after the arrival of the excitatory pulse in both IN and PY, inhibition in the PY sets in and restrains or even prevents further PY output (Figure 2). In fact, multiple studies have provided evidence for strong excitatory input to PV^+ basket cells from thalamocortical projection neurons and cortical PYs, which exceeds that observed in other IN groups and even PY neurons (Armstrong and Soltesz, 2012; Cruikshank et al., 2007; Kim et al., 2014; Rotaru et al., 2005; Xu and Callaway, 2009). As quickly as PV^+ basket cells are engaged in activity, as promptly can they be shut off due to inhibition by other PV+ basket cells, by other interneuron types and autapses, and a sudden drop of excitation by the PYs with which they are reciprocally connected (Bacci and Huguenard, 2006; Bacci et al., 2003; Hu et al., 2014; Otsuka and Kawaguchi, 2009; Pfeffer et al., 2013). Thus, PV^+ cells are embedded in multiple negative feedback loops. Moreover, the excitatory inputs PV^+ cells receive are of a depressing nature, which are defined by an initial large-amplitude EPSP but subsequently steadily declining EPSPs (Beierlein et al., 2003; Reyes et al., 1998). Hence, these INs are precisely tuned to the onset of PY activity. As they are tightly time-locked to excitatory input to PYs, they control the probability and timing of action potentials of PYs (Haider and McCormick, 2009; Hu et al., 2014; Rudy et al., 2011; Xue et al., 2014).

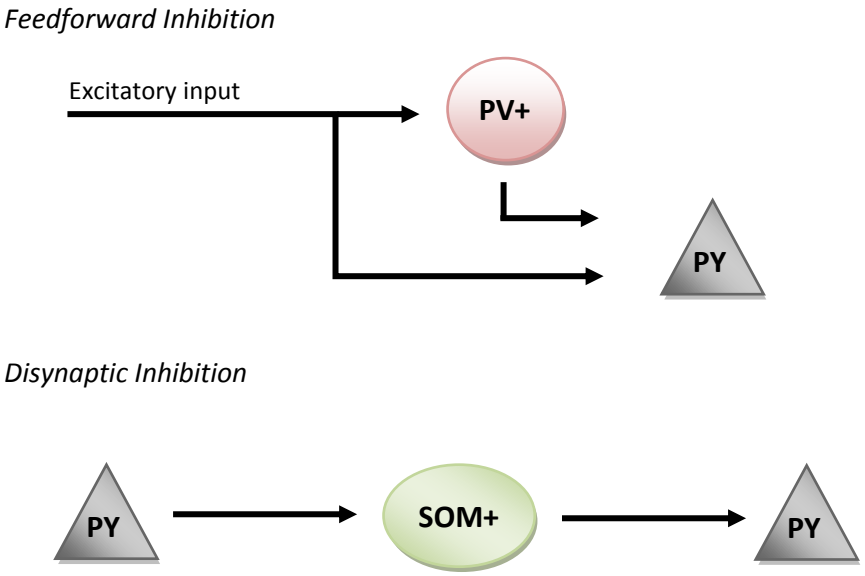

FIGURE 2: TWO DIFFERENT INHIBITORY PATHWAYS.

1.3.2 SOM+ Martinotti cells

SOM$^+$ Martinotti INs are the counterpart to PV$^+$ basket INs in multiple respects and seem to take on a complementing functional role within the inhibitory network as will be outlined below.

Martinotti cells can be identified by their ascending axonal arbors and collaterals, which mostly terminate in layer I. They spread laterally and innervate tuft, apical and basal dendrites of PY cells across multiple columns (Fino et al., 2013; Gupta et al., 2000; Kawaguchi and Kubota, 1996, 1997; de Lima and Morrison, 1989; Ma et al., 2006; Wang et al., 2004). In contrast to PV$^+$ basket cells, which form local subnetworks with neighboring PYs, the excessive branching and connectivity allow one Martinotti cell to innervate a multitude of PY targets even at great distance.

Silberberg and Markram (2007) argued that most of the inhibition to PYs provided by Martinotti cells is restricted to the dendrites due to the long electrotonic distance of the synapse to the soma. In contrast to the powerful perisomatic inhibition by PV$^+$ basket INs, dendritic inhibition is inadequate to control pyramidal somatic membrane potential and action potential output. However, it is well suited to prevent action potential-induced calcium spike generation in dendrites. This hypothesis was supported by *in vivo* and *in vitro* research, which showed that calcium signals are strong during phases of Martinotti cell inactivity (Gentet et al., 2012; Murayama et al., 2009), but considerably diminished especially by inhibition of apical dendrites provided by these INs (Marlin and Carter,

2014). Thus, Martinotti cells are presumably responsible for adjusting distal excitatory input in PYs through the control of dendritic integration (Silberberg and Markram, 2007).

Not only morphological aspects clearly distinguish Martinotti cells from basket cells, but also their electrophysiological finger print and their firing pattern. In general, they have action potentials of much longer duration, a higher input resistance and a more depolarized resting membrane potential than PV^+ basket cells (Kawaguchi and Kubota, 1996; Wang et al., 2004). The latter two of these characteristics make Martinotti cells more excitable and sensitive to electrical stimuli (Fanselow et al., 2008). Unlike PV^+ basket cells, Martinotti cells cannot be clearly identified on the basis of their firing pattern. Some show a fast-spiking firing pattern similar to that of PV^+ basket cells and fewer display a so-called stuttering or irregular-spiking firing pattern, but most are regular-spiking, which is characterized by an increase of the inter-spike interval over the duration of a depolarizing current step. Most regular-spiking cells fire a single spike at the onset of a depolarization step (classic onset); only few start with a spike doublet or an outright burst of spikes (Wang et al., 2004). Martinotti cells' accommodating firing patterns allow for fundamentally different functionality in comparison to PV^+ basket cells. Whereas basket cells supply local feedforward or feedback inhibition which is instant and strong, but also depressing, inhibition provided by Martinotti cells increases gradually and in proportion to the rate and duration of presynaptic discharges (Fino et al., 2013; Silberberg and Markram, 2007). This is partly the result of facilitating synapses connecting presynaptic PYs to postsynaptic Martinotti cells, but also a result of the wide dynamic firing range of Martinotti cells. Even though they settle to 3-10 Hz when excited, they are capable of transiently firing with up to 50 Hz, which makes them more flexible than PV^+ basket cells and adaptable to different network conditions (Fanselow et al., 2008).

In terms of the network architecture, Martinotti cells are involved in a so-called disynaptic pathway, where they receive excitatory input from presynaptic PYs and mediate inhibitory output to neighboring postsynaptic PYs (Figure 2) (Silberberg and Markram, 2007). Unlike PV^+ basket cells, they rely on local cortical information and are not or only sparsely innervated by thalamic afferents, depending on the cortical layer. Thus, disynaptic inhibition may serve as an intracortical mechanism to contain spontaneous PY activity and to mediate synchronization of PY action potential firing (Berger et al., 2010).

1.4 Spontaneous network activity *in vitro* is regulated by INs

The comparison of two types of INs in the preceding chapter illustrates exemplarily the diversity of GABAergic inhibition in neocortex. Firing modes of INs, their dendritic and axonal morphology, and the spatial distribution, postsynaptic targets and short-term plasticity of the synapses they establish,

are key factors determining their potential impact on cortical activity. The electrophysiological characteristics of INs have mostly been determined via intracellular stimulation or with the cortical network driven into action by sensory or artificial stimuli. In acute brain slices *in vitro*, such experiments were usually carried out on a background of nearly complete neuronal silence. However, it has increasingly been recognized that a neurophysiologically realistic picture of cortical function must incorporate spontaneous network activity, that is, neuronal activity which is not caused by external stimuli but is an emergent property of the neuronal networks. Spontaneous network activity is innate to the mammalian central nervous system including neocortex. Numerous studies have shown that the constant synaptic input into neurons caused by spontaneous activity has a profound impact on the integration properties of neurons (Destexhe et al., 2003), a feature which is routinely built into models of cortical networks. Spontaneous activity is thus both a factor influencing neuronal information processing and a naturally emerging, homeostatically regulated characteristic of cortical networks (Desai et al., 1999).

In cortical networks *in vitro*, spontaneous activity originates in layer 5 and takes the form of 'bursts' ('UP' states), which are phases of recurrent network activity, alternating with 'silent periods' ('DOWN' states), which are characterized by relative neuronal silence (Sanchez-Vives and McCormick, 2000). There are some differences in the properties of UP states between different *in vitro* preparations, especially between acute brain slices and organotypic slice cultures. In slice cultures, the rate of UP states is about an order of magnitude higher than in acute slices, most likely due to their high degree of synaptic connectivity (Drexler et al., 2010; Gähwiler et al., 1997; Johnson and Buonomano, 2007; Klostermann and Wahle, 1999). Regardless of the type of preparation, spontaneous UP/DOWN state-like activity requires glutamatergic excitation and is shaped by GABAergic inhibition. Specifically, the diverse classes of INs are believed to govern UP states in diverse ways. Especially PV^+ INs have the highest action potential firing rate during UP states in comparison to other INs (Neske et al., 2015), where they seem to be especially active in the beginning and at the end of an UP state (Puig et al., 2008). While their role as restrainers of PY firing activity might suggest that the absence of PV^+ activity during UP states would lead to even longer activity phases, the opposite was found. Multiple studies showed that the blockade of $GABA_AR$ and especially the prevention of PV^+ IN activity shortened UP states and led to more intense, high-frequency firing in the initial phase of the bursts (Kawaguchi, 1997; Kuki et al., 2015; Mann et al., 2009; Sanchez-Vives et al., 2010). Pharmacological enhancement of GABAergic currents either shortens or prolongs UP states, depending on the molecular mechanism (Antkowiak, 1999; Drexler et al., 2009; Razik et al., 2013). These findings collectively suggest that finely tuned IN activity is an important, but also incompletely understood, factor in shaping UP states.

Within UP states, cortical networks engage in high-frequency oscillatory activity over a wide frequency range (Steriade et al., 1996). Oscillations in the gamma band (40-80 Hz) arise from an interplay between excitatory and inhibitory neurons. Particularly PV^+ INs have been suggested to be the initiator of gamma rhythms (Hasenstaub et al., 2005; Kuki et al., 2015). Due to electrical and chemical coupling of PV^+ cells amongst each other, synchronized output is possible leading to gamma oscillations (Fries et al., 2007; Gibson et al., 1999).

In contrast to PV^+ INs, which play an important role within UP states, SOM^+ INs have been reported to fire during both UP and DOWN states (Fanselow and Connors, 2010; Neske et al., 2015). Their role in UP state modulation is not clear. Although they have been proposed in the past to be responsible for the termination of UP states (Fanselow and Connors, 2010; Krishnamurthy et al., 2012), recent work could not support this hypothesis (Neske et al., 2015). Kuki et al. (2015) showed the involvement of SOM^+ INs in the generation of delta oscillations embedded within UP states, which is the first time that low frequency bands have been associated with this IN type.

ACh has been shown to modulate the neocortical interneuronal system via nicotinic and muscarinic ACh receptors (Alkondon et al., 2000; Aracri et al., 2010; Lucas-Meunier et al., 2009; Xiao et al., 2009; Yi et al., 2014). In the following, evidence is presented for the hypothesis that GABAergic interneurons are crucially involved in bringing about the change of cortical activity patterns seen upon cholinergic stimulation.

1.5 ACh and GABA INs

PV^+ basket cells are the largest group of INs in cortex and thus one of the main study objects when the effect of ACh on inhibition is investigated. Intriguingly, the intrinsic properties of PV^+ basket cells remain unchanged in the presence of ACh and thus it has been concluded that they are not directly or only marginally activated by bath or focal ACh application (Gulledge et al., 2007; Kawaguchi, 1997; Yi et al., 2014). Alitto and Dan (2013) stimulated basal forebrain cholinergic neurons and analyzed calcium imaging signals from PV^+ basket cells in mouse layer 1 and 2/3 of visual cortex. About half of the cells responded with excitation, while the other half showed less activity. Additional application of CNQX, a competitive AMPA/kinate receptor antagonist, blocked the positive responses and thus confirmed the glutamate-dependence of ACh-induced excitation in PV^+ cells. Conclusively, PV^+ basket cells do not respond to ACh directly; however, ACh increases the glutamatergic excitatory input to PV^+ cells, which can be detected as an increase of EPSP frequency in PV^+ cells. As a result, their firing probability increases (Pafundo et al., 2013). It is likely that ACh-activated cortical PYs and thalamocortical input are the source of PV^+ cell depolarization. Usually, this excitation would initiate the inhibitory feedback-loop where PV^+ cell firing dampens prospective PY output. Surprisingly,

paired recordings from PV^+ basket cells and PY cells revealed a cholinergic suppression of inhibitory postsynaptic currents (IPSCs) in PYs (Kruglikov and Rudy, 2008; Yamamoto et al., 2010). Thus, GABA release from presynaptic PV^+ basket cell terminals was extenuated by ACh as a result of the activation of inhibitory presynaptic muscarinic M2/M4 receptors. Their presence on PV^+ basket cells has been confirmed by immunohistochemistry for hippocampus and visual cortex (Disney and Aoki, 2008; Hájos et al., 1997). Consequently, the inhibition of GABA release from these INs decreases feedback inhibition of PY cells in cortex. Due to this mechanism, the time window of signal transduction from thalamus to cortex is broadened and hence thalamocortical communication is improved.

Not as much detail is known about the interaction of ACh with SOM^+ INs. In general, these INs have been shown to react with strong depolarization when ACh was applied (Chen et al., 2015; Kawaguchi, 1997), which seems to be mediated via muscarinic but not nicotinic ACh receptors (Fanselow et al., 2008; Porter et al., 1999). Chen et al. (2015) recently provided evidence for a connection between SOM^+ and PV^+ INs, suggesting that SOM^+ activation directly inhibits PV^+ activity, which in turn would reduce somatic inhibition to PY cells. Thus, the activation of SOM^+ INs through the cholinergic system and the ensuing inhibition of pyramidal dendrites but disinhibition of pyramidal somata very likely contributes to above-mentioned switch of neocortex' modus operandi.

The observation that different IN types are differentially sensitive to ACh argues strongly in favor of an ACh-mediated qualitative switch of GABAergic inhibition. An important, but thus far largely uninvestigated ramification of such a switch is implied in the coupling of IN classes to specific postsynaptic $GABA_AR$ subtypes (Figure 3). For example, as briefly mentioned above, fast-spiking PV^+ basket cells establish synapses with mostly α_1 subunit-containing $GABA_AR$ which possess fast decay kinetics. Therefore, a cholinergically mediated shift of the activation of IN types should also result in a differential activation of $GABA_AR$ subtypes. This raises the intriguing possibility of investigating the effect of ACh on GABAergic inhibition by $GABA_AR$ subtype-specific pharmacology. Before this central idea of the present study can be further developed, the composition, properties and pharmacology of $GABA_AR$ need to be explained.

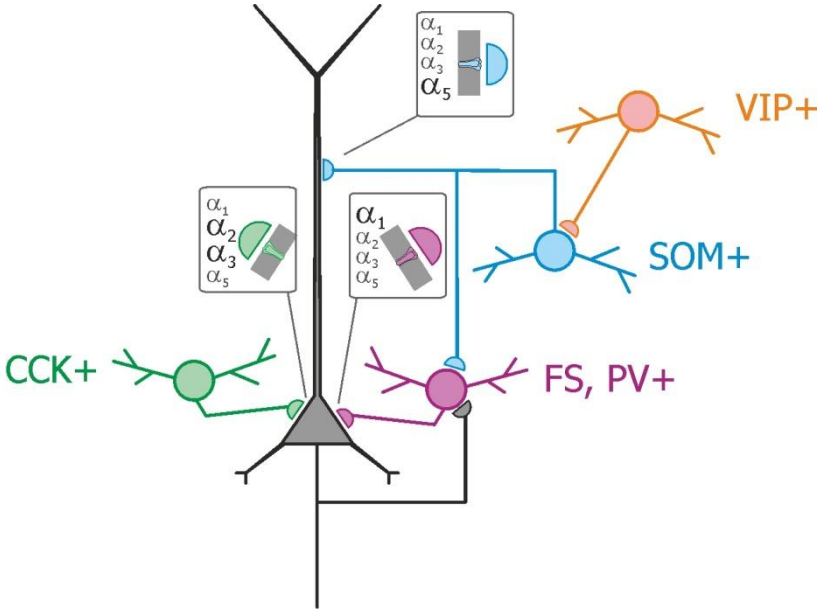

FIGURE 3: SCHEMATIC OF PY-IN COUPLING IN NEOCORTEX.

1.6 Coupling of $GABA_AR$ subunits to presynaptic IN types

$GABA_ARs$ are ligand-gated chloride channels. Activation of the receptor by GABA leads to an opening of the channel and, if the membrane potential is above the equilibrium potential of chloride, an inflow of chloride ions into the cell, which causes a hyperpolarization of the membrane potential. Independent of an effect on the membrane potential, opening of the receptor increases the membrane conductance, leading to a 'shunt' of excitatory input. $GABA_ARs$ assemble as heteropentamers. Thus far, 19 subunits have been identified: α_{1-6}, β_{1-3}, γ_{1-3}, δ, ε, θ, π, and 3 ρ subunits (Olsen and Sieghart, 2009). The most common stoichiometry is 2 α : 2 β : 1 γ. Due to the diversity of subunits, a very large number of combinations would be possible. However, the number of observed and physiologically relevant receptor subtypes is limited. 60% of $GABA_ARs$ consist of $\alpha_1\beta_2\gamma_2$ (Rudolph and Antkowiak, 2004), the most prevalent $GABA_AR$ subtype. The ultrastructural distribution of $GABA_AR$ is subunit-specific. Receptors containing α_{1-3}, β_{1-2} and γ_2 subunits can mostly be found in the synaptic cleft, where they mediate phasic inhibition. α_4 and α_6 $\beta_x\delta$ subtypes are typical extrasynaptic receptors which are sensitive to low ambient concentrations of GABA; these receptor subtypes mediate tonic inhibition (Fritschy and Panzanelli, 2014; Korpi and Sinkkonen, 2006; Winsky-Sommerer, 2009). Receptors containing α_5 (with $\beta_3\gamma_2$) subunits mediate both slow phasic and tonic currents and are located extracellularly and in pyramidal dendritic regions (Ali and Thomson, 2008; Fritschy and Panzanelli, 2014; Serwanski et al., 2006; Yamada et al., 2007).

Benzodiazepines, a group of psychoactive drugs which mediate sedative, anxiolytic and anticonvulsant effects, are highly affine, positive allosteric modulators of $GABA_AR$. They prolong the open times of the receptors. As a consequence, tonic and/or phasic inhibitory postsynaptic currents (IPSCs) and/or above-mentioned shunting effect are enhanced, leading to stronger inhibition of the postsynaptic cell (Rudolph and Antkowiak, 2004). The classical benzodiazepine binding site lies between the α and γ subunit of the $GABA_AR$. Specifically, these substances have high affinities for $GABA_AR$ containing $\alpha_{1\text{-}3,5}$ and γ_2 subunits, lower affinities for receptors with γ_1 and γ_3 subunits, and no affinity for receptors with α_4 and α_6 subunits (Olsen and Sieghart, 2009). Although most benzodiazepines like diazepam are characterized by a broad pharmacological bandwidth and are thus not subunit-selective, some benzodiazepines and related drugs do show preferences for receptors with certain subunits. One prominent example is zolpidem, a non-benzodiazepine, which is more likely to bind to receptors containing the α_1 subunit (and temperature- and concentration-dependently, α_2/ α_3) than to those containing α_5 (Munakata et al., 1998; Olsen and Sieghart, 2009; Puia et al., 1991; Sanna et al., 2002; Sigel and Buhr, 1997). This characteristic in combination with specific receptor subunit knock-in mice makes these substances a valuable tool to investigate functional differences between $GABA_AR$ subtypes.

To illustrate this last point, a study by Ali and Thomson (2008) will be described in more detail, in which zolpidem and diazepam were employed to study the association of cortical INs with postsynaptic $GABA_AR$ subtypes. Research in hippocampal slices had already suggested a specific IN type - $GABA_AR$ coupling (Freund, 2003; Nyíri et al., 2001). For example, PV^+ INs preferentially form synapses with $GABA_ARs$ containing the α_1 subunit, whereas PV-negative IN synapses have a low density of α_1 (Klausberger et al., 2002; Thomson and Jovanovic, 2010; Thomson et al., 2000). For cortex, much less is known about IN-receptor subunit coupling. Ali and Thomson (2008) showed that neocortical $GABA_AR$ subunit insertion is also presynaptic neuron-specific. In this study, dual whole-cell recordings were performed from IN-PY cell pairs and IPSPs were recorded from PYs in the presence of different $GABA_AR$ modulators. When zolpidem at a concentration of 0.4 µM was applied, IPSPs generated by PV^+ INs were enhanced while SOM^+ IPSPs remained stable. Keeping in mind zolpidem's preference for $GABA_ARs$ containing the α_1 subunit at the chosen concentration, the idea was supported that PV^+ INs form synapses with this specific type of receptor. Diazepam, on the other hand, enhanced SOM^+ IN-mediated IPSPs. This effect was attenuated by an α_5-specific antagonist. Since the α_5 subunit has been identified in dendritic synapses (Serwanski et al., 2006) and SOM^+ INs target PY dendrites, this subunit is the suggested postsynaptic partner for SOM^+ neurons mediating the increase in inhibition seen with diazepam (Figure 3). Nonetheless, it needs to be stressed that IN-PY $GABA_AR$ coupling in neocortex is almost exclusively based on above-mentioned study or inferred from data derived from hippocampus.

1.7 Project motivation

In summary, INs play a crucial role in restraining and shaping excitation, and the neuromodulator ACh is believed to alter the contribution of the various IN types to inhibition. Although knowledge on the cholinergic excitability of the various IN classes and their interconnectivity is growing, a complete picture of cholinergic modulation of GABAergic inhibition is still far off. The impacts of activating pre- and postsynaptic nicotinic and muscarinic receptors on INs, and the mutual GABAergic inhibitory connections between INs are only two of numerous factors defining the complexity of cholinergic-GABAergic interactions.

The main hypothesis of the current project was that the population of $GABA_AR$ subtypes contributing to GABAergic inhibition should differ depending on the cholinergic status of neocortex. The approach to study these interactions was pursued based on $GABA_AR$ pharmacology. It was hypothesized that a $GABA_AR$ subtype-preferring pharmacological enhancement or depression of GABAergic inhibition should have quite different impacts in different cholinergic states. $GABA_AR$ modulators with different receptor subtype preferences were tested in the presence and absence of ACh to investigate this general hypothesis. Because ACh activates some classes of INs, it was hypothesized that ACh might be able to enhance the effect of these modulators, as seen by an overall increase in inhibition.

The first part of the project was dedicated to the effects of ACh alone. In this context, organotypic co-cultures of the cholinergic cell-containing basal forebrain (BF) and the somatosensory neocortex were established. Ideally, in such preparations cholinergic neurons would fire spontaneously and provide neocortex with a close to physiological mode of delivery and level of ACh. Although the anatomy of this system has been described in the past, there are no electrophysiological results until the present day (Baratta et al., 1996; Distler and Robertson, 1992; Ha et al., 1999). Co-cultures were made from a mouse mutant expressing GFP in ACh neurons. Thus, it was possible to specifically target them in basal forebrain and monitor their activity with current clamp recordings during spontaneous network activity. However, as a success of this approach could not be predicted, conventional application of ACh via the bath solution was applied in all further experiments.

Since Martinotti cells have been shown to depolarize in the presence of ACh but their overall contribution to network activity is still incompletely known, one experimental series was designed to understand their activity level in the presence and absence of ACh. A mouse mutant with GFP-labelled Martinotti cells was used to reliably identify this cell type and specifically record from these cells during different ACh states in organotypic cultures and acute slices.

For the main part of the project, different $GABA_AR$ modulators were bath-applied to somatosensory cortical organotypic cell cultures while ACh (ACh^+ condition) or cholinergic receptor antagonists

atropine and mecamylamine (*ACh*$^-$ condition) were co-applied. The preferences of $GABA_AR$ modulators for specific receptor subtypes were used as a pharmacological tool to enhance inhibition at certain synapses but not at others. The main substances used were zolpidem and diazepam. While zolpidem (depending on its concentration) preferentially binds to $GABA_AR$ containing the α_1 subunit (and $\alpha_{2/3}$ in higher concentrations), diazepam binds to $GABA_ARs$ containing the $\alpha_{1,2,3,5}$ subunits and is thus a less specific $GABA_AR$ modulator than zolpidem.

Due to the sensitivity of SOM^+ INs to ACh and their association with α_5 subunit-containing receptors, a notable difference between the *ACh*$^+$ and *ACh*$^-$ condition was hypothesized for $GABA_AR$ modulators acting via these receptors (diazepam and L-655,708). Specifically, it was hypothesized that in the *ACh*$^+$ condition positive allosteric modulation of these receptors would be enhanced compared to the *ACh*$^-$ condition because SOM^+ IN activation by ACh would lead to an increase in GABA release. Since SOM^+ IN activity was recently linked to decreased delta power and ACh has also been shown to shift spectral power from delta to higher frequencies, it was expected that the combined application of ACh and $GABA_AR$ modulators acting via α_5 would lead to reduced power in the lower frequency spectrum (Kalmbach and Waters, 2014; Kuki et al., 2015). Moreover, the increase of SOM^+ cell activity in the presence of ACh seems to be a fundamental cause of ACh's desynchronizing and decorrelating effects (Chen et al., 2015). Hence, diazepam in combined application with ACh was expected to have especially strong decorrelating effects.

The outcome of the combination of mostly α_1-preferring substances like zolpidem at low concentrations with ACh was harder to predict. As previously described, ACh does not directly activate PV^+ basket cells presynaptic to the α_1 subunit-containing $GABA_ARs$. Presynaptic M_2 receptors might even inhibit GABA release from PV^+ INs. Additionally, Chen et al. (2015) provided evidence for direct inhibition of PV^+ cells by activated SOM^+ cells. Hence, it was believed that the $GABA_AR$ modulator in combination with ACh might result in less network inhibition than in the absence of ACh. According to Kuki et al. (2015), the reduced activity of PV^+ cells might manifest itself as shortened activity phases and a decrease in higher frequencies.

In order to characterize the IN-$GABA_AR$ coupling and the effects of ACh further, inhibitory postsynaptic potentials were recorded from cells in neocortex with the same $GABA_AR$ modulators under *ACh*$^+$ and *ACh*$^-$. This specific project was designed to focus specifically on the change of inhibition in the network and resolve the results received from the extracellular experiments described above in more detail.

2 Methods

2.1 Animals

For most of the experiments, organotypic cultures and acute slices were prepared from C57Bl/6 mice (Charles River, Sulzbach, Germany). Additionally, some experiments were carried out with strains Tg(Gad1-EGFP)98Agmo/J, henceforward called X98 for convenience, and B6.Cg-Tg(RP23-268L19-EGFP)2Mik/J, furtheron called Mik (both by The Jackson Laboratory, Bar Harbor, Maine, USA). X98 and Mik animals were housed in groups of three in an animal housing facility with food and water available *ad libitum*. A 12/12-hour light/ dark cycle was used with lights on at 07.00 A.M.

2.2 Preparation system

2.2.1 Organotypic cultures of somatosensory neocortex

All procedures were approved by the local animal care committee (Eberhard-Karls-University, Tübingen, Germany) and were in accordance with German law on animal experimentation. Organotypic cultures of mouse neocortex mostly comprised of the somatosensory part were prepared and maintained *in vitro* using the roller-tube technique (Gähwiler, 1981; Antkowiak & Helfrich-Förster, 1998). Mice of postnatal age three to five days (P3-5) were deeply anesthetized with isoflurane and killed by decapitation. Once the brain was removed, it was cooled down in ice-cold dissection medium composed of Gey's balanced salt solution (GBSS, Sigma-Aldrich, Taufkirchen, Germany) with 60 mM glucose (50%, Sigma-Aldrich) and 11 mM $MgCl_2$ (Applichem, Darmstadt, Germany). With the cerebellum removed, the cerebrum was glued to the stage of a vibratome (NVSLMI Motorized Advance Vibroslice, World Precision Instruments, Berlin, Germany) and 300 µm thick slices were cut in the solution specified above. Pieces of neocortex were dissected, placed on glass cover slips and fixed with a coagulate of chicken plasma and thrombin (both Sigma-Aldrich), transferred into plastic tubes containing 750 µl of culture medium and incubated in a roller drum (Heracell 240, Thermo Scientific (Heraeus), Waltham, MA USA) at 10 rev/h at 37°C. The culture medium consisted of 50 % Basal medium Eagle, 25 % Hank's balanced salt solution and 25 % horse serum and had a final concentration of 1 mM l-glutamine and 61 mM glucose (Table 1). One day after preparation, the medium was changed and anti-mitotics were added to reduce glial proliferation. Thereafter, the culture medium was changed twice a week. After preparation and after each medium renewal, the cultures were incubated 1-2 h in an atmosphere of 5% carbon dioxide in room air, attaining a pH of 7.2-7.4. Cultures were used between two to six weeks of incubation.

Substances	Supplier	Traditional culture medium	Alternative culture medium
Horse serum	Life Technologies	25%	25%
Basal medium Eagle with phenol red, without glutamine (BME)	Sigma-Aldrich	50%	50%
Hank's balanced salt solution with phenol red (HBSS)	Sigma-Aldrich	25%	--
HBSS substitute	self-made	--	25%
Glucose	Sigma-Aldrich	61 mM	30 mM
L-glutamine	Sigma-Aldrich	1 mM	1mM
Sodium Pyruvate (for cholinergic neurons)	Sigma-Aldrich	2.5 mM	--
Urea (for cholinergic neurons)	Sigma-Aldrich	10 µM	--

TABLE 1: ORGANOTYPIC CULTURE MEDIA. The alternative culture medium was developed to potentially unify firing patterns.

2.2.2 Co-cultures of basal forebrain and neocortex

In the majority of experiments presented in this study ACh was applied externally via the bath solution, mimicking ambient ACh (e.g. Descarries (1998)). However, as there is also a phasic/synaptic component of ACh signaling (Sarter et al., 2009, 2014), an experimental series was dedicated to the investigation of this mode of cholinergic release. Co-cultures of basal forebrain (origin of cholinergic projection neurons) and neocortex were prepared. Organotypic cultures were prepared as stated above, except that a piece of neocortex was placed next to a piece of basal forebrain on a glass cover slip, both prepared from Mik mice of postnatal age three days. To provide a more physiological pH environment for the slices during the dissection process, GBSS-based dissection medium (pH = 8.20 at room temperature) was substituted by Dulbecco's phosphate buffered saline (DPBS; pH = 7.24 at room temperature; Sigma-Aldrich).

It has been shown that neuronal growth factor (NGF) enhances cholinergic cell development, especially in the presence of urea (Mobley et al., 1986; Zassler et al., 2005). Thus, 10 µM urea (Sigma-Aldrich) were added to the culture medium while 0.005µg/ml NGF (Sigma-Aldrich) were pipetted directly into the culture tubes upon culture medium change for the first two weeks. Additionally, pyruvate (2.5 mM; Sigma-Aldrich) was added to the culture medium as an energy source (Hodgkins and Schwarcz, 1998; Holmgren et al., 2010).

One of the problems observed when recording from organotypic cultures was a drift in neuronal activity from initially long phases of activity to shorter but more frequent bursts within minutes (data not shown). It was hypothesized that the sudden change in ionic concentrations between the culture medium and the artificial cerebral spinal fluid (aCSF) in the bath chamber, particularly the decline of

the potassium concentration, caused this phenomenon. The traditional nutrition medium cultures received for at least two weeks contained > 5 mM K^+, a concentration chosen to promote neuronal activity and health during early development. On the other hand, the K^+ concentration of the recording aCSF corresponded to rodent CSF with 3.5 mM K^+. It appeared conceivable that cortical and basal forebrain neurons could be differentially susceptible to such sudden changes in the ionic environment. In order to exclude this factor as a confound, an alternative medium was created for this experimental series which had the same concentration of major ions (Na^+, K^+, Ca^{2+}, Mg^{2+}, Cl^-) as the aCSF. Basal medium Eagle (BME) and horse serum were considered indispensable constituents of the medium as they contain numerous amino acids and other substances vital for long-term neuronal survival. The third component of the classical nutritional medium, Hank's balanced salt solution (HBSS), was substituted by a tailor-made medium (Table 2). The resulting ionic concentrations of the alternate medium were identical to those of the aCSF. Finally, the glucose concentration was halved from 60 mM to 30 mM (Table 1). Cultures received the traditional medium with high K^+ from the day of preparation until day nine *in vitro* for optimal early cell development, and the alternative medium with low K^+ and low glucose from day ten on until the recording day.

Substances	HBSS concentration (mmol/l)	HBSS substitute concentration (mmol/l)
KCl	5,366	--
NaCl	137,931	133.61
CaCl2 2H2O	1,258	0.00
D-glucose	5,551	65.13
KH2PO4	0,439	--
MgCl2 6H2O	0,000	1.32
MgSO4	0,812	--
NaHCO3	4,166	16.66
NaH2PO4	0,399	2.36
Phenolred*Na	0,029	--
KCl	--	1.10

TABLE 2: HBSS VS HBSS SUBSTITUTE

2.2.3 Acute slices of neocortex

For acute slice preparations, animals were deeply anesthetized with isoflurane and killed by decapitation. The brain was removed quickly and placed into ice-cold modified aCSF containing (in mM): NaCl 110.0, KCl 2.5, NaH_2PO_4 1.13, $NaHCO_3$ 26, $MgCl_2$ 10.0, $CaCl_2$ 0.5, D-glucose 10, buffered to pH 7.4 and saturated with 95% O_2 and 5% CO_2 (Table 3). After the brain was cooled down for about one minute, it was blocked at the cerebellum and the cerebrum was then glued to the stage of a

microslicer (DTK-1000, Dosaka, Kyoto, Japan) with the dorsal side leaning against an agar block for enhanced mechanical stability during cutting. The stage was filled with ice-cold modified aCSF, which was continuously oxygenated. Using the microslicer, 300 µm thick slices were cut. Slices were immediately transferred into a holding chamber containing aCSF of the following composition (in mM): NaCl 120.0, KCl 3.5, NaH_2PO_4 1.13, $NaHCO_3$ 26, $MgCl_2$ 1.0, $CaCl_2$ 1.2, D-glucose 11.0, buffered to pH 7.4 and oxygenated (Table 3). Slices were incubated in the holding chamber for one hour at 34°C and then maintained at room temperature until recording.

Substances	Prep aCSF acute slices (in mM)	Recording aCSF acute slices/ Organotypic cultures
NaCl	110.0	120.0
KCl	2.5	3.5
NaH_2PO_4	1.13	1.13
$MgCl_2$	10.0	1.0
$CaCl_2$	0.5	1.2
D-glucose	10.0	11.0
$NaHCO_3$	26.0	26.0

TABLE 3: ACSF COMPOSITION

2.3 Electrophysiological recordings

2.3.1 In vitro extracellular recordings

In vitro extracellular recordings were performed at 33-34°C under continuous superfusion with aCSF (flow rate 1 ml/min for cultures and 2 ml/min for acute slices). The aCSF was gassed with a mixture of 95 % O_2/5 % CO_2. In experiments with drug application, organotypic cultures were placed into the recording chamber for 30 minutes prior to baseline recordings. Thus, cultures had time to adapt to the ionic differences between the culture medium and the aCSF. Extracellular recordings were carried out with aCSF-filled glass electrodes with resistances of 3-5 MΩ. For each recording, one electrode was placed in the supragranular layers II/III and a second electrode in the infragranular layer V of neocortex. Signals were amplified with a MultiClamp 700A amplifier (Axon Instruments, Union City, CA, USA) or a Microelectrode AC Amplifier 1800 (A-M Systems, Sequim, WA, USA) and digitized by a Digidata 1440A digitizer (Molecular Devices, Union City, CA, USA). Data were collected with a sampling rate of 10-20 kHz. Signal acquisition was performed using pCLAMP 10 software (Molecular Devices, Sunnyvale, CA, USA).

One known confounding factor in the analysis of recordings from organotypic cultures is the systematic difference of activity patterns between different culture batches. To control for this

variability, at least three different culture batches were used per experimental block. Furthermore, one batch was usually used (if possible) for more than one experimental block so that between-batches variability was apportioned roughly equally across experimental groups.

2.3.2 Whole-cell voltage clamp recordings

Whole-cell voltage clamp recordings were obtained from neurons in layer V of organotypic neocortex cultures. Glass pipettes (1.3-2.7 MΩ tip resistance with recording solution) were pulled from borosilicate glass (World Precision Instruments, Sarasota, FL, USA) with a laser puller (P-2000, Sutter Instrument Company, Novato, CA, USA) and filled with an intracellular solution containing (in mM): CsCl 145.0, $MgCl_2$ 1.0, EGTA 5.0, HEPES 10.0, ATP 4.0, QX 314 5.0, Alexa 555 0.05, pH 7.2. The theoretical liquid junction potential of this solution, determined with Clampex software (Molecular Devices), was -6.6 mV and was corrected for during the experiment. Cells were held at -70 mV in order to record inhibitory postsynaptic currents (IPSCs). Recordings were performed only when the initial access resistance did not exceed 9 MΩ and did not change by more than 40% during the course of the experiment. The NMDA and AMPA receptor antagonists, AP5 (50µM) and CNQX (10µM) (both Sigma-Aldrich), respectively, were added to the extracellular bath solution to block glutamatergic currents. Signals were amplified with a MultiClamp 700A amplifier and sampled and digitized at a frequency of 20 kHz with a Digidata 1440A digitizer and pCLAMP 10 software. Neurons filled with Alexa 555 (Invitrogen/ Life Technologies, Darmstadt, Germany) were visualized by epifluorescence with a mercury arc lamp mounted on an Axioskop 2 FS plus microscope (Zeiss, Jena, Germany). PY cells were distinguished from interneurons by their large pyramidal-like shaped cell body, and apical dendrite and spines.

2.3.3 Whole-cell current clamp recordings

Whole-cell current clamp recordings were performed on Bl6 organotypic cultures, X98 organotypic neocortex cultures/ acute slices and MIK basal forebrain-neocortex co-cultures with simultaneous network activity recording by an extracellular electrode (applicable for cultures only). Patch glass pipettes (3-4 MΩ tip resistance with recording solution) were pulled from borosilicate glass (World Precision Instruments, Sarasota, FL, USA) and filled with an intracellular solution containing (in mM): K-gluconate 138.0, EGTA 10.0, $CaCl_2$ 0.5, HEPES 10.0, $MgCl_2$ 2.0, Na_2ATP 3.0, GTP-Na 0.3, Na_2-phosphocreatine 10.0, pH 7.2. For visualization, either neurobiotin (5%, Linaris, Dossenheim, Germany) or Alexa 555 (0.05 mM) were added to the pipette solution. Signals were amplified with a MultiClamp 700A amplifier in current clamp mode. Series resistance was compensated for and generally between 10 – 20 MΩ. The calculated liquid junction potential of -17 mV was corrected for

offline. Temperature was kept at 33-34°C. After the initial break-through and sufficient time for cell stabilization, baseline activity was recorded.

Depolarizing current pulses of increasing amplitude (duration, 400 ms) were used to stimulate action potentials, from which numerous cell characteristics were evaluated, including spike waveform, spike width at half-maximal amplitude, and stimulus-response curves for the spike rate including the maximal firing rate. However, the reaction of the neurons to current injection depended on spontaneous activity (Razik et al 2013): while during network bursts the responses were distorted and either amplified or depressed, they were as a rule depressed by the hyperpolarized membrane potential in immediate post-burst phases. Thus, obtaining undistorted responses would have required many repetitions of current injections, triggered to spontaneous bursts, which would have left less recording time for stimulation protocols which were deemed more important. Therefore, usually the sequence of depolarizing current injections was applied twice or thrice and the maximal firing rate determined from the least distorted response; this parameter is termed “approximate maximal firing rate” to indicate this fact.

Small negative current pulses (140-300 ms, current adjusted to result in hyperpolarizing responses of 5-10 mV amplitude) were repetitively injected into the cells; fitting single exponentials to the resulting hyperpolarizing membrane potential responses allowed the extraction of membrane resistance and time constant (see also paragraph 'current clamp analysis'). Together, these parameters were used in addition to morphological characteristics to classify cells.

Cultures containing neurobiotin-loaded cells were fixed by immersion in 4% paraformaldehyde at 4°C overnight before they were washed three times for ten minutes each in 0.01 M phosphate-buffered saline (PBS). Then they were incubated in fresh 1.5% H_2O_2 in 0.01 M PBS and again washed three times for ten minutes each in 0.01 M PBS and three times for ten minutes each in Triton 4% in 0.01 M PBS. Cultures were incubated in the avidin-biotin complex (Vectastain Elite ABC kit, Vector Labs, Burlingame, CA, USA) for at least 60 minutes followed by washing them with 0.1 M phosphate buffer (PB) three times for ten minutes each and incubating them with DAB (Vector) for two to four minutes. Cultures were rinsed with 0.1 M PB twice for 20 minutes each, dehydrated in graded ethanol, washed with Xylol and covered with DePex. Not all cells could be stained sufficiently. Stained cells were visualized under a Leitz Orthoplan microscope with an oil immersion objective 25x and photographed with a Pentax K20D camera.

2.3.4 Applied substances

All drugs were administered via O_2/CO_2-saturated aCSF. The drug-containing aCSF was delivered to the perfusion chamber via a system of gas-tight syringes (Hamilton, Reno, NV, USA) driven by syringe pumps (Harvard Apparatus, Holliston, MA., USA) and connected to teflon tubing.

For the central part of the thesis, $GABA_AR$ modulators with different $GABA_AR$ subunit affinities were compared in two conditions marked by the presence and absence of tonic cholinergic activity, henceforth called ACh^+ and ACh^-, respectively. For the ACh^+ condition, a constant cholinergic tone was created by bath-applying ACh (1 or 10 µM) together with the ACh esterase inhibitor neostigmine (1 µM). For ACh^-, the cholinergic system was completely blocked by the application of muscarinic receptor antagonist atropine (1 µM) and the nicotinic receptor antagonist mecamylamine (3 µM). An overview over all application schemes is provided in table 4.

Experiment	Control	Drug 1	Drug 2	Wash
CC *ACh*$^+$	aCSF	ACh & Neo	/	aCSF
VC *ACh*$^+$	aCSF	ACh & Neo	Atr & Mec	aCSF
VC TTX & *ACh*$^+$	aCSF	TTX	ACh & Neo	/
Extra *ACh*$^+$ & *ACh*$^-$	aCSF	ACh (1/ 10 µM) & Neo	Atr & Mec	aCSF
CC & Extra Co-culture Mik	aCSF	Neo	Atr & Mec	aCSF
CC & Extra X98	aCSF	ACh & Neo	/	aCSF
VC *ACh*$^+$ sham	ACh & Neo	ACh & Neo	Atr & Mec	ACh & Neo
VC ACh & Ana	ACh & Neo	Zolpi (1/ 0.2 µM)/ Dia	Atr & Mec	ACh & Neo
Extra *ACh*$^+$ & Ana	aCSF	ACh & Neo	Zolpi (1/ 0.2 µM)/ Dia/ Dia in α1 mutant/ L655,708	aCSF
Extra *ACh*$^-$ & Ana	aCSF	Atr & Mec	Zolpi (1/ 0.2 µM)/ Dia/ Dia in α1 mutant/ L655,708	aCSF

TABLE 4: DRUG APPLICATION DESIGN. Experiments are ordered according to order of appearance in results section.

The common drug application scheme started with a six-minute recording of the baseline condition, during which the cultures or acute slices received aCSF alone. After a twelve-minute wash-in period of the substance(s), a second six-minute recording followed. In a subset of experiments, a second drug was applied for another twelve minutes, followed by a further six-minute recording. The experiment ended with a twelve-minute wash-out period of all drugs followed by a final recording in

order to assess the reversibility of the drug effects. Specific drug applications are explained in the results section.

Five different $GABA_AR$ modulator conditions were tested in the current work. Concentrations of substances were chosen in a way to modulate specific single $GABA_AR$ subunits or combinations of subunits in the most effective way. Zolpidem was used in two different concentrations distinguished by differential $GABA_AR$ subunit preferences. While a concentration of 0.2 µM preferentially binds to receptors with the α_1 subunit as reported in the literature, 1.0 µM additionally modulates receptors containing the α_2 and α_3 subunit (Munakata et al., 1998). To indicate preference (instead of selectivity), zolpidem (0.2 µM) is later on marked in figures as $\alpha_{1\,(2,\,3)}$, while zolpidem (1.0 µM) is marked as $\alpha_{1,\,2,\,3}$.

Diazepam was used to target $GABA_AR$ containing $\alpha_{1,}$ $\alpha_{2,}$ α_3 and α_5 subunits. The concentration used here was chosen based on Drexler et al. (2010b), who showed a concentration-dependent biphasic action of diazepam. Between 50 nM to 6.25 µM, diazepam had a plateau effect in decreasing the firing rate by about 20%. Starting at 12.5 µM, firing rate decreased constantly in a concentration-dependent manner. The $GABA_AR$ antagonist bicuculline only partially antagonized these effects, suggesting unspecific binding of diazepam in high concentrations. Additionally, Puia et al. (1991) showed that the affinity for the α_3 subunit-containing receptors increases disproportionately to receptors with the other three subunits diazepam binds to with increasing concentrations. Thus, the concentration used in the current project (1 µM) was chosen from the plateau concentration range, since a clear, $GABA_AR$-specific effect was expected at this concentration with a relatively balanced activation of all four receptor classes. Nonetheless, the exact weighting of the different receptor classes for this concentration is not known. Diazepam was also applied in the α_1-knock-in mouse strain, in which $GABA_ARs$ containing the α_1 subunit cannot be modulated by benzodiazepines. This paradigm was used to investigate the modulation of receptors with the α_2, α_3 and α_5 subunits.

Lastly, L-655,708 was employed, which is a highly specific, negative allosteric modulator of $GABA_AR$ containing the α_5 subunit. In the case of L-655,708, concentrations were not as critical since a 50-fold selectivity of this drug for $GABA_AR$ containing the α_5 subunit over $GABA_AR$ with α_1, α_2, α_3, and α_6 has been shown, and concentrations differing by a factor of 10 had nearly the same effect on tonic inhibitory currents in hippocampus (Caraiscos et al., 2004; Quirk et al., 1996). L-655,708 was applied at 5 µM in the current project for effective blockage of α_5 subunit-containing receptors. All drugs, their supplier and concentrations used for specific experiments are listed in table 5.

Substance	Abbreviation	Concentration	Target site and action	Supplier	Experiments
Acetylcholine	ACh	1 µM 1 µM & 10 µM	Agonist of muscarinic and nicotinic cholinergic receptors	Sigma-Aldrich	CC Bl6 cultures CC/extra Mik co-culture CC X98 acute/ culture VC Bl6 Extracellular Bl6 cultures
(2R)-amino-5-phosphonovaleric acid	AP5	50 µM	Antagonists on NMDA receptor	Tocris	VC Bl6
Atropine		1 µM	Antagonists on muscarinic cholinergic receptors	Sigma-Aldrich	Extracellular culture Bl6 CC/extra Mik co-culture VC Bl6
6-cyano-7-nitroquinoxaline-2,3-dione	CNQX	10 µM	Antagonists on AMPA/kianate receptors	Sigma-Aldrich	VC Bl6
Diazepam-Lipuro	Dia	1 µM	Positive allosteric modulator on $GABA_AR$ containing $\alpha_{1, 2, 3, 5}$ subunits	Uni-pharmacy	Extracellular Bl6/ α1 mutant VC Bl6
L-655,708		5 µM	Negative allosteric modulator on $GABA_AR$ containing α_5 subunit	Tocris/Biotrend	Extracellular Bl6
Mecamylamine	Mec	3 µM	Antagonist on nicotinic cholinergic receptors	Sigma-Aldrich	Extracellular culture Bl6 CC/extra Mik co-culture VC Bl6
Neostigmine	Neo	1 µM	Inhibitor of acetylcholinesterase	Sigma-Aldrich	CC Bl6 cultures Extracellular Bl6 cultures CC/extra Mik co-culture CC X98 acute/ culture VC Bl6
Tetrodotoxin	TTX	1 µM	Na^{2+} channel blocker	Tocris	VC Bl6
Zolpidem	Zolp	0.2 µM 1 µM	Positive allosteric modulator of $GABA_AR$ containing α_1 subunit Positive allosteric modulator of $GABA_AR$ containing $\alpha_{1, 2, 3}$ subunit	Sigma-Aldrich	Extracellular Bl6 VC Bl6

TABLE 5: SUBSTANCE LIST. All drugs used were listed for each experiment; VC: voltage clamp; CC: current clamp; Bl6: black 6 mouse strain; X98: X98 mouse mutant strain

2.4 Data analysis

2.4.1 Extracellular data from spontaneously active organotypic cultures

All data analyses described below were performed in custom-written programs in Matlab (R2008a-R2014a).

Most data collected for this thesis project were obtained from experiments on cortical organotypic slice cultures (Figure 4A). A distinguishing feature of these cultures in comparison to cortical acute slice preparations is their spontaneous network activity. The typical activity pattern is marked by alternating phases of high network activity (bursts) and low collective neuronal activity (silent periods) as displayed in figure 4B. Hence, the first step of analysis consisted of quantifying and describing the degree and pattern of this activity by parameterizing bursts and action potential activity. To this end, the raw extracellular signal was split up via digital Butterworth bandpass filters into local field potential (LFP; passband 1-100 Hz) and action potential (AP; passband 300-5000 Hz) signals (Figure 4B). Filtering was performed in both forward and reverse direction (via Matlab routine 'filtfilt'), resulting in zero phase shifts. The LFP signal was used for the detection of network bursts (Figure 4C). Network bursts were variable in shape, often composed of a large initial transient and smaller, oscillatory signal excursions, here collectively termed 'burstlets'. In order to capture both positive and negative burstlet components the LFP was rectified.

A threshold was set, and sub- to suprathreshold transitions of the LFP were defined as the beginning of a burstlet. The end of a burstlet was defined as the point in time when the LFP signal made a supra- to subthreshold transition across a second threshold, which was set to 20-100% of the first threshold (Figure 4C). A series of burstlets separated by less than 400-700 ms was defined as a burst. Single burstlets of less than 20 ms duration usually represented artifacts and were rejected. Multi-unit action potentials were detected in the high frequency-containing signal (300-5000 Hz) by setting a threshold to about four times the standard deviation of the base line noise, and registering the times of sub- to suprathreshold transitions of the signal.

Once the detection of bursts and action potentials was concluded, a wide range of parameters describing activity (e.g. burst length, action potential rate) was computed. Of these, a subset of six parameters was chosen for analysis and statistical comparisons between drug conditions, based on the following considerations:

a) As LFP and AP signals reflect different aspects of neuronal activity (mostly synaptic input versus suprathreshold excitation), parameters based on both signals were picked.

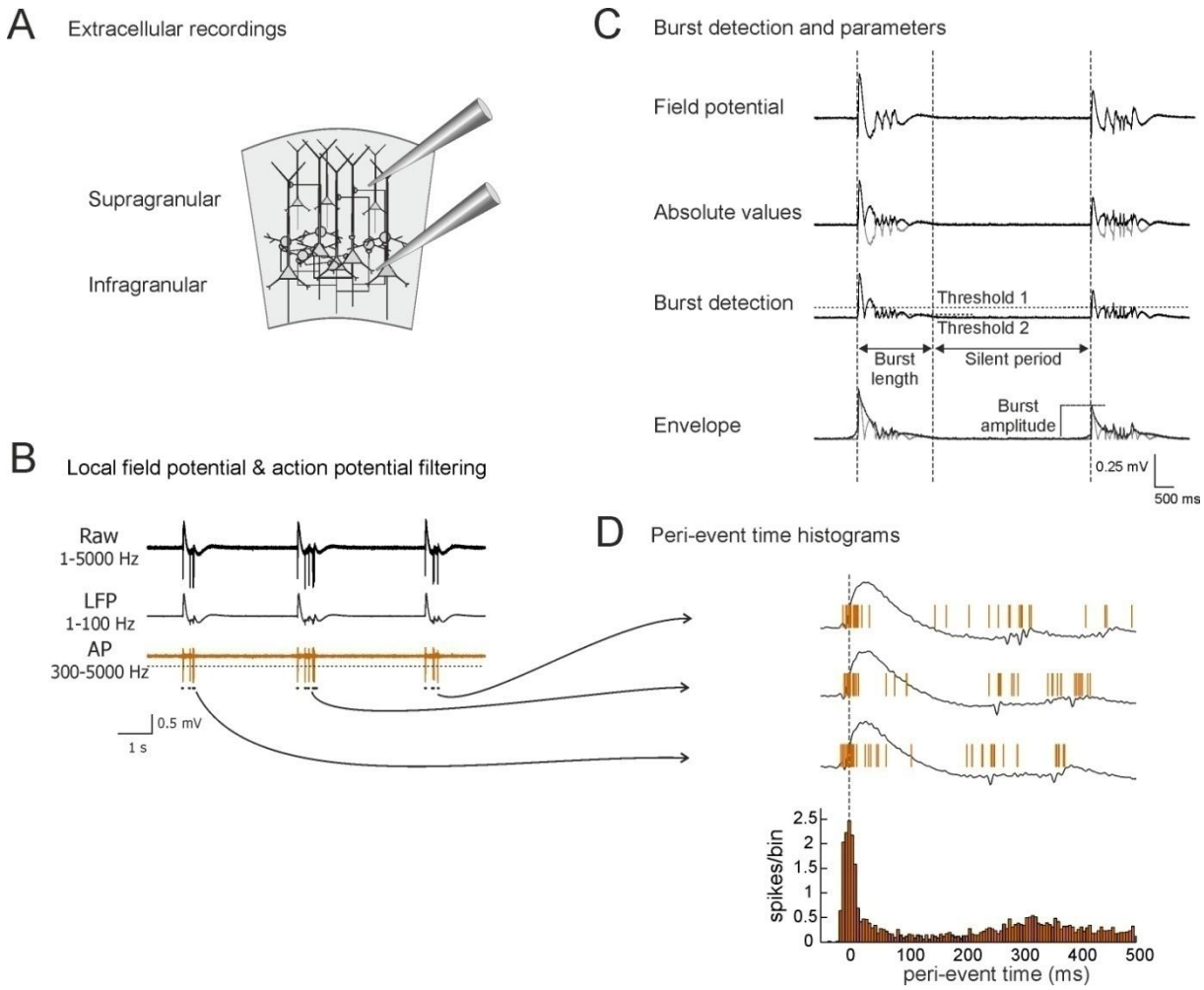

FIGURE 4: SCHEMA OF EXTRACELLULAR RECORDING AND DATA ANALYSIS. ***A.*** Scheme of cortical organotypic culture and electrode placement during extracellular recordings. ***B.*** Raw data (upper trace) was filtered to extract the local field potential (LFP; middle trace) and action potential activity (AP; bottom trace). ***C.*** For burst detection, the absolute value (second trace) of the LFP (first trace) was used. Then, two thresholds were used to define the beginning and the end of the burst phases, respectively (third trace). Burst length is measured from the beginning to the end of a burst (time in ms), while silent periods were measured from burst end to beginning of the next burst. The burst amplitude is determined from the burst envelope (fourth trace). ***D.*** Construction of peri-event time histograms (PETH) of APs. APs were collected in bins covering pre-and post-burst time as determined on the basis of the LFP. Time point zero of the PETH is the burst beginning.

b) As specific manipulations of GABAergic inhibition result in specific, fingerprint-like alterations of burst structure, burst shape and the overall degree of activity (Razik et al., 2013; Sanchez-Vives et al., 2010), parameters describing these aspects of spontaneous activity were chosen.

Thus, the following parameters were chosen: action potential rate, fraction of time bins containing action potentials, relative time spent in burst, burst rate, burst length (Figure 4C) and burst peak amplitude (Figure 4C last trace). A summary explaining the derivation of all parameters can be found in table 6.

Parameter	Unit	Description
Action potential rate	Hz	Time-averaged multiunit action potential frequency (number of action potentials divided by recording length)
Burst rate	Hz	Field-potential based burst frequency (number of field potential bursts divided by recording length)
Fraction of active bins	Dimensionless (range 0 – 1)	Recording is subdivided into time bins (100 ms). The number of bins containing action potentials is divided by the total bin count.
Relative time in burst	Dimensionless (range 0 – 1)	Time occupied by bursts divided by total recording time. It is the fraction of time the networks spend in a neuronally active state. Equivalent to “fraction of active bins”, but based on local field potential.
Burst length	ms	Median length of bursts as detected in the field potential
Burst amplitude	mV	Mean peak amplitude of envelope of field potential within first 500 ms of bursts

TABLE 6: DESCRIPTION OF EXTRACELLULAR ACTION POTENTIAL AND BURST PARAMETERS.

Beyond this 'classical' burst and action potential analysis, spectral analysis was performed. Each recording was divided into segments with a length of 16.384 seconds and an overlap of 8.192 seconds. Each segment was windowed with the Blackman-Harris window function; a Fast Fourier Transform was applied and the power spectral density (PSD) was computed for the frequency range 0.5 to 200 Hz. The resulting PSDs were averaged across segments.

Furthermore, the synchrony and similarity of the LFP signals between recording sites (supragranular vs. infragranular layer) were quantified via cross-correlations. Cross-correlation analysis was performed for broadband LFP signals ([1-200] Hz, here termed 'wide band') as well as for bandpass filtered signals in five different frequency bands: δ [2-5] Hz, θ [6-12] Hz, β [15-30] Hz, γ [30-50] Hz, high γ [50-80] Hz. Filtered LFP traces were divided up into 30 second long segments. Pairs of segments were cross-correlated and for all signals the largest positive peak of the cross-correlation in an interval of [-0.25 0.25] seconds was determined.

In order to describe the relation between action potential and LFP signals at each recording site, a spike density function was computed from the spikes detected at the site. This was done by representing each detected spike by a triangular window (half-width 6 ms) and adding the resulting triangular waveforms (Nawrot et al., 1999; Szűcs, 1998). This resulted in a discrete time series here termed 'instantaneous firing rate' (ifr) which was cross-correlated with the LFP signals from the same recording electrode (segment length was 30 s as above). Specifically, ifr were correlated with the LFP filtered in the δ, θ, and β band, and with the envelope of γ and high γ band. The analysis was meant to assess the correlation between the magnitude of action potential firing and the magnitude of the oscillations; the timing of action potentials within the oscillation cycle was not of interest. Therefore,

the envelope of the cross correlations were computed, and the peak of the envelope was determined in an interval of [-0.25 0.25] seconds.

Lastly, the temporal profile of action potential activity during network bursts (as defined via the local field potential) was quantified via peri-event time histograms (PETHs) (Figure 4D). Peri-burst time was divided into bins of 10 ms length; the number of APs falling into each bin was counted for each individual burst and the values converted to Hz by dividing the counts, averaged across bursts, by the bin width (Figure 4D).

2.4.2 Whole-cell current clamp analysis

In organotypic cultures, intracellular signals recorded in current clamp mode reflect spontaneous network activity as well as extracellularly recorded signals (Czarnecki et al., 2012; Razik et al., 2013). Therefore, spontaneous bursts and action potentials in current clamp data traces were detected by threshold analysis in a manner similar to that employed for extracellular signals. Prior to analyses of the average pre-, post and within-burst membrane potential explained below, action potentials in the voltage traces were pruned by replacing the spike waveforms by a linear fit through the membrane potential values flanking the spike waveforms (2 ms on either side).

Spontaneous activity strongly influences cellular parameters like membrane resistance and time constants (Destexhe and Paré, 1999). In some neurons in organotypic cultures, the low membrane resistance as observed during bursts recovers only very slowly (on the order of seconds) to high, 'resting' values (Razik et al., 2013). In order to obtain values of these parameters during a most stable and precisely defined state of the network, they were determined from responses to hyperpolarizing current injections only in silent periods up to 1 s before each burst. In similar vein, the resting membrane potential (Em_{rest}) was analyzed in fixed intervals of [-1500 -200] ms before bursts. The membrane potential within bursts (Em_{burst}) was analyzed in an interval of [15 80] ms after burst beginning. Last, the difference between the Em before and after each burst (Em_{before} and Em_{after}, respectively) was analyzed. The median Em was determined in a 0.40 s time interval before each burst and 2.00 to 10.00 s after each burst with interval length from 0.20 s up to 5.00 s (depending on the burst frequency in each recording). Then, the difference between Em_{before} and Em_{after} was calculated per burst and the median of this difference was calculated for each recording under control, ACh and wash condition. In this manner, changes in Em in relation to bursts were evaluated for different drug conditions.

2.4.3 Whole-cell voltage clamp analysis

'Classical' analysis of data traces containing spontaneous inhibitory postsynaptic currents (IPSCs) consists of isolating individual events and quantifying their frequency, amplitude and decay and rise times. Due to the high degree of synaptic connectivity in the cultures the frequency of inhibitory postsynaptic currents was quite high, leading to a substantial overlap between IPSCs. This posed a challenge insofar as single events with an uninterrupted decay phase were rare and an analysis based solely on a very small subset of events can be expected to be biased in several ways. The analysis of IPSC data was therefore two-pronged, consisting of i) a classical routine adapted to a frequent overlap of IPSCs and ii) an approach pioneered by Glykys and Mody (2007) which did not rely on the detection of IPSCs (Figure 5 presents details of the analysis).

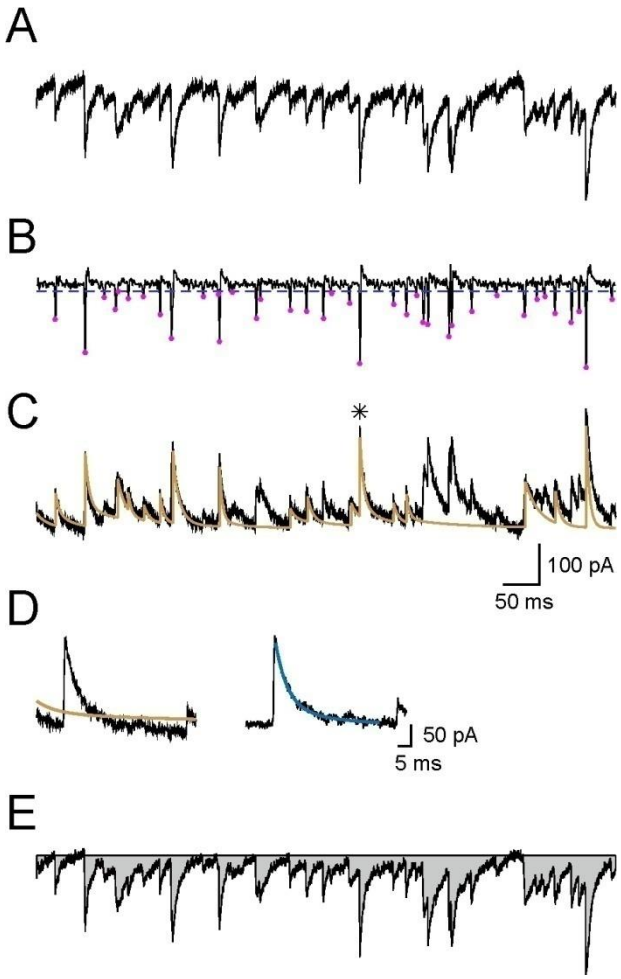

FIGURE 5: ANALYSIS OF IPSCS. ***A.*** Exemplary current trace from a cortical cell under drug-free condition featuring numerous overlapping IPSCs. ***B.*** Pseudo-differentiated current trace representing the rising phase of IPSCs as negative 'spikes'. Blue dotted line is the threshold used for detecting IPSCs (marked by magenta dots). ***C.*** Same current trace as in ***A***, but inverted and with $I_{predict}$ overlaid in ochre (see main text). Minimal fit quality was R^2=0.3. Note that about half of the detected IPSCs were not incorporated in $I_{predict}$ as they either did not

conform to the minimal fit quality criterion or were spaced too closely to each other. IPSC marked by a star did satisfy the quality criteria for both inclusion in $I_{predict}$ and the final selection and is illustrated in ***D***. ***D.*** Left, IPSCs marked by star in C. Overlaid trace is $I_{predict}$ prior to fitting of this IPSC. Right, same IPSC as left, but with $I_{predict}$ subtracted. Blue overlaid trace is the double exponential fit to this IPSC. ***E.*** Same current trace as in ***A***, shown to illustrate the quantification of inhibitory current independent of the detection of IPSCs. Gray area is the integral of the current trace, assuming a base line (thin black line) as described in the main text, corresponding to a 'total phasic current' of -43.2 pA in the excerpt shown.

2.4.3.1 Adapted classical analysis

Inhibitory postsynaptic current traces were first passed through a 'pseudodifferentiation' routine, which consisted of running a boxcar filter of 0.5-1.0 ms length through the data and subtracting the resulting signal by a copy of itself shifted by 0.5-1.0 ms to the left (Banks et al., 2000). The pseudodifferentiation isolated the rapid rising edge of the IPSCs and eliminated both the much slower decay of the IPSCs and fluctuations of the base line, similar to a highpass filter. A time point at which this signal crossed a manually set threshold was defined as the time of occurrence of an IPSC. IPSCs thus detected were cut out and passed through a Savitzky-Golay filter (polynomial order 5, frame size 1.0-1.2 ms), which efficiently eliminated noise but preserved the steep rise phase of the IPSCs. From each of the cutouts, the base line was computed and subtracted from the waveform, followed by a computation of the peak amplitude and 10-90% rise time. Thus, up to this stage the routine yielded values of IPSC frequency, rise time and amplitude independent of any fitting procedure. For the computation of all other parameters, which were based on fitting the decay components of individual IPSCs to a double exponential function, unfiltered current traces were used. The fitting algorithm accommodated overlaps between IPSCs to some degree by subtracting from each IPSC the extrapolated current decays of preceding IPSCs (Figure 5). This was done in a sequential way as follows: starting with the first IPSC, each IPSC was investigated for the length of its decay phase uninterrupted by subsequent (detected) IPSCs. A double exponential fit was performed if the uninterrupted decay phase was at least 8-12 ms long, otherwise the IPSC was discarded. The length of the actual decay fitted was limited by the lesser of [time of occurrence of a subsequent IPSC, end of maximal fit interval of 35-40 ms]. If the fit quality parameter R^2 (discussed below) exceeded a threshold of 0.3-0.6 the IPSC's decay was extrapolated up to ten times its weighted decay time constant. The resulting extrapolated current trace was added to a template array (initialized with zeros) which matched the length of the whole recording and is here termed '$I_{predict}$' for convenience. From each of all subsequent IPSCs matching excerpts of this extrapolated current were subtracted prior to fitting, and the process described above repeated. The algorithm was not able to trace bursts of IPSCs separated by less than the minimal time interval required for fitting, but it did resolve a proportion of IPSC doublets and occasionally triplets with an inter-event separation which was above said limit but still so short as to compromise the following IPSCs (Figure 5C, D).

R^2, the coefficient of determination (range 0 to 1), indicated which proportion of the variance in the data (decay phase of IPSC) was explained by a decay over time as quantified by a double exponential fit. Its value depended strongly on the ratio of IPSC amplitude to current noise amplitude, being low for low ratios. Hence, a threshold value of 0.3-0.6 can be regarded as conservative, preferring large, well-fit IPSCs. Note that at this stage the chosen value of R^2 determined only the inclusion of IPSCs into $I_{predict}$; the final selection of IPSCs for analysis followed an additional criterion designed to reflect the quality of the fit in a manner less dependent on IPSC amplitude:

$$mse_{nc} = \frac{mse_{fit} - mse_{noise}}{amp_{IPSC}}$$

where

mse_{fit} is the mean squared error of the fit to the data

mse_{noise} is the mean squared error of the noise, obtained from a highpass-filtered version of the IPSC (-3dB frequency of 500 Hz)

amp_{IPSC} is the amplitude of the IPSC.

mse_{nc} (nc = noise-corrected) is a measure of the fit error, expressed as the deviation of the data from the fit, corrected for the deviation expected given the current noise level, and scaled by IPSC amplitude. The cutoff value ranged between 0.8 and 1.0.

Finally, from the IPSCs/fits fulfilling the quality criteria, the following parameters were computed: weighted decay time, weighted amplitude, and charge per IPSC (Table 7).

Parameter full name	Unit	Description
Weighted decay time τ	ms	Time from peak until IPSC decays to 36.8 % (100/e) of its peak amplitude
IPSC frequency	Hz	Number of IPSCs divided by recording length
IPSC amplitude	pA	Mean amplitude of peak IPSCs
Phasic current	pA	Integral of inhibitory currents divided by recording time

TABLE 7: DESCRIPTION OF IPSC PARAMETERS.

As the analysis of IPSCs in the aforementioned way involved many subjective choices of analysis parameters, the results may be biased. Furthermore, particularly in recordings with a substantial overlap of IPSCs only a minority of IPSCs could be retained for analysis on the basis of above-mentioned criteria. The sequential selection of IPSCs based on fit quality explained above usually

resulted in a 50-95% loss of events relative to the initial detection stage. The implication of this strong pruning of IPSCs would have been a severe underestimation of the total charge transferred by all IPSCs. This parameter was of interest here because it quantifies the sum of all inhibitory inputs experienced by the cell recorded from. Therefore, a method independent of the detection of individual IPSCs based on the approach by Glykys and Mody (2007) was used and is described in the next paragraph.

2.4.3.2 Current analysis independent of IPSC detection

The whole recording was passed through a Savitzky-Golay filter as described above and divided into segments of 4 s, and from each of these segments an all-points histogram (bin width 2 pA) was computed. Due to the presence of IPSCs, the histograms were skewed toward negative values. A Gaussian was fitted to the unskewed part of the histogram up to the bin representing the first peak. The abscissa value of the Gaussian's maximum was taken as the baseline of the data segment, and subtracted. The integral of the trace thus obtained, divided by its duration, yielded the total charge transferred per time, here termed 'total phasic current' (Figure 5F). In a final step, values from all segments were averaged.

2.5 Statistical analysis

2.5.1 Normality and homoscedasticity of analyzed data

A characteristic of spontaneous activity in cortical cultures is the large variability of burst- and silent period duration and frequency in different preparations and culture batches as described in more detail by Johnson and Buonomano (2007) and Razik et al. (2013). Even in one culture and under constant conditions, short and long bursts can appear. The baseline variability has to be taken into account in the choice of statistical analyses of such data.

First, values for all extracted parameters were plotted as histograms and boxplots to visually characterize the distributions in terms of normality and homoscedasticity (homogeneity of variance), respectively. A number of tests are available to statistically predict if a sample originated from a normally distributed population. However, simulation data has shown that normality tests are especially susceptible to small sample sizes because power is too small and thus, normality test results are heavily biased (Öztuna et al., 2006; Razali and Wah, 2011). Because sample sizes within this thesis project can all be considered "small", no adequate test-based prediction about the underlying distributions could be made. Therefore, non-parametric statistical tests, which do not depend on normality, were used for the analysis. For independent data sets, the Kruskal-Wallis omnibus test was used followed by the Wilcoxon ranksum test for specific group comparisons. Dependent data were analyzed with Friedman's test to compare more than three groups and

Wilcoxon signed rank test for post-hoc analysis. Although non-parametric statistics do not rely on the assumption of normality, they very well assume approximately equal variances (Erceg-Hurn and Mirosevich, 2008). Therefore, all data sets were tested for homoscedasticity with the non-parametric Brown-Forsythe test (data not shown). For the Brown-Forsythe test, the median was subtracted from each individual value of a sample data set. The resulting absolute differences from the median were compared between samples to evaluate the equality of variances. Almost all compared data sets passed the test for homoscedasticity. However, in some rare cases where variances were unequal, *p*-values were marked with a '†' since test assumptions were violated. In some cases, results of variance analyses were reported as test result since large differences of variances can be interpreted as treatment drug effect.

Even though *p* values were reported for reader reference, an evaluation of the statistical significance of a result was based on a robust measure of effect size, *area under the receiver operating characteristics curve* (AUROC) and corresponding confidence intervals (see paragraph below).

2.5.2 Effect size and confidence intervals: Auroc

The Measures of Effect Size toolbox for Matlab by Hentschke and Stüttgen (2011) was used for statistical analysis to determine differences between experimental treatment conditions. For all analyses between two groups, effect sizes with 95% confidence intervals (CI) were reported in addition to traditional Chi^2 (X^2) and *p*-values. For the comparison of two groups, the *p*-value alone only gives the probability of obtaining a difference between the groups as large or larger than the one observed, given the Null Hypothesis of no difference (which is usually rejected if $p < 0.05$). A measure of effect size was provided to quantify the actual size of the difference between two samples. Thus, it could be explicitly stated how large the treatment effect actually was in comparison to a control condition. A number of measures are available to quantify the size of an effect. A non-parametric and robust effect size – one which does not depend on normality and homoscedasticity – is AUROC (Grissom and Kim, 2012) and was used for all data sets analyzed. A detailed and enlightening description of the calculation and interpretation of AUROC is given in an article by Brown and Davis (2006).

For the purpose of this study, AUROC can be interpreted as the probability of superiority. It means that the probability (Pr) that a randomly sampled score of sample X (X_i) exceeds (is superior to) a randomly sampled score from sample Y (Y_i) as in Pr ($X_i > Y_i$) (Grissom and Kim, 2012). AUROC can range from 0 to 1, where 0 refers to the case when none of the values in X exceed Y (Pr ($X_i > Y_i$) = 0 (floor effect: all scores of sample X are smaller than scores of sample Y)), and 1 means that all values in X exceed those in Y (Pr ($X_i > Y_i$) = 1 (ceiling effect: all scores of sample X are larger than scores of sample Y)). In both of these extreme examples, there is no overlap between the two sample

distributions. For 0.5, values in X and Y exceed each other equally often, hence there is no difference between the two samples.

As an example, consider the following values for group X and group Y:

Group X	Group Y	Result
5	7	5 **<** 7; 5 > 3; 5 > 4
6	3	6 **<** 7; 6 > 3; 6 > 4
8	4	8 > 7; 8 > 3; 8 > 4

Now, all values in group X will be compared to all values in group Y. Out of nine possible comparisons (3 x 3), values in group X exceed values of group Y seven times and two values in X are smaller than in Y. Here, Pr ($X_i > Y_i$) = 7/9 = 0.78. When interpreting the thesis results later in the results section, it is important to keep in mind that the superiority of X over Y is calculated and thus, the input order of variables into the equation matters. In all cases, the order of input variables into the statistical equation reflected the drug application order during the experiment. Thus, a *decrease* of a parameter relative to control would present as an AUROC value *above* the null effect value of 0.5.

In order to decide if an effect is small or large, the following index was provided by Grissom (1994): AUROC of 0.56 can be considered as a small effect, 0.64 is a medium effect, and 0.71 is a large effect.

To evaluate the precision of the effect, 95% confidence intervals (CIs) were calculated by bootstrapping. CIs can be interpreted in different ways depending on their usage. Here, the CI is meant as a range covering the true population mean with a confidence of 95% (Cumming et al., 2007).

3 Results

3.1 Effects of tonic acetylcholine (*ACh*$^+$) on spontaneous activity in organotypic cortical cultures

Data for this thesis project were gained from electrophysiological recordings *in vitro* with the main focus on spontaneous activity of organotypic cultures of somatosensory neocortex. Some of the experimental series were also performed on co-cultures of basal forebrain and cortex and cortical acute slices. Spontaneous network activity in cultures was examined during the combined application of $GABA_AR$ modulators with ACh and neostigmine or cholinergic receptor antagonists. These substance combinations were studied to investigate how cholinergic modulation alters GABAergic inhibition in neocortex. Before this main question was tackled, the sole role of ACh on the cortical network was extensively tested with extracellular, current clamp, and voltage clamp experiments.

3.1.1 Lack of substantial cholinergic tone in neocortical cultures

In the first experimental block, three independent series (I-III) of paired extracellular recordings from supra- and infragranular somatosensory cortical layers were conducted. The goal was to assess if the neuronal network state differed with externally supplied ACh and without (presumably a state of cholinergic inactivity). Each of the three series began with a control recording in the absence of any drug. Following control, no external ACh was supplied in the sham condition (series I), or ACh (1 µM) and the acetylcholine esterase-inhibitor neostigmine (1 µM) were applied together (series II) or ACh (10 µM) and neostigmine (1 µM) were applied (series III) (Table 8). Each of these three conditions was followed by and contrasted with the *ACh*$^-$ condition defined by the application of the muscarinic receptor antagonist atropine (1 µM) and the nicotinic receptor antagonist mecamylamine (3 µM). The rationale for applying cholinergic blockers and thus ensuring the absence of any cholinergic action in the *ACh*$^-$ condition was an assessment not only of the effects of externally supplied ACh, but also of the intrinsic cholinergic tone in the cortical networks: Even though the main source of ACh in cortex is provided by cholinergic projection neurons from basal forebrain, cortex also contains cholinergic INs (Consonni et al., 2009; Engelhardt et al., 2007). Reversibility of the drug effects was screened in a wash-out condition terminating each experiment.

For statistical comparison of the three experimental series with each other, the modulatory effects of putative intrinsic ACh (sham – series I) and externally supplied ACh (series II and III) were expressed as changes in activity in the *ACh*$^-$ condition. Specifically, within each experiment, data from the *ACh*$^-$ condition were normalized to the preceding conditions (Table 8); these normalized data sets were

compared with each other via a Kruskal-Wallis test, followed by specific pairwise comparisons in the case of a significant omnibus effect (supplementary material Table S1).

Codition	**Drug application order**			
I **Sham**		Control (drug-free)	***ACh*$^{-}$** (Atropine (1 µM) & Mecamylamine (3 µM))	Wash-out (drug-free)
II **ACh (1 µM)**	Control (drug-free)	*ACh*$^{+}$ (ACh (1 µM) & Neostigmine (1 µM))	***ACh*$^{-}$** (Atropine (1 µM) & Mecamylamine (3 µM))	Wash-out (drug-free)
III **ACh (10 µM)**	Control (drug-free)	*ACh*$^{+}$ (ACh (10 µM) & Neostigmine (1 µM))	***ACh*$^{-}$** (Atropine (1 µM) & Mecamylamine (3 µM))	Wash-out (drug-free)

TABLE 8: DRUG APPLICATION SCHEME. Data in the three ACh- conditions (in bold) were each normalized to the preceding condition (ACh+ or control) and then statistically compared to each other.

Six parameters of neuronal activity were investigated, which were: action potential rate, fraction of active bins, burst rate, relative time in burst, burst length and burst amplitude. Action potential rate, fraction of active bins and relative time in burst were chosen to allow statements about the degree of activity; burst rate and burst length revealed firing pattern changes, and burst amplitude was used to evaluate the shape of activity (see Methods section for a detailed description).

Since the antagonism of cholinergic receptors should reverse *ACh*$^{+}$-induced effects, it was hypothesized that changes of neuronal activity from *ACh*$^{+}$ to *ACh*$^{-}$ should be noticeable. Contrasting these effects with those of *ACh*$^{-}$ without previous ACh application would reveal the strength of the intrinsic cholinergic tone. Judged by visual inspection of exemplary raw data (Figure 6), cholinergic blockade altered spontaneous activity notably if it was preceded by either of the two *ACh*$^{+}$ conditions (Figure 6B, C), but less so if it was preceded by the drug-free control condition (sham) (Figure 6A). Boxplots in Figure 6 indicate that *ACh*$^{-}$ following drug-free control increased the median burst rate while having no effect on burst amplitude (Figure 6A, n = 13). By contrast, *ACh*$^{-}$ decreased burst rate and increased burst amplitude when applied subsequent to the *ACh*$^{+}$ conditions (Figure 6B, n = 21 and C, n = 14). In accordance with these observations, differences between the three groups were detected for burst rate, burst length and burst amplitude.

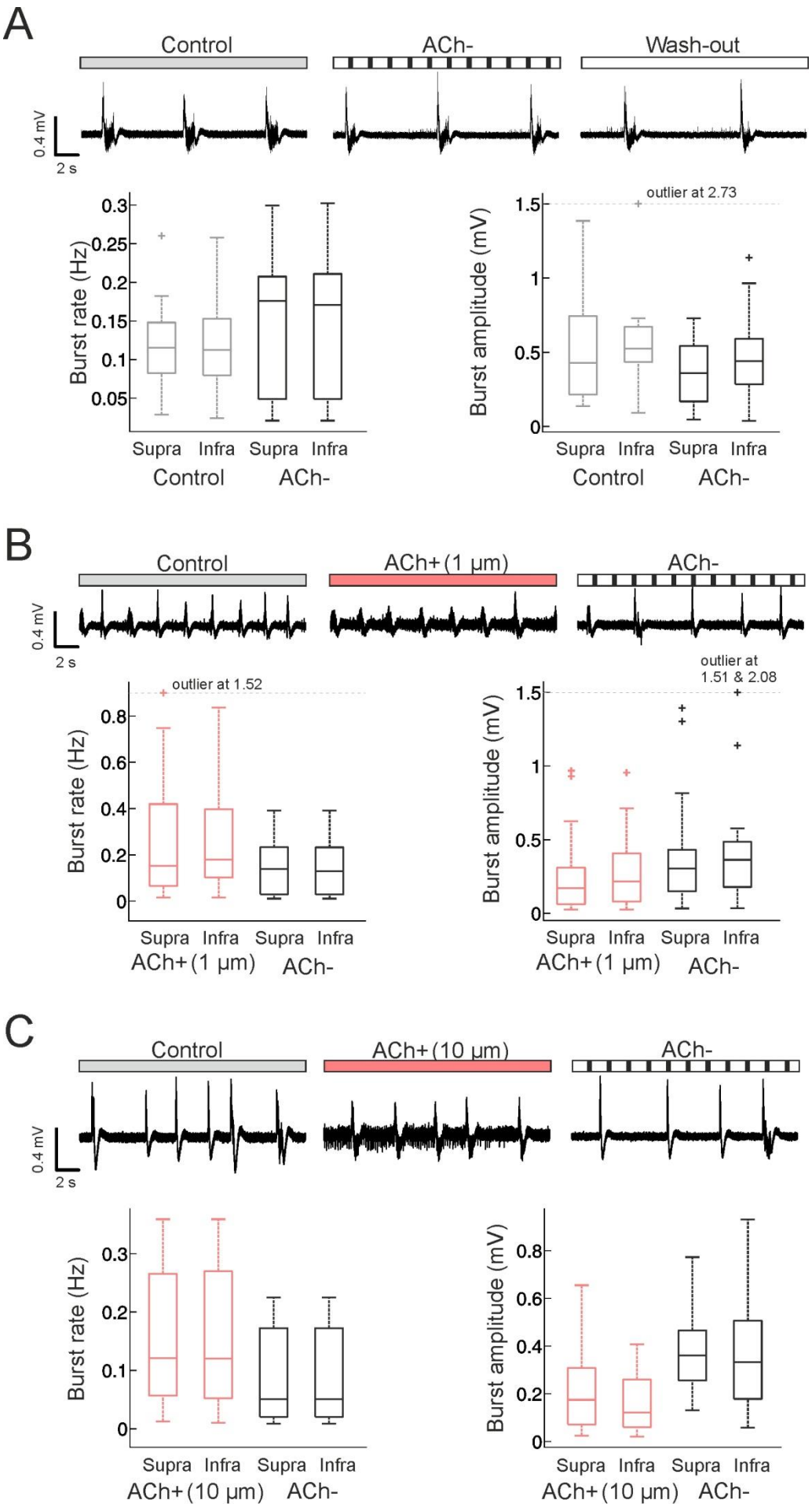
A
Control
ACh-
Wash-out
0.4 mV
2 s
Burst rate (Hz)
0.3
0.25
0.2
0.15
0.1
0.05
Supra Infra Supra Infra
Control ACh-
Burst amplitude (mV)
outlier at 2.73
1.5
1
0.5
0
Supra Infra Supra Infra
Control ACh-
B
Control
ACh+(1 µm)
ACh-
0.4 mV
2 s
outlier at 1.52
Burst rate (Hz)
0.8
0.6
0.4
0.2
0
Supra Infra Supra Infra
ACh+(1 µm) ACh-
outlier at
1.51 & 2.08
Burst amplitude (mV)
1.5
1
0.5
0
Supra Infra Supra Infra
ACh+(1 µm) ACh-
C
Control
ACh+(10 µm)
ACh-
0.4 mV
2 s
Burst rate (Hz)
0.3
0.2
0.1
0
Supra Infra Supra Infra
ACh+(10 µm) ACh-
Burst amplitude (mV)
0.8
0.6
0.4
0.2
0
Supra Infra Supra Infra
ACh+(10 µm) ACh-

FIGURE 6: CHOLINERGIC MODULATION OF EXTRACELLULARLY RECORDED SPONTANEOUS NETWORK ACTIVITY. *A.* Effects of cholinergic receptor blockade (*ACh*$^-$) following a drug-free control. Top row, exemplary raw data. Boxplot (left) shows burst rate (Hz) for supra- and infragranular layers during control and *ACh*$^-$. Boxplot (right) shows burst amplitude for the same recording sites and drug conditions. In all box plots, data points considered outliers in each group were collectively marked by a single '+' symbol placed at the threshold (dotted horizontal line) and their values were given as text. Bonferroni correction: $p < 0.025$; CI 0.975. ***B.*** Similar depiction of data as in A for effects of cholinergic receptor blockade (*ACh*$^-$) following cholinergic stimulation (1 µM ACh + 1 µM neostigmine, termed *ACh*$^+$). ***C.*** Similar depiction of data as in B for effects of cholinergic receptor blockade (*ACh*$^-$) following cholinergic stimulation with 10 µM ACh + 1 µM neostigmine.

For example, differences for burst rate between *ACh*$^-$ normalized to control (I), *ACh*$^-$ normalized to *ACh*$^+$ (1 µM) and *ACh*$^-$ normalized to *ACh*$^+$ (10 µM) were detected with an omnibus test (supragranular layers: $X^2(2) = 9.47$, $p = 0.009$) (Figure 7A). Directly contrasting the burst rate for *ACh*$^-$ normalized to control (I) to *ACh*$^-$ normalized to either of the two *ACh*$^+$ conditions (II & III) revealed differences (I & II supra: $p = 0.01$, auroc [95% confidence intervals (CIs)] = 0.77 [0.56 0.94]; I & III supra: $p = 0.005$, auroc 0.82 [0.60 0.97]) (Figure 7B). Auroc values and corresponding CIs for burst rate, burst length and burst amplitude are displayed in Figure 7B. An auroc value of 0.5 can be interpreted as no difference between conditions; 0 and 1 describe maximal effects (calculations and interpretation of auroc are described in great detail in the Methods section). For the three other parameters, no differences were detected (supplementary material Table S1).

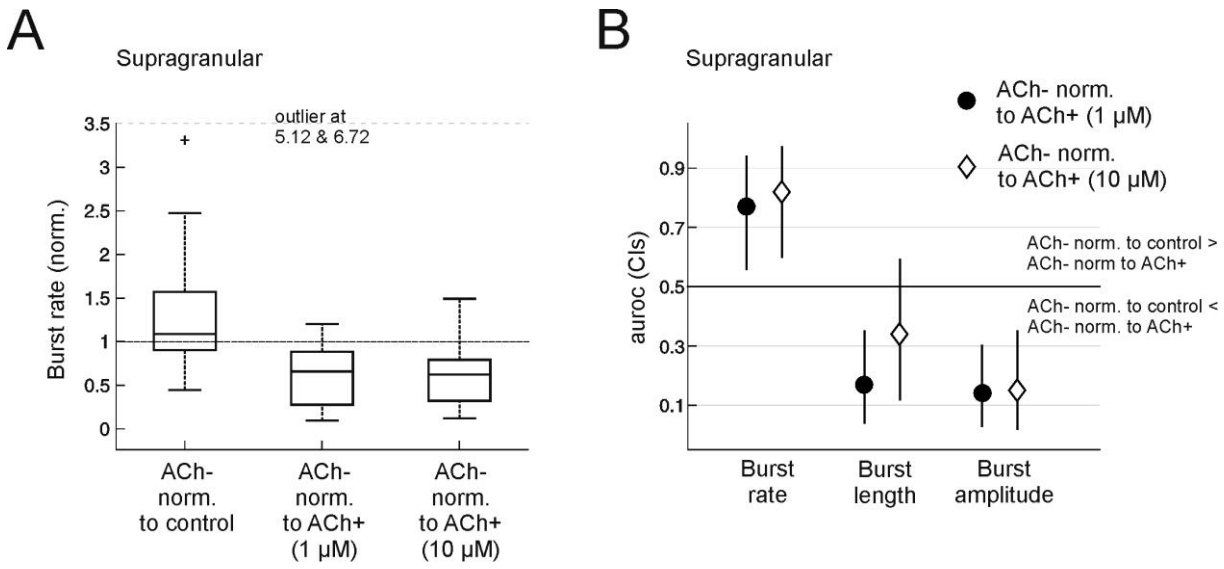

FIGURE 7: COMPARISON AND STATISTICAL ANALYSIS OF THE EFFECTS OF CHOLINERGIC RECEPTOR BLOCKADE (*ACH*$^-$) FOLLOWING CONTROL (DRUG-FREE) OR *ACH*$^+$ (1 OR 10 MM) CONDITIONS. *A.* Effects of *ACh*$^-$ on burst rate in the supragranular layer. Data from the *ACh*- condition were normalized to either the preceding control (drug-free; left data set), *ACh*$^+$ (1 µM; middle data set) or *ACh*$^+$ (10 µM; right data set) conditions. Pairs of data sets thus normalized were compared statistically and the results plotted in ***B***. ***B.*** Effect size (auroc) values with 95% confidence intervals (CI) from pairwise comparisons of normalized effects of *ACh*- for three burst parameters. Dotted horizontal line depicts the auroc 'null' value.

Lastly, differences between the *ACh*$^{+}$ and *ACh*$^{-}$ condition were analyzed based on PETHs (Figure 8). First, comparing the effect of *ACh*$^{-}$ following the control condition revealed no difference between the two conditions (Figure 8A, left panel) as PETHs were almost congruent. This observation was verified by the auroc effect size values for each bin, which were close to 0.5. When *ACh*$^{-}$ was compared to wash-out (Figure 8, right panel), firing rates for each bin stayed approximately the same with corresponding auroc values of about 0.5 indicating no change. Thus, in agreement with previous analyses, the *ACh*$^{-}$ condition did not have an effect on firing patterns. Figure 8B and C display PETHs for control and *ACh*$^{+}$ (1 µM) and *ACh*$^{+}$ (10 µM) (left panel), respectively. For both concentrations, but more so for the higher ACh concentrations, firing rates were higher prior to burst beginning (before time point 0) in the presence of ACh (auroc value above 0.5) and lower during the initial phase of the burst (~ first 50 ms) in comparison to the control conditions (auroc value below 0.5). When cholinergic blocker were applied and compared with the two *ACh*$^{+}$ conditions (Figure 8B & C, right panel), firing in bins prior to burst beginning decreased (auroc below 0.5), but increased during the initial burst phase. Thus, cholinergic effects were reversed by blocker.

In summary, antagonizing effects of cholinergic blockers were shown following the *ACh*$^{+}$ condition for two different concentrations of ACh but not for the sham condition. The main conclusion drawn from this experimental set is the absence of significant endogenous release of ACh in organotypic cultures of cortex. Since the two conditions *ACh*$^{+}$ and *ACh*$^{-}$ differed substantially, they were used for subsequent experiments studying the effects of ACh alone and as baseline conditions during experiments with $GABA_AR$ modulators. The lower ACh concentration (1 µM) was sufficient for a notable contrast between *ACh*$^{+}$ and *ACh*$^{-}$ and was further on the standard ACh concentration.

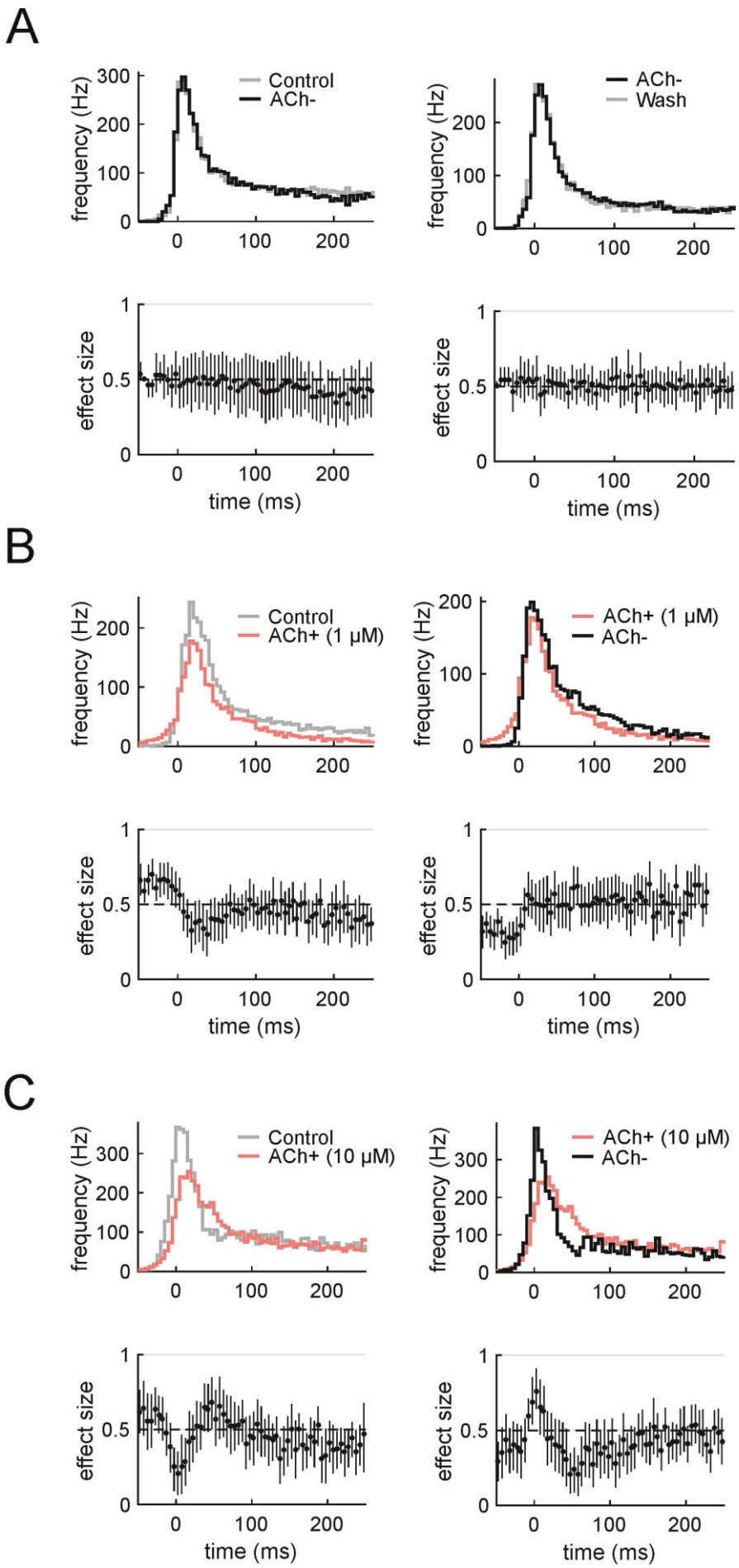
A
frequency (Hz)
Control
ACh-
ACh-
Wash
effect size
time (ms)
B
Control
ACh+ (1 µM)
ACh+ (1 µM)
ACh-
C
Control
ACh+ (10 µM)
ACh+ (10 µM)
ACh-

FIGURE 8: PETHS AND EFFECT SIZES FOR ACH-, ACH+ (1 µM) AND ACH+ (10 µM). All results shown in this figure were recorded in infragranular layers. ***A, left.*** PETHs are shown for control (grey) and ACh- (black) (n = 13). ***A, right.*** PETHs are shown for ACh- (black) and wash (n = 12). Below, auroc effect sizes are presented to show effects of ACh- in comparison to control and wash, respectively. ***B, left.*** PETHs are shown for control (grey) and ACh+ (1 µM) (rosé) (n = 20). ***B, right.*** PETHs for ACh+ (1 µM) (rosé) and ACh- (n = 20). Below, auroc effect sizes are presented to show effects of ACh+ in comparison to control and ACh-, respectively. ***C.*** Same as B, except that ACh+ was applied in higher concentration (10 µM), n= 14.

3.1.2 ACh altered the activity pattern and reduced membrane potential excursions in current clamp experiments

To gain a more detailed understanding of the effects of tonic ACh on spontaneous neuronal activity in organotypic cortical cultures, first, a variety of neuron types across cortical layers were recorded in whole-cell current clamp mode (n = 13). Recordings of spontaneous activity were performed under three successive conditions (in order of application): (I) drug-free control, (II) ACh^+ (as defined above), and (III) wash-out. The first block of analyses dealt with characterizing changes in activity by means of the same parameters as employed for the extracellular data analysis. Thus, comparisons between the present current clamp data set and extracellularly recorded data described in chapter 3.1.1 were possible. For all parameters, the ACh^+ condition (II) was compared with both drug-free control (I) and wash-out (III) conditions. The change of activity from the control condition (I) to the ACh^+ condition (II) was termed ACh^+ effect, whereas the transition from ACh^+ (II) to wash-out (III) was termed wash effect. To illustrate the effects visually, auroc effect sizes and 95 % confidence intervals (CIs) for ACh^+ and wash effects for each parameter were plotted (Figure 9). Results showed that ACh changed the activity in comparison to the control recording in a reversible manner (Figure 9, supplementary material Table S2). Action potential rate, fraction of active bins, burst rate and relative time in burst increased during the ACh^+ condition (auroc < 0.5); burst length was shortened (auroc > 0.5). The largest effect was observed for burst rate, which almost doubled (median [25^{th} & 75^{th} quantile]: Ctrl = 0.08 [0.04 0.11] Hz; ACh^+ = 0.14 [0.09 0.20] Hz; p = 0.003; auroc [95 % confidence intervals] = 0.30 [0.13 0.41]). Overall, these findings were in good agreement with the results from the extracellular recordings described above. For each parameter, the effect induced during the ACh^+ condition was reversible as seen by the mirror-symmetry of ACh^+ effect and wash effect values. Summing up, the overall intracellular activity level increased and network patterns changed notably during the ACh^+ condition.

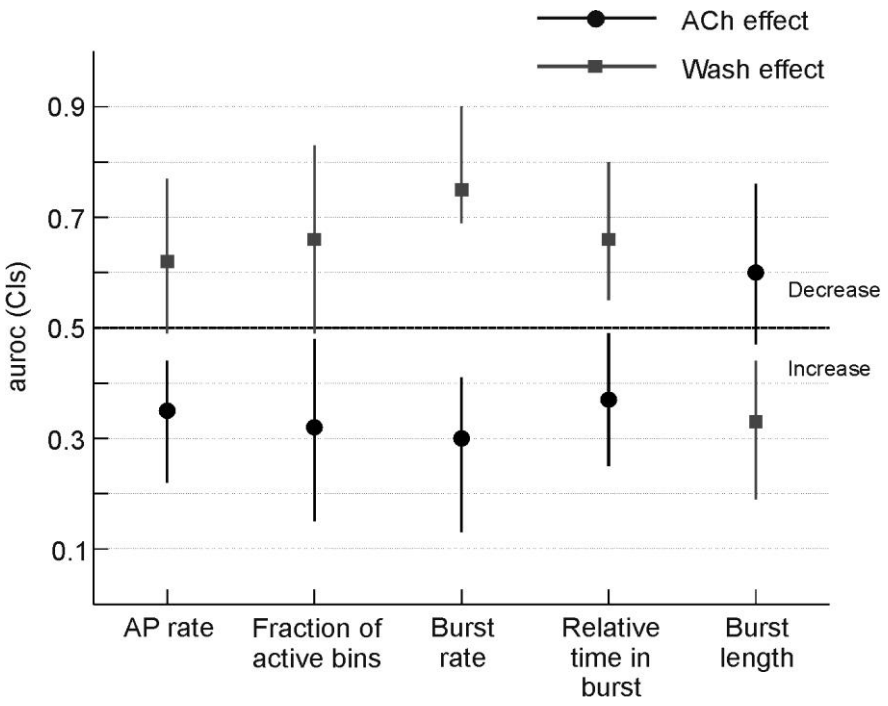

FIGURE 9: EFFECT SIZE ANALYSIS OF ACH TREATMENT ON AP AND BURST PARAMETERS AS ASSESSED IN CURRENT CLAMP RECORDINGS. The plot shows auroc values (filled symbols) and 95 % confidence intervals (vertical bars) for two sets of pairwise comparisons: "ACh effect" is the effect of *ACh+* in relation to the preceding control (drug-free) condition. "Wash effect" is the effect of wash in relation to the preceding *ACh+* condition. Note the mirror-symmetry of the auroc values around the null effect value of 0.5, illustrating reversibility of the modulatory effects of *ACh+*.

Next, intracellular parameters were analyzed to gain a more detailed understanding of cholinergic modulatory effects. Two raw data examples are displayed in Figure 10. In Figure 10A, recordings from a neuron from supragranular layers are shown. The cell was identified by its high input resistance (155.28 MΩ), spike width at half amplitude of 1.05 ms and approximate maximal firing frequency of about 26 Hz - electrophysiological characteristics typical for regular-spiking INs in culture (Czarnecki et al., 2012) (It cannot be ruled out that the cell was possibly a PY neuron. However, measured parameters fit better with the description of regular-spiking INs in culture by Czarnecki et al. (2012) than the characterization of PYs in culture by Klostermann and Wahle (1999)). Under control conditions, the neuron displayed activity typical of neurons in spontaneously active neocortical organotypic cultures (Antkowiak and Helfrich-Forster, 1998; Czarnecki et al., 2012; Johnson and Buonomano, 2007): regularly recurring, strong depolarizations accompanied by action potential activity, an activity pattern termed network 'bursts', separated by periods of relative neuronal quiescence ('silent periods'). In the ACh^+ condition, the resting membrane potential (Em_{rest}) was slightly depolarized, bursts were shortened and their rate of occurrence increased. The second neuron (Figure 10B) was a fast-spiking cell from infragranular layers (input resistance: 39.45 MΩ; spike width at half amplitude: 0.48 ms; approximate maximal firing frequency: 119 Hz).

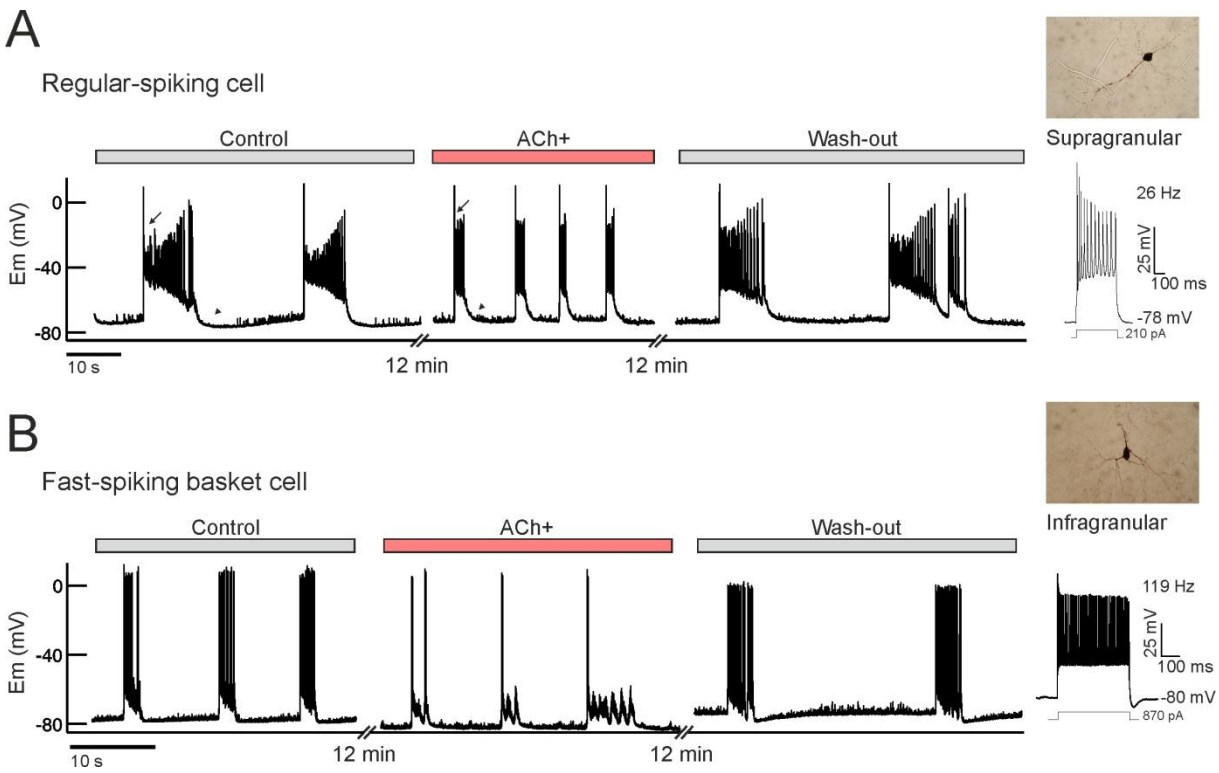

FIGURE 10: CURRENT CLAMP RECORDINGS IN THE PRESENCE OF ACH. ***A.*** Raw data traces from current clamp recordings of a regular-spiking cell. Data was recorded during control (drug-free), ACh^+ and wash-out. Drug-application or wash-out time was 12 minutes. Note the strong depolarization of the membrane potential followed by a dip in spike amplitude at burst begin (control condition, arrow) and a notable burst afterhyperpolarization (control condition, arrowhead), all of which are much less prominent in the ACh^+ condition. Rightmost panels show adapting spiking pattern elicited by current step injection (approximate maximal firing rate was 26 Hz) and microscopic image of the biocytin-filled cell. ***B.*** Raw data traces recorded from a fast-spiking cell (approximate maximal AP rate 119 Hz, see rightmost panel).

Similar to the neuron described above, spontaneous activity occurred in clearly separable bursts, but during ACh^+ Em_{rest} hyperpolarized. Possibly as a consequence of this hyperpolarization, the cell fired less during bursts. For all recorded cells, ACh^+ had no effect on cell resistance R (median [25^{th} & 75^{th} quantile]): $R_{control}$ = 106.01 [61.57 173.04] MΩ; R_{ACh} = 109.84 [85.73 130.87] MΩ; $R_{wash\text{-}out}$ = 98.55 [81.72 126.98] MΩ; X^2 = 0.67, p = 0.72. However, as mentioned above, visual inspection of the raw data traces suggested that ACh exerted strong effects on Em. Hence, changes in Em were analyzed by selecting three time windows around bursts (Figure 11A): (a) directly before the bursts (Em_{rest}), (b) during burst beginnings (Em_{burst}), and (c) after the bursts terminated. Due to spontaneous activity in organotypic cultures, the baseline mean Em_{rest} was determined in a pre-burst time window of [-1500 -200] ms. Results were averaged for each cell under control, ACh^+ and wash condition and summarized in Figure 11D. No consistent effect of ACh^+ was observed: some cells were slightly depolarized while others were hyperpolarized (one cell was excluded because of a missing wash recording, n = 12; median [25^{th} & 75^{th} quantile]): $Em_{rest\text{-}control}$ = -77.20 [-78.97 -74.27] mV; $Em_{rest\text{-}ACh}$ = -74.56 [-79.43 -71.35] mV; $Em_{rest\text{-}wash\text{-}out}$ = -72.69 [-75.88 -70.62] mV; X^2 = 4.67, p = 0.10.

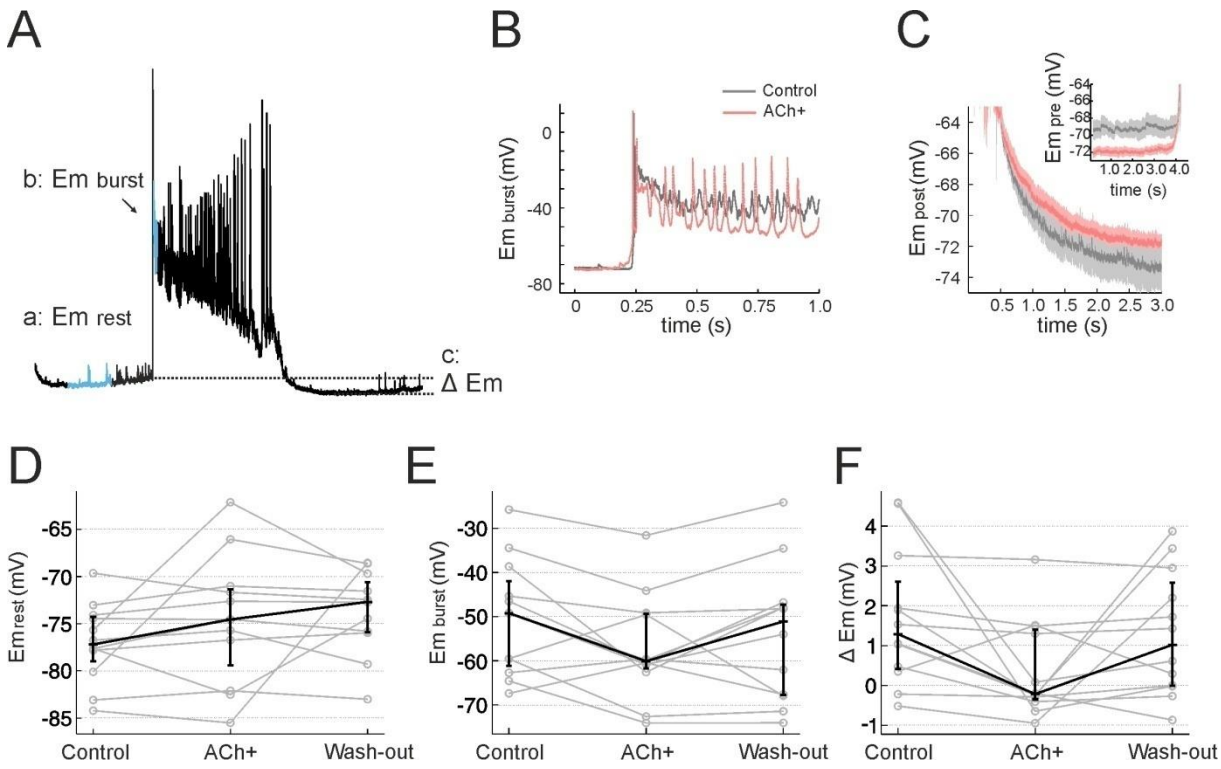

FIGURE 11: RESULTS OF CURRENT CLAMP RECORDINGS IN THE PRESENCE OF ACH. ***A.*** Example of a spontaneous network burst illustrating peri-burst time windows and differences between time windows used for membrane potential analysis. ***Aa.*** Em_{rest} [-1500 -200] ms prior to burst beginning. ***Ab.*** Em_{burst} [15 80] ms after burst beginning. ***Ac.*** Δ Em = Em_{pre} [-400 0] ms before burst beginning - Em_{post} [burst end +2.000] to [burst end +10.000] ms. ***B.*** Exemplary excerpts of bursts illustrating the difference in initial depolarization and spiking ability between control and ACh+. ***C.*** Example of difference between Em in control (grey) and ACh+ (rosé) after burst end (Em_{post}) and before burst beginning (Em_{pre}). Thick traces and shaded areas are averaged traces and standard deviations, respectively, from one recording. ***D.*** Plot of Em_{rest} for the three different drug conditions. Grey points and lines are from individual experiments, black lines and vertical bars represent medians with 25th and 75th quantile. ***E.*** Plot of Em_{burst} for three different drug conditions. Grey points and lines are from individual experiments, black lines and vertical bars represent medians with 25th and 75th quantile. ***F.*** Plot of ΔEm. Grey points/ lines from individual experiments; black lines/ vertical bars are medians with 25th and 75th quantile. Note that median value of ΔEm is close to zero during the ACh+ condition.

This finding confirmed the diversity of effects of ACh on different cortical cell types as reported by other groups (Gulledge et al., 2007; Kawaguchi, 1997).

Even though the action of ACh^+ on Em_{rest} was very cell-specific, some coherent effects were observed. Under control condition, most cells went into a depolarization block in the first phase of a burst. During this time, Em was briefly depolarized to a degree that cells were unable to fire action potentials until Em reached a more negative level again. When ACh^+ was applied, the depolarization block was greatly reduced or even removed completely in some cases, resulting in a more regular firing pattern throughout bursts as seen in figure 11B. For analysis, action potentials were removed (see Methods) and Em was averaged in a time window [15 80] ms after burst beginning and compared between control, ACh^+ and wash condition (Figure 11E), median [25^{th} & 75^{th} quantile]): Em_{burst} control = -49.21 [-61.14 -42.01] mV; Em_{burst} ACh^+ = -60.10 [-61.71 -49.35] mV; Em_{burst} wash-out

= -51.12 [-67.78 -47.35] mV; X^2 = 6.00, p = 0.05. Posthoc analysis with a Wilcoxon signed rank test and auroc between Em_{burst} control and Em_{burst} *ACh*$^+$ revealed that the Em during the first phase of a burst was on average less depolarized during the *ACh*$^+$ condition, p = 0.03, auroc [95% CI] = 0.65 [0.51 0.82]. This result is consistent with the finding that ACh diminished peak amplitudes of the bursts as recorded extracellularly (Figure 6, 7B). Although the general trend towards a less depolarized Em within the burst is supported by the statistical results, it should be noted that three cells reacted with stronger depolarization to *ACh*$^+$ application, which again highlights the heterogeneous effects of *ACh*$^+$.

During the control condition, a burst was usually followed by a long-lasting afterhyperpolarization, resulting in a slowly rising Em before the next burst. Visual inspection of the recorded traces suggested that ACh abolished this rhythmic change of the Em. Therefore, Em around bursts was examined (Figure 11C). Em directly before burst beginning (Em_{pre}) was averaged in a [-400 0] ms time window and after burst end (Em_{post}) in a window of variable size ranging from [burst end +2.000] to [burst end +10.000] ms depending on the kinetics of the afterhyperpolarization and the silent period length between bursts. The difference of membrane potentials (Δ Em) between both time windows was calculated for each burst (Δ Em = Em_{pre} – Em_{post}) and averaged per recording for control, *ACh*$^+$ and wash-out condition. Statistical analysis revealed a difference between the three groups (median [25th & 75th quantile]): Δ Em control = 1.29 [0.41 2.60] mV; Δ Em *ACh*$^+$ = -0.22 [-0.35 -1.40] mV; Δ Em wash-out = 1.02 [-0.01 2.58] mV; X^2 = 9.5, p = 0.01). Post-hoc analysis between Δ Em control and Δ Em *ACh*$^+$ showed that the difference between Em_{pre} and Em_{post} decreased, p = 0.01, auroc [95% CI] = 0.76 [0.63 0.92] (Figure 11F). Thus, the analysis confirmed the impression of a more constant resting membrane potential during the *ACh*$^+$ condition.

In summary, the results supported the notion of ACh modulating excitation as well as inhibition. On the one hand, cell and network activity notably increased, as indicated by an increase in action potential and burst frequency during the *ACh*$^+$ condition – indication of increased excitation. On the other hand, inhibitory components of the effect of ACh on the networks were manifest in the form of dampened in-burst peak depolarizations and shortened bursts. This increase in inhibition could be due to heightened GABAergic IN activity (Mann et al., 2009; Razik et al., 2013). Since ACh is known to excite specific GABAergic INs, the next experimental series investigated the hypothesis of an ACh-mediated increase of GABAergic inhibition in the cortical network.

3.1.3 ACh increased the total inhibitory current in IPSC recordings

Whole-cell voltage clamp recordings were obtained from visually identified cortical PYs in culture (n = 8). In order to record GABAergic inhibitory postsynaptic currents (IPSCs), blockers of glutamatergic receptors (CNQX and AP5) were added throughout the experiments and the neurons were filled with a chloride-based solution and held at -70 mV. Neurons were recorded under control, the ACh^+, and the ACh^- condition equivalent to the extracellular recording procedure described in chapter 3.1.1 (see an exemplary recording in Figure 12A).

The decay time of IPSCs, their frequency, amplitude and the 'total phasic current' (the time-averaged current carried by IPSCs) were analyzed for all three tested drug conditions (for detailed description of parameters see Methods Table 7). In the control condition, IPSCs had a median decay time of 7.78 [6.52 10.37] ms, an amplitude of 23.73 [19.57 30.51] pA, and occurred with a frequency of 6.51 [4.47 9.97] Hz. In the ACh^+ condition the decay time remained unaffected, but IPSCs became more frequent and had larger amplitudes (Figure 12, supplementary material Table S3). Thus, the overall inhibitory current in the ACh^+ condition increased almost five times in comparison to the control and ACh^- conditions (median [25^{th} & 75^{th} quantile]): control = -2.09 [-3.67 -1.10] pA; ACh^+ = -9.68 [-11.38 -6.19] pA; ACh^- = -2.12 [-4.01 -1.64] pA; X^2 =12.25, p = 0.002 (Figure 12A & B, supplementary material Table S3).

Parameter values of the control condition and the ACh^- condition were clearly similar, indicating that the blockade of cholinergic receptors solely reversed the effects of externally supplied ACh and neostigmine. If intrinsic cholinergic neurons had been active and released ACh in physiologically relevant amounts, blockade of cholinergic receptors should have reduced IPSC frequency and/or amplitude below control levels. In agreement with the extracellular data set described previously, no evidence was found to suggest significant intrinsic release of ACh in cortex.

The magnitude of the cholinergic effect on IPSCs suggested that ACh fostered action potential activity of GABAergic INs. To confirm that the observed changes were action potential-dependent, a subseries of experiments was performed in which tetrodotoxin (TTX), a blocker of voltage-gated sodium channels, was applied prior to the ACh^+ condition (Table 9, Figure 13A). To compare effects of ACh^+ and [TTX & ACh^+] treatments, data were normalized to their preceding control condition, which was either drug-free aCSF for the ACh^+ condition or TTX-containing aCSF for [TTX & ACh^+]. Normalized data sets were directly compared with a Wilcoxon ranksum test which showed major differences between ACh^+ and [TTX & ACh^+] for all parameters, particularly IPSC frequency and amplitude (Figure 13B, supplementary material Table S4).

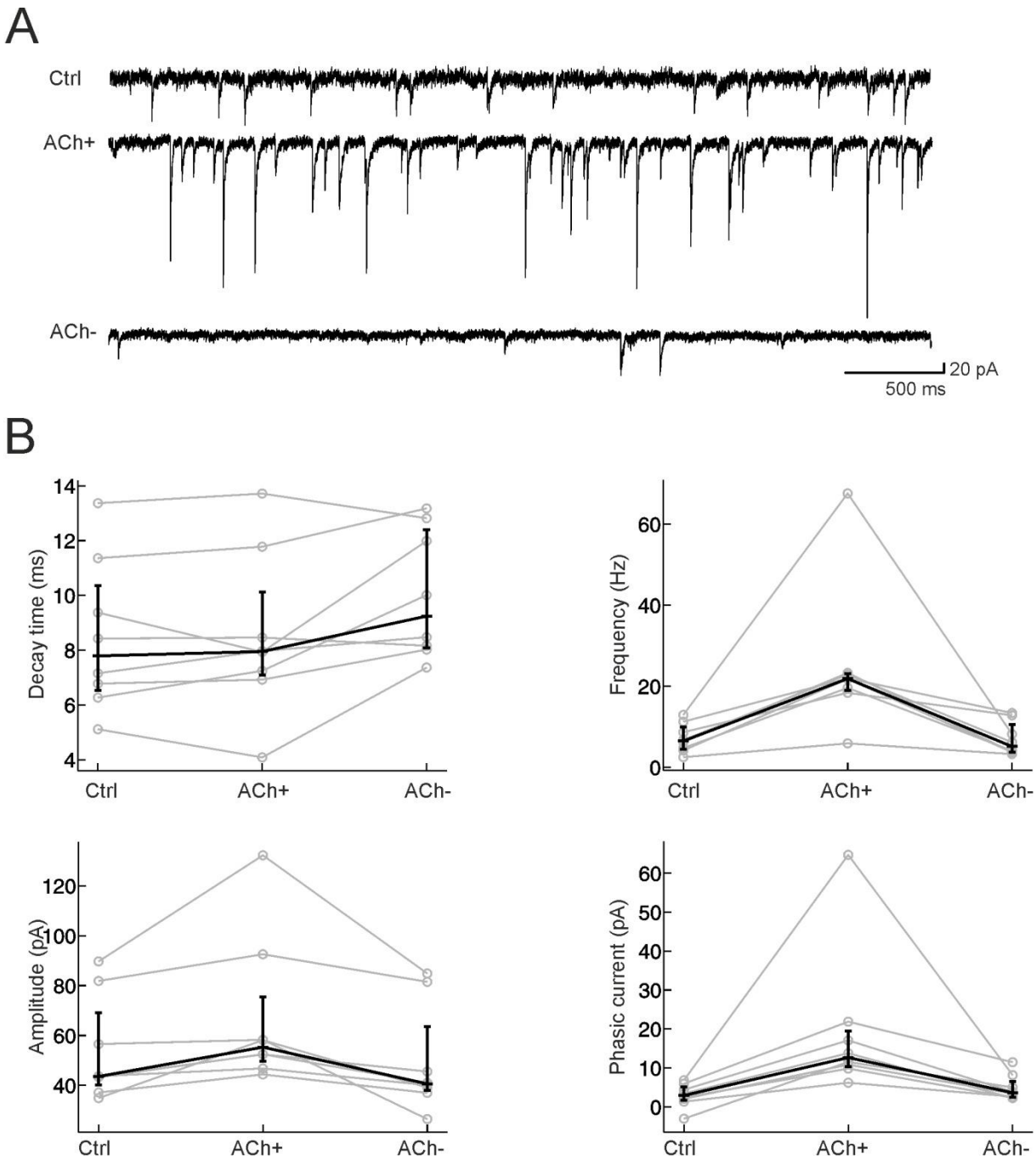

FIGURE 12: IPSC RECORDINGS IN THE PRESENCE OF ACH. ***A.*** Example recording of IPSCs in control (ctrl, drug-free), ACh^+ and ACh^- in the presence of AP5/CNQX. IPSC frequency increased and high-amplitude IPSCs appeared during ACh administration. ***B.*** Summary results (n = 8 cells) for decay time, frequency, amplitude and phasic current (gray, individual cells; black, median and 25th and 75th quantile).

Condition	Drug application order		
I ***ACh*$^+$**	Control (drug-free)	*ACh*$^+$ (ACh (1 µM) & Neostigmine (1 µM))	*ACh*$^-$ (Atropine (1 µM) & Mecamylamine (3 µM))
II **[TTX & *ACh*$^+$]**	Control (drug-free)	TTX (TTX (1 µM))	TTX & *ACh*$^+$ (TTX (1 µM) & ACh (1 µM) & Neostigmine (1 µM)

TABLE 9: DRUG APPLICATION SCHEME AND NORMALIZATION FOR *ACH*$^+$ AND [TTX & *ACH*$^+$].

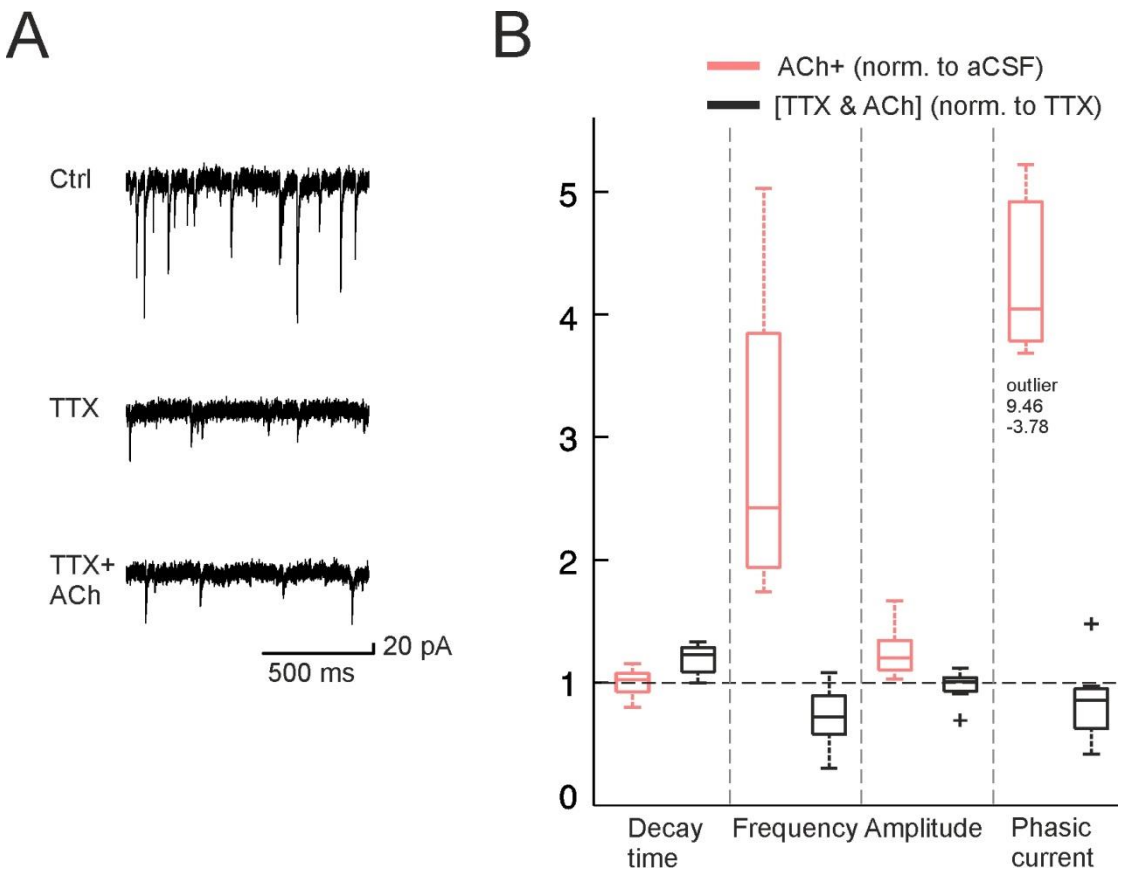

FIGURE 13: *A.* EXAMPLE RECORDING OF IPSCS IN CONTROL, AFTER THE ADDITION OF TTX AND [TTX & ACH]. Note the absence of any notable effect of ACh+ in the presence of TTX. ***B.*** Summary comparison of cholinergic effects on IPSCs. IPSC parameters were compared between *ACh*$^+$ normalized to preceding control (drug-free)] and [TTX & *ACh*$^+$] normalized to preceding TTX condition].

To sum up, voltage-clamp experiments suggested that ACh excites GABAergic INs directly, and that the resulting enhancement of inhibition can be profound. Indirect activation of INs via glutamatergic transmission could be excluded since CNQX and AP5 were co-applied in these experiments. Finally, the similarity of IPSC parameter values in control and *ACh*$^-$ conditions (Figure 12B) suggested that

either intrinsic cholinergic neurons in the networks were not active or that the amount of ACh they released was not sufficient to drive GABAergic IN activity appreciably.

3.1.4 ACh release in basal forebrain-neocortex co-culture system

For all previously described experiments, ACh was applied via the bath perfusion system and hence, measured ACh effects were attributed to a constant ACh concentration. One part of the project was devoted to the question if an *in vitro* model could be developed which would provide neocortex with physiologically released ACh instead. As stated before, neocortex *in vivo* receives prominent cholinergic innervations from basal forebrain. To date, no acute slice preparation has been described which preserves these projections. However, in co-cultures of both brain regions, cholinergic axons from basal forebrain grow into cortex (Distler and Robertson, 1993). Therefore, these preparations were tested for their suitability of providing cortex with ACh. Co-cultures were prepared from the 'Mik' mouse mutant, which expressed GFP in cholinergic cells so that these could be specifically targeted (for detailed specification see Methods section). To test the connectivity between the two brain regions, paired recordings were performed. One electrode was placed extracellularly in layer V of neocortex to record spontaneous network activity, while the second electrode was used for current clamp recordings from cholinergic neurons in basal forebrain (n = 8; Figure 14A). Cell parameters of cholinergic neurons were determined via hyper- and depolarizing current injection (median [25^{th} and 75^{th} quantile]): R = 106.58 [71.61 170.21] MΩ; τ = 8.39 [6.99 16.67] ms; spike width at half amplitude = 1.33 [1.19 1.71] ms; approximate maximal firing rate = 24.85 [19.95 27.63] Hz; Em_{rest} = -74.88 [-76.67 -66.74] mV. An example is shown in figure 14B. Electrophysiological properties of cholinergic cells described here greatly differ from those of cholinergic cells in acute slices (Unal et al., 2012). Both cell populations described by Unal et al. (2012) showed a membrane resistance about six times greater, a six to seven times greater time constant τ, and slightly wider spikes. Moreover, cells in acute slices were more depolarized than cholinergic cells in cultures described here, which will be elaborated on in the discussion.

Visual inspection of the firing pattern under control condition revealed that most cholinergic cells were spontaneously active in culture, albeit at low rates (median firing rate [25^{th} and 75^{th} quantile]: 0.66 [0.11 1.79] Hz). In most cases, they depolarized and fired synchronously with neocortex; however, some neurons fired action potentials independent of cortical bursts, and two neurons showed weak hyperpolarization and inhibited firing time-locked to cortical bursts. To investigate if ACh released by neurons in the basal forebrain had any effect on the network activity recorded in neocortex, first neostigmine (1 µM) was washed in, followed by the application of atropine (1 µM) and mecamylamine (3 µM). An example is shown in Figure 14C. Local field potentials and action

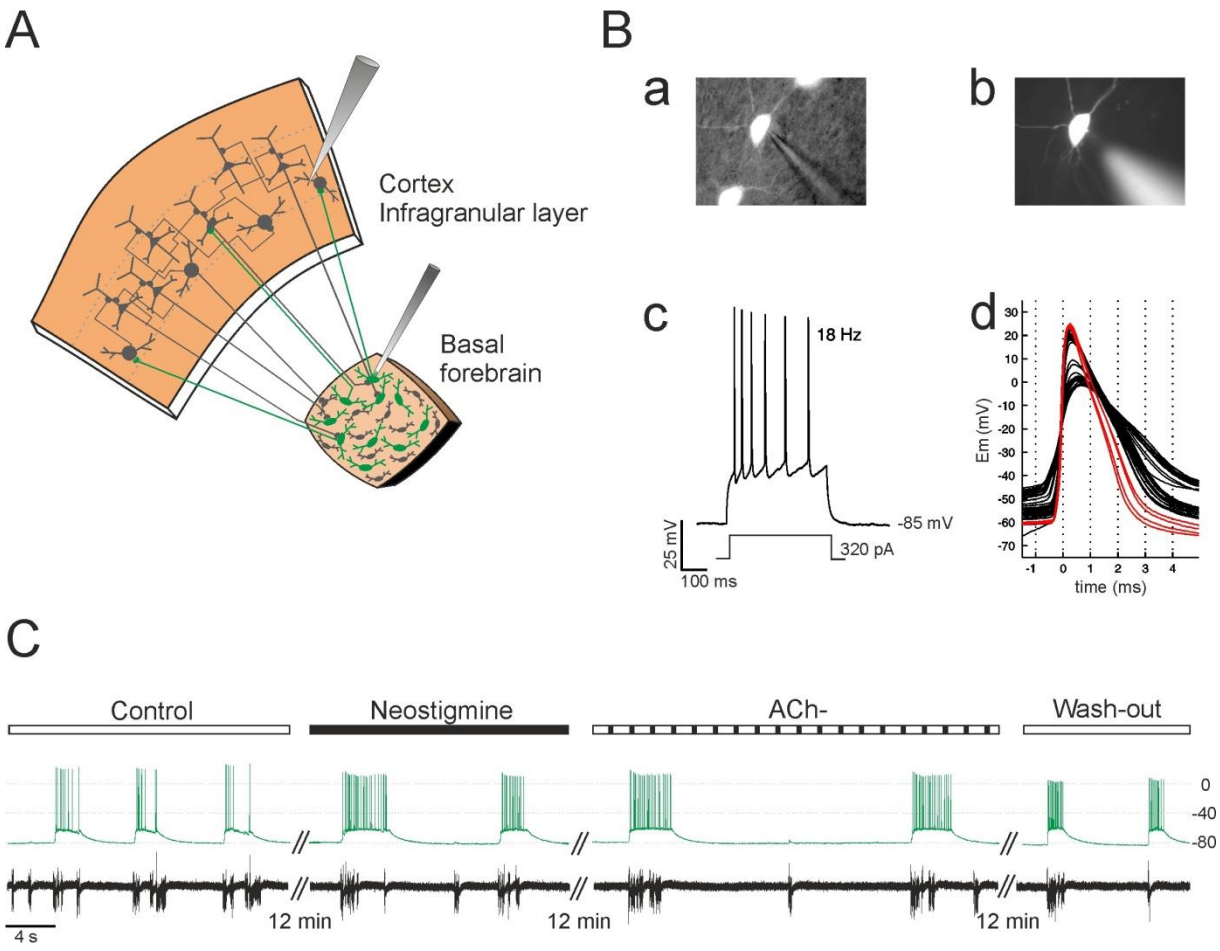

FIGURE 14: PAIRED CURRENT CLAMP AND EXTRACELLULAR RECORDINGS FROM BASAL FOREBRAIN-CORTEX CO-CULTURE MODEL. ***A.*** Schematic illustration of co-culture model between basal forebrain and neocortex. Extracellular recordings were made from infragranular layers in cortex, current clamp recordings were made from basal forebrain cholinergic cells. ***Ba.*** Mixed fluorescent/bright field microscopic image of GFP-expressing, cholinergic neurons in basal forebrain *in vitro* derived from Mik mouse line. ***Bb.*** Fluorescent image of the same neuron as shown in Ba, center, after current clamp recording and filling of the cell with the fluorescent dye Alexa 555. ***Bc.*** Typical firing pattern of a cholinergic neuron upon injection of a current step. Note decreasing AP amplitude. ***Bd.*** Overlay plot of APs of a single cholinergic neuron, obtained from injection of a high-amplitude current step. First four spikes within train are marked in red; APs widened with increasing time. For best comparison with acute slice data, only the narrowest APs were used for characterization of spike width at half-maximal amplitude (red traces). ***C.*** Example of a paired recording from a co-culture of basal forebrain and cortex. Intracellular activity in basal forebrain (green trace) and extracellular activity in neocortex (black trace) were recorded during control (drug-free), neostigmine, *ACh*$^{-}$, and wash-out conditions.

potentials were analyzed and compared between conditions. In some experiments, drug treatment had notable effects, but the effects diverged widely between experiments. On average, no consistent drug effect was found for any LFP- or action potential-based parameter intra- or extracellularly, except for a small effect between control and neostigmine conditions on cortical relative time in burst (supplementary material Table S5). However, the effect was not reversible with cholinergic blockers and was thus not regarded as result of the presence of ACh.

In order to illuminate possible causes of the absence of cholinergic effects, more detailed analyses of firing patterns were undertaken. First, the timing of basal forebrain action potentials relative to cortical bursts was investigated. Figure 15A shows examples of peri-event time histograms (PETHs) of single-neuron action potentials in basal forebrain and multi-unit action potentials in neocortex, aligned to the beginning of extracellular bursts in neocortex as determined on the basis of the LFP. In this example, characterized by vigorous activity levels in both neuronal tissues, action potential firing in cortex preceded firing in basal forebrain by about 15 ms, suggesting that activity in neocortex drove activity in basal forebrain. As basal forebrain firing rates in most cultures were quite low, this spike-based analysis was suitable only for a minority of experiments. Therefore, in a second analysis, values of the average membrane potential of cholinergic neurons were compared for three peri-event time intervals (because only the control condition was used for this analysis, two more cells could be added for a total n = 10): (1) Em_{base} [-300 -200] ms before extracellular burst start; (2) $Em_{pre-burst}$ [-25 0] ms before; (3) $Em_{in-burst}$ [20 100] ms after burst start (figure 15B). If cholinergic neurons were de- or hyperpolarized ahead of neocortical activity, Em_{base} and $Em_{pre-burst}$ should differ. By contrast, if cholinergic neurons were de- or hyperpolarized concomitant with or after neocortex, a difference between the intervals $Em_{pre-burst}$ and $Em_{in-burst}$ should be detectable. Results were plotted in figure 15C. There was no difference between Em_{base} and $Em_{pre-burst}$ but between $Em_{pre-burst}$ and $Em_{in-burst}$ (median [25^{th} & 75^{th} quantile]): Em_{base} = -74.88 [-76.67 -66.74] mV; $Em_{pre-burst}$ = -73.55 [-77.33 -66.11] mV; $Em_{in-burst}$ = -66.85 [-72.16 -64.15] mV; $X^2 = 6.2$, $p = 0.05$; Em_{base} & $Em_{pre-burst}$: $p = 0.43$, auroc [95% CI] = 0.49 [0.36 0.59]; $Em_{pre-burst}$ & $Em_{in-burst}$: $p = 0.03$, auroc [95% CI] = 0.32 [0.14 0.48]). The specific comparisons between groups indicate that Em of basal forebrain cholinergic neurons changes substantially after neocortical bursts begin but not before.

In conclusion, neurons of basal forebrain in the co-culture system showed weak action potential activity predominantly initiated by neocortex. Likely, this dependence on cortical drive, and/or the low level of activity were causal for a lack of a consistent modulation of neocortical activity (although other or additional causes are plausible, see discussion). In view of these results, co-cultures of basal forebrain and cortex were not used as a complement to bath application of ACh in subsequent experiments. However, this model system might be suitable for optogenetic experiments, which would allow specific activation of basal forebrain cholinergic fibers by light stimuli independent of cortical activity.

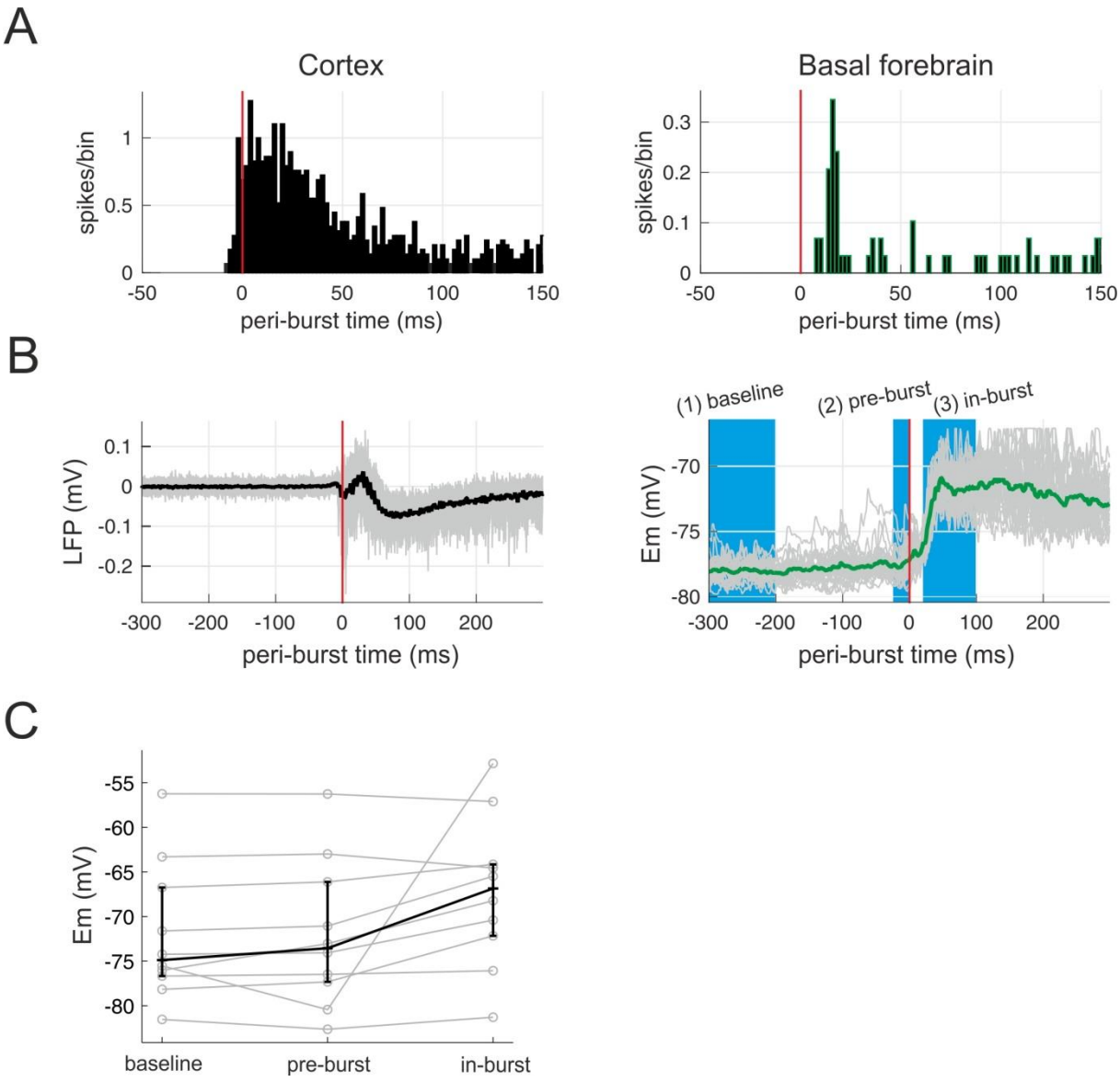

FIGURE 15: ANALYSIS OF ACTIVITY PATTERNS IN COCULTURES OF BASAL FOREBRAIN AND NEOCORTEX. ***A.*** Example of peri-event time histograms (PETHs) of multi-unit action potentials in neocortex (left) and single-neuron action potentials in BF (right), aligned to extracellular burst beginning in neocortex on LFP basis (see *Ab* below). ***B.*** Peri-burst cutouts of cortical LFP (left) and corresponding Em of cholinergic neuron (right) for one experiment. Cutouts were aligned according to cortical burst begin (time zero). Individual cutouts are in grey, averages in black and green, respectively. Blue rectangles in right plot illustrate peri-burst time intervals used for analysis of Em of cholinergic neurons: (1) Em_{base} [-300 -200] ms; (2) $Em_{pre\text{-}burst}$ [-25 0] ms; (3) $Em_{in\text{-}burst}$ [20 100] ms. ***C.*** Summary data for peri-burst Em analysis of cholinergic neurons (grey lines and symbols, individual cells; black, median and 25th and 75th quantile).

3.1.5 The response of X98 Martinotti cells to ACh application

One main aspect of cholinergic modulation may be the influence of ACh on SOM+ GABAergic INs, as illustrated in the introduction. The next part of the thesis project was therefore assigned to study the effects of ACh on Martinotti cells in the 'X98' mouse line (Ma et al., 2006). In these mice, a subset of SOM+ cells identified as Martinotti cells are GFP-labeled and can thus be specifically targeted for electrophysiological recordings. So far, very few studies exist with this mouse line beyond the paper in which they were first introduced, and none of them in neocortex (Ma et al., 2006; Nassar et al., 2015). Whole-cell current clamp recordings were performed from Martinotti cells in layer V of organotypic cultures and acute slices from X98 mice. Results from recordings in culture will be described first. Figure 16A (left) shows a typical SOM+ cell in culture with cell resistance R = 52.60 MΩ, time constant τ = 10.35 ms, approximate maximal firing frequency = 65.15 Hz and spike width at half-maximal amplitude = 0.96 ms. Parameter averages for all cells (n = 10) are listed in table 10. In comparison to electrophysiological characteristics of X98 SOM+ cells in acute slices reported here later on and by (Ma et al., 2006), cells in culture had a ten times smaller cell resistance, six times faster membrane time constant τ, slightly narrower spikes, and were more hyperpolarized.

Parameter	Culture (n = 10)		Acute (n = 12)
Resistance (MΩ)	52.92 [43.40 58.62]	<	299.10 [222.91 390.18]
Time constant τ (ms)	5.69 [4.39 6.06]	<	36.05 [27.49 38.32]
Approximate firing frequency (Hz)	95.59 [81.63 105.26]	>	67.60 [55.58 83.16]
Spike width at half amplitude (ms)	0.68 [0.59 0.73]	>	0.60 [0.52 0.71]
Resting Em (mV)	-76.49 [-80.28 -72.72]	<	-81.64 [-82.69 -79.83]

TABLE 10: CHARACTERISTICS OF X98 SOM+ CELLS FOR CULTURES AND ACUTE SLICES. All values are medians [25^{th} & 75^{th} quantile].

Recordings were obtained from one electrode in current clamp mode attached to a SOM+ IN in infragranular layers and concurrently from a second extracellular electrode placed in the same column in supragranular layers (Figure 16B). As in previous experiments, recordings were made from organotypic cultures during a drug-free control condition, an ACh^+ drug condition, and a wash-out (Figure 16B). The cell resistance was mostly unaffected by ACh application (supplementary material Table S6). In contrast to whole-cell recordings from undefined cortical cell types (section 3.1.2), ACh had a consistent, large effect on Em_{rest} but not on Em during bursts (Em_{burst}) of X98 SOM+ cells. During the ACh^+ condition, Em_{rest} was more depolarized in the majority of cells and synaptic input to the cells increased as measured in fluctuations of Em_{rest}, but there was no uniform effect on Em_{burst} (supplementary material Table S6, Figure 16Ca).

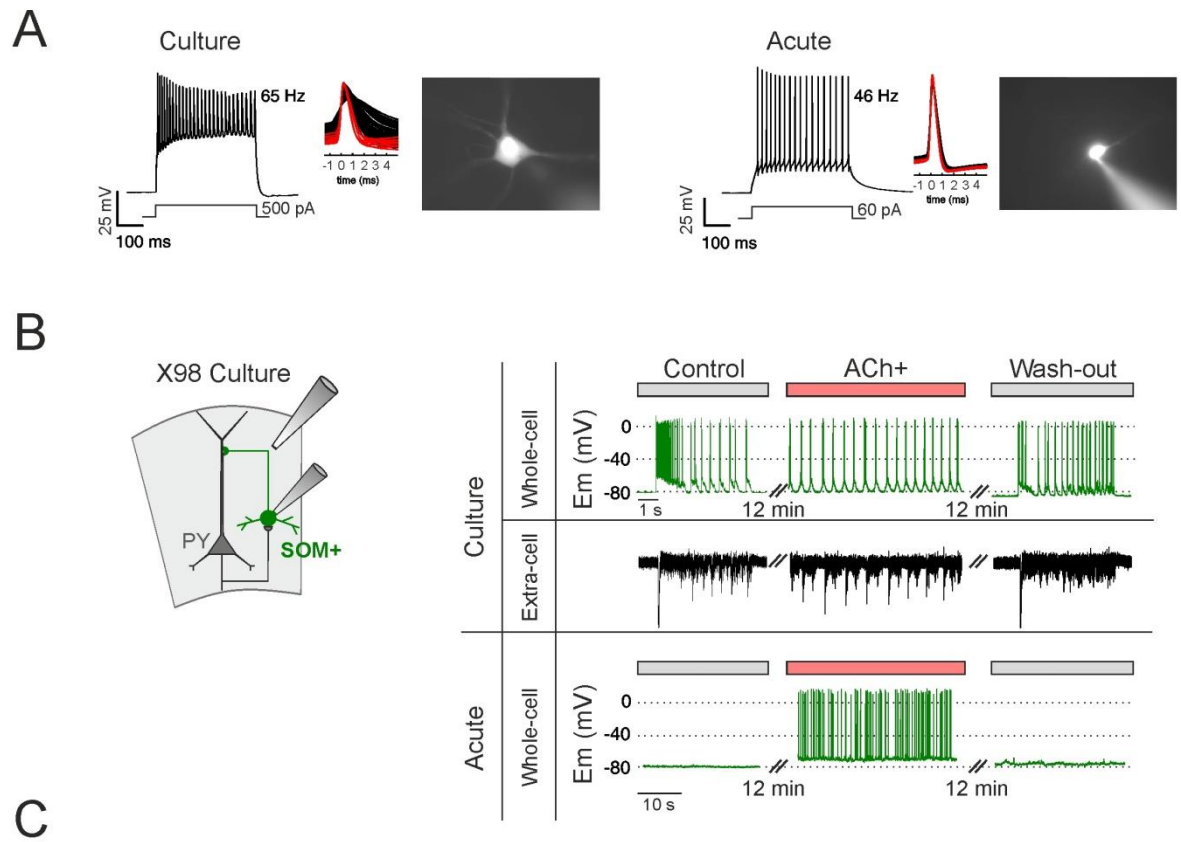
A
Culture
65 Hz
25 mV
500 pA
100 ms
-1 0 1 2 3 4
time (ms)
Acute
46 Hz
25 mV
60 pA
100 ms
-1 0 1 2 3 4
time (ms)
B
X98 Culture
PY
SOM+
Control
ACh+
Wash-out
Culture
Whole-cell
Em (mV)
0
-40
-80
1 s
12 min
12 min
Extra-cell
Acute
Whole-cell
Em (mV)
0
-40
-80
10 s
12 min
12 min
C
Culture
a
Em (mV)
-50
-60
-70
-80
Em fluct (mV)
10
5
0
Control
ACh+
Wash-out
b
AP rate (Hz)
10
5
0
Fraction APs in silent periods
0.5
0.4
0.3
0.2
0.1
0
Control
ACh+
Wash-out
Acute
c
Em (mV)
-65
-70
-75
-80
-85
Em fluct (mV)
6
5
4
3
2
1
Control
ACh+
Wash-out
d
AP rate (Hz)
2.5
2
1.5
1
0.5
0
Control
ACh+
Wash-out

FIGURE 16: CURRENT CLAMP RECORDINGS FROM GFP-EXPRESSING, PUTATIVE MARTINOTTI CELLS IN THE PRESENCE OF ACH (X98 MOUSE STRAIN). ***A left.*** Firing pattern of a typical Martinotti cell in culture induced by injection of a current step. AP cutouts are depicted in the inset (first APs in train marked in red). Note decrease of amplitude concomitant with an increase of AP width. The neuron recorded from was filled with the fluorescent dye Alexa 555 and is depicted in the microscopic image. ***A right.*** Firing pattern, AP cutouts and fluorescent microscopic image of a typical Martinotti cell in an acute slice. ***B left.*** Schematic illustration of paired extra- and intracellular recordings in neocortical slice cultures derived from X98 mice. Current clamp recordings were performed from Martinotti cells in infragranular layers; an extracellular recording electrode was placed in the supragranular layers of the same column. In acute slices, only intracellular recordings were performed (not illustrated) ***B right.*** Example raw signals from cultures and acute slices during control, ACh+ and washout conditions. ***C.*** Comparison of modulatory effects of ACh on Martinotti cells in cultures and acute slices. ***Ca & c.*** Summary data for Em (main plots) and fluctuation of the Em ('noise', insets). Grey, individual cells; black, median and 25^{th} and 75^{th} quantiles (due to the low number of cells recorded in acute slices no averages are given in these figures). ***Cb & d.*** Summary data for AP rates (main plots). Inset in Cb depicts the fraction of AP in occurring outside bursts in culture, demonstrating activation of Martinotti cells by ACh.

To test cell excitability, a sinusoidal ramp current was injected into the cell and thereby stimulated action potentials were counted (Figure 17A). Under control, cells reached a median [25^{th} & 75^{th} quantile] of 4.00 [3.19 5.09] spikes, while the spike count almost doubled under the ACh^+ condition (7.50 [6.08 8.58]) (supplementary material Table S6, Figure 17B), likely due to the ACh-induced depolarization of the resting membrane potential. Thus, SOM+ neurons were more excitable in the presence of ACh^+.

Although cell excitability increased, median action potential firing rates did not change with ACh application (median [25^{th} & 75^{th} quantile]): Ctrl = 2.57 [0.79 6.51]; ACh^+ = 2.88 [1.24 3.52]; wash = 1.34 [0.52 2.77]; X^2 = 2.21, p = 0.33) (Figure 16Cb, supplementary material Table S6). However, firing patterns were affected by the ACh^+ condition (Figure 16Cb inset). During the control condition, all cells fired action potentials within bursts, whereas during the ACh^+ condition two thirds of them also fired during silent periods (one third remained unaffected). The dichotomy of cell activity during silent periods evoked by ACh was expressed by significantly different variances between control, ACh^+ and wash-out (median [25^{th} & 75^{th} quantile]): Ctrl = 0.00 [0.00 0.02]; ACh^+ = 0.14 [0.01 0.40]; wash = 0.00 [0.00 0.02]; Brown-Forsythe test F (2, 24) = 15.55, p = 0.00005; auroc [95% CI] Ctrl-ACh^+ = 0.15 [0.00 0.29] (Figure 16Cb inset). In other words, ACh caused SOM+ INs to fire more independently of cortical bursts.

For the examination of the relation between extracellular multiunit action potential activity and the firing of SOM+ cells with and without ACh, a cross-correlation analysis was employed. Results revealed that spike-firing between the two signals was well correlated during the control condition, but decreased significantly during the ACh^+ condition – an effect that was partially reversible during wash-out (supplementary material Table S6). This finding indicates that SOM+ cells fired less in synchrony with other cortical cells in the presence of ACh.

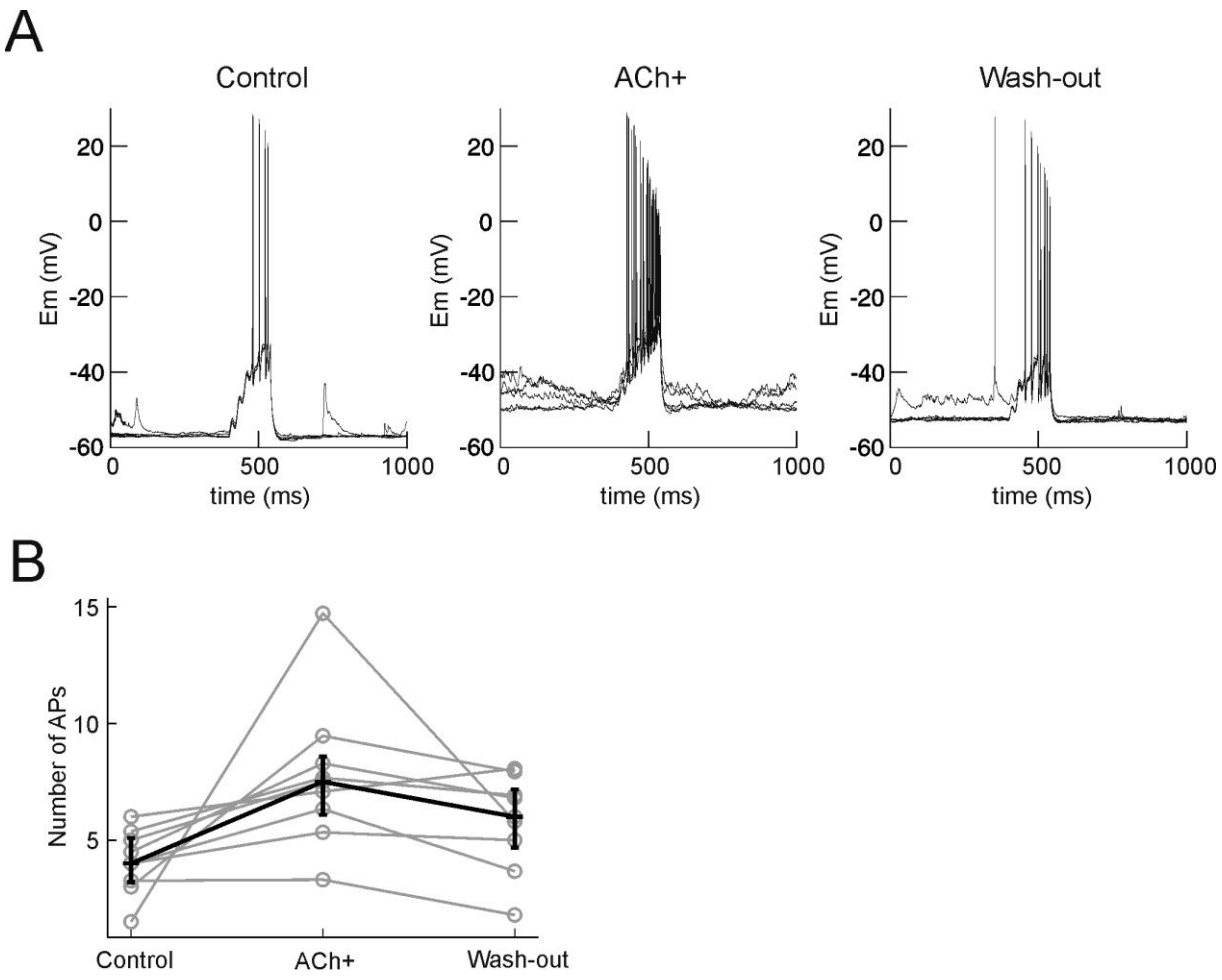

FIGURE 17: ACH-INDUCED CHANGE IN EXCITABILITY OF MARTINOTTI CELLS IN CULTURE. ***A.*** Excerpts of current clamp recordings during injection of a sinusoidal ramp current in control, ACh+ and wash conditions. Note the stronger response of the neuron to current injection during ACh+. For analysis, the number of AP induced during current injection was counted. ***B.*** Summary data for AP count during current injection (grey, individual cells; black, median and 25th and 75th quantiles).

To validate findings from organotypic cultures, ACh was also applied to acute slices of X98 mice. An overview of all cell parameters is presented in table 10 (n = 12). Unlike in organotypic cultures, in acute slices SOM+ cells were not spontaneously active under the control condition. Overall, electrophysiological characteristics were more comparable to values reported by Ma et al. (2006). For *ACh*$^{+}$ effect analysis, Em_{rest} was analyzed from five cells (the other seven cells could not be held for the ACh condition). During the *ACh*$^{+}$ condition, Em_{rest} was more depolarized, cells likely received more synaptic input, which was quantified by the increased fluctuation of Em (Figure 16Cc), and the rate of spontaneous action potentials rose from zero to about 2 Hz (Figure 16Cd). Due to the small sample size, no statistical analysis was applied to this data set. Nonetheless, ACh had a clearly excitatory (depolarizing) effect on all four cells, which agrees with previous reports (Kawaguchi, 1997).

3.2 The action of $GABA_AR$ modulators in the presence and absence of ACh

3.2.1 Effect of $GABA_AR$ modulators on extracellularly recorded network activity under different cholinergic conditions

The main objective of this thesis project was to elucidate if ACh alters GABAergic inhibition in neocortex. Central to this endeavor was an experimental modulation of the cholinergic status as described before in conjunction with a subunit-specific modulation of GABAergic inhibition. Extracellular experiments were performed in organotypic cultures of somatosensory neocortex with one electrode placed in the supragranular layers, while the second electrode was placed in the infragranular layers of the same column. Within each experiment, spontaneous network activity was recorded in four different drug conditions. An initial drug-free condition was followed by either the ACh^+ or the ACh^- condition, which served as cholinergic baseline condition. Next, with the cholinergic condition maintained, a $GABA_AR$ modulator was applied, followed by a wash-out of all drugs (Table 11). The $GABA_AR$ modulators used were zolpidem (in two concentrations), diazepam, diazepam in cultures derived from α_1 knock-in mice, and L-655,708. Different $GABA_AR$ modulators were chosen to modulate specific combinations of $GABA_AR$ subunits (see Methods section 2.3.4). Briefly, zolpidem (0.2 µM) was used to mainly modulate $GABA_AR$ containing the $\alpha_{1\,(2,3)}$ subunit, zolpidem (1.0 µM) was used for $\alpha_{1,\,2,\,3}$, diazepam (1.0 µM) for $\alpha_{1,\,2,\,3,\,5}$, and diazepam (1.0 µM) in the α_1-knock-in genotype for $\alpha_{2\,,3,\,5}$. L-655,708 (5 µM), the only negative allosteric modulator used, was specific for $GABA_AR$ containing the α_5 subunit. Thus, there were five different means of $GABA_AR$ modulation in two different cholinergic conditions, resulting in ten unpaired experimental series. In the analyses described below, all parameters computed for the combined cholinergic/GABAergic condition were normalized to the preceding ACh^+ or ACh^- condition (Table 11). These normalized parameter values were statistically compared between the ACh^+ and ACh^- series in order to assess the dependence of each type of $GABA_AR$ modulation on the cholinergic status. As the effects of the ACh^+ and ACh^- conditions per se have been investigated in detail in previous experiments, it was not of interest to evaluate them again in these experimental series.

Condition	**Drug application design**			
I **ACh+**	Control (drug-free)	ACh^+	**ACh^+ &** **$GABA_AR$ modulator**	Wash-out (drug-free)
II **ACh-**	Control (drug-free)	ACh^-	**ACh^- &** **$GABA_AR$ modulator**	Wash-out (drug-free)

TABLE 11: DRUG-APPLICATION DESIGN. Conditions in bold were statistically compared. Bold conditions were normalized to respective previous conditions.

Three analysis approaches were pursued: 1) classical action potential and burst analysis as with previously analyzed extracellular data sets (chapter 3.2.1.1), 2) spectral analysis (chapter 3.2.1.2), and 3) cross-correlation analysis between LFP signals filtered at specific frequency bands from the supra- and infragranular layers and cross-correlation analysis between the instantaneous firing rate (ifr) based on action potentials and LFPs filtered at specific frequency bands, respectively (3.2.1.3).

3.2.1.1 Cholinergic status differentially changed effects of $GABA_AR$ modulators on action potential- and burst parameters

The first approach to analyze the data was to quantify the effects of the different substance combinations on action potential and burst parameters. All results are listed in table S7 of the supplementary material. Differences between the ACh^+ and ACh^- condition in combination with $GABA_AR$ modulators surfaced in very specific parameters and layers. Affected parameters were burst rate, burst length and time spent in burst. No differences between the ACh^+ and ACh^- condition in combination with $GABA_AR$ modulators were found on the action potential rate, the fraction of active bins or the burst amplitude.

In figure 18A, a raw data example is given for ACh^+ and diazepam (Figure 18Aa) and ACh^- and diazepam (Figure 18Ab). As can been seen in this example, the application of ACh^+ had notable effects on the bursting pattern (Figure 18Aa second trace), while the addition of diazepam did not further modify the effect (Figure 18Aa third trace). On the other hand, diazepam substantially shortened burst phases and increased the burst rate when it was applied under the ACh^- condition (Figure 18Ab third trace). The results for diazepam with regard to burst rate, burst length, and relative time in burst were summarized for the infragranular layers as box plots in figure 18B. As depicted in the raw data sample, diazepam had different effects in ACh^+ than in ACh^-. Overall, diazepam evoked a change in the burst pattern within the ACh^- condition (shorter bursts and higher burst rate), but had no impact on the absolute amount of network activity since the total time spent in burst remained stable.

In Figure 18C, auroc values for all parameters, both layers and all $GABA_AR$ modulators were summarized. For diazepam ($\alpha_{1, 2, 3, 5}$), the effects on burst rate, burst length and relative time in burst were similar for both layers. Zolpidem (0.2 µM and 1.0 µM), on the other hand, evoked small to medium effects between ACh^+ and ACh^- in the supragranular layers, while large differences in the infragranular layer were found (Figure 18C). The most affected parameter was the relative time in burst. For zolpidem (1 µM) ($\alpha_{1, 2, 3}$) this effect was the result of a combination of decreases in burst rate and burst length under the ACh^+ condition, but the single effects were not large enough to bring about a significant difference on their own. For zolpidem (0.2 µM) ($\alpha_{1\,(2, 3)}$), additionally to the relative time in burst, the burst rate was dramatically lower in the ACh^+ than ACh^- condition (Figure 18C).

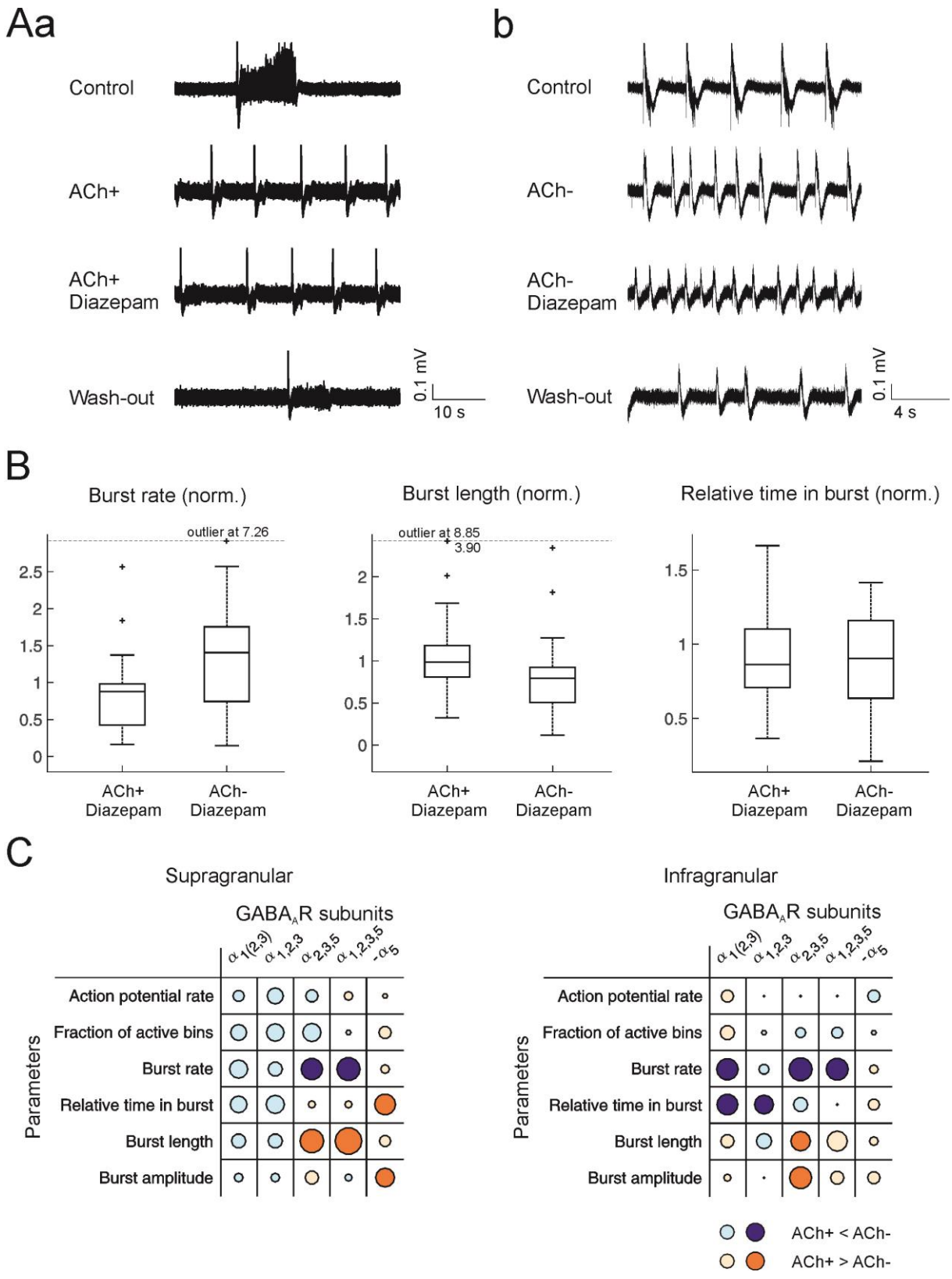

FIGURE 18: ANALYSIS OF AP AND LFP PARAMETERS FROM EXTRACELLULARLY RECORDED DATA. *A.* Raw data example of extracellular activity in control (drug-free), *ACh$^+$ (a)* or *ACh$^-$ (b)*, [*ACh$^+$ (a)* or *ACh$^-$ (b)* & Diazepam], and wash-out. ***B.*** Exemplary summary data for three of the six parameters describing alteration of neuronal activity by GABA$_A$R modulators in contrasting cholinergic conditions. Here, the effect of diazepam in supragranular layers is depicted. Data for [*ACh$^+$* & GABA$_A$R modulator] and [*ACh$^-$* & GABA$_A$R modulator] conditions were normalized to the preceding *ACh$^+$* or *ACh$^-$* conditions, respectively. Pairs of data sets thus normalized were compared statistically (the results are depicted in C). ***C.*** Summary of comparisons between

ACh^{+} and *ACh*$^{-}$ conditions for all tested $GABA_AR$ modulators and both layers. Rows list the six analysis parameters, columns list the primary α-subunit(s) of the $GABA_AR$ modulated by the chosen drugs: α_1 – zolpidem 0.2 µM; $\alpha_{1,2,3}$ – zolpidem 1 µM; $\alpha_{2,3,5}$ – diazepam in α_1-knock-in; $\alpha_{1,2,3,5}$ – diazepam in WT; -α_5 – L-655,708. The colored circles represent the auroc effect size of the comparison *ACh*$^{+}$ versus *ACh*$^{-}$. Areas of the circles are proportional to the effect size (=distance of the auroc value from the null value of 0.5). The superiority of the *ACh*$^{+}$ condition was always tested over the *ACh*$^{-}$ condition. Thus, **blue circles** signify that values in *ACh*$^{+}$ fall mostly below those of *ACh*$^{-}$ (auroc < 0.5), dark blue indicates significance (α) at the 0.05 level. **Orange circles** signify that values in *ACh*$^{+}$ are mostly above those of *ACh*$^{-}$(auroc > 0.5), dark orange indicates significance at 0.05 level.

L-655,708, a negative allosteric modulator of α_5-containing $GABA_AR$ (-α_5), was clearly more effective in the supra- than in the infragranular layer. Under the *ACh*$^{+}$ condition, the substance caused higher network activity (more time spent in burst) and higher burst amplitudes in comparison to the *ACh*$^{-}$ condition in the supragranular layer only.

3.2.1.2 Spectral power differed between cholinergic conditions with modulation of $\alpha_{1,2,3}$ and –α_5 subunit-containing $GABA_AR$s

Beyond studying the combined effects of ACh and $GABA_AR$ modulators on firing activity and bursting pattern, changes of spectral power were investigated. ACh is known to reduce the power in low frequency bands (1-10 Hz) (Chen et al., 2015; Metherate et al., 1992). Since EEG studies have revealed effects of diazepam and zolpidem on spectral power (Arbon et al., 2015; Brunner et al., 1991; Scheffzük et al., 2013), it was of interest to investigate if cholinergic modulation would interact with $GABA_AR$ modulator-induced changes of spectral power. Moreover, action potential and LFP parameter analyses described previously were limited to recordings with clearly identifiable bursts and silent periods. Cultures with oscillating or highly 'desynchronized' activity could not be properly analyzed. To include such data in the analysis, spectral power in the delta [2 5] Hz, theta [6 12] Hz, beta [15 30] Hz, gamma low [30 50] Hz and gamma high [50 80] Hz frequency bands were analyzed. For each frequency band, the median spectral power across experiments was calculated, normalized to the preceding ACh condition and compared for all $GABA_AR$ modulators in both ACh conditions. An example is provided for zolpidem (1 µM) and L-655,708 (Figure 19). In figure 19A (right panel) it can be seen that zolpidem decreased the delta power strongly following both ACh conditions. However, the effect was stronger in the presence of *ACh*$^{+}$ (median [25th & 75th quantile]): *ACh*$^{+}$ = 0.16 [0.09 0.30]; *ACh*$^{-}$ = 0.33 [0.23 0.46]; auroc 0.34 [0.21 0.47], p = 0.02. As previously reported for zolpidem, when action potential and burst parameters were analyzed (section 3.2.1.1), differences between cholinergic conditions were restricted to infragranular layers (Figure 19A).

L-655,708 differed between both cholinergic conditions in the theta frequency band in the supragranular layers, where the normalized power was higher under the *ACh*$^{+}$ than the *ACh*$^{-}$ condition (median [25th & 75th quantile]): *ACh*$^{+}$ = 1.31 [0.81 2.34]; *ACh*$^{-}$ = 1.05 [0.63 1.48]; auroc 0.64 [0.53 0.75], p = 0.02†; Figure 19B).

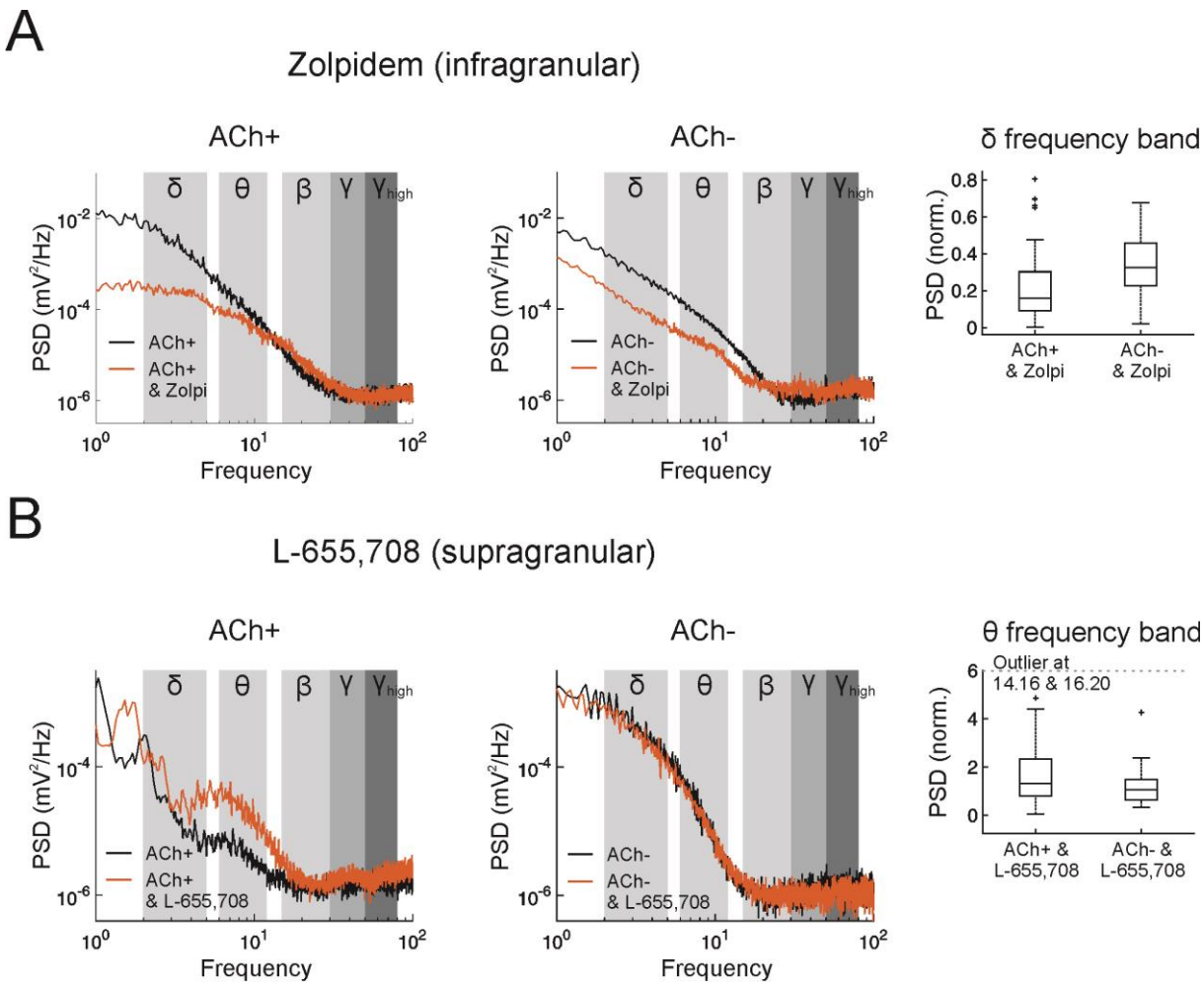

FIGURE 19: POWER SPECTRAL ANALYSIS OF LFP SIGNALS IN CORTICAL CULTURES WITH CHOLINERGIC AND GABAERGIC MODULATION. *A.* Left, exemplary power spectral density (PSD) plots of data recorded from the infragranular layer. Black trace shows the PSD in the *ACh*$^+$ condition; orange trace after additional application of zolpidem (1 µM). Grey windows depict five different frequency bands in which the PSD was integrated and compared between drug conditions: δ [2 – 5] Hz, θ [6 – 12] Hz, β [15 – 30] Hz, γ [30 – 50] Hz, and high γ [50 – 80] Hz. Center, identical depiction of a data example with the *ACh*$^-$ condition (black) preceding *ACh*$^-$ & zolpidem (1 µM). Right, summary from all experiments of the effects of zolpidem (1 µM) on δ PSD in infragranular layers in the *ACh*$^+$ condition (left data set) and in the *ACh*$^-$ condition (right data set). Data were normalized to the preceding ACh condition. *B.* PSD plots of LFP data recorded in the presence of L-655,708 (left and center) and summary data (right). Data were recorded from supragranular layers. Same conventions as in A apply.

It also evoked differences in the gamma and high gamma range in the infragranular layers, where the power was smaller under the *ACh*$^+$ than the *ACh*$^-$ condition (gamma: median [25th & 75th quantile]): *ACh*$^+$ = 0.92 [0.80 1.09]; *ACh*$^-$ = 1.04 [0.94 1.16]; auroc 0.37 [0.25 0.49], p = 0.04; high gamma: median [25th & 75th quantile]): *ACh*$^+$ = 0.94 [0.77 1.05]; *ACh*$^-$ = 1.05 [0.93 1.15]; auroc 0.35 [0.24 0.46], p = 0.01).

Thus, with regard to spectral changes of spontaneous network activity, effects of $GABA_A$Rs modulation containing the $\alpha_{1,2,3}$ subunit in combination with ACh application were delta-frequency specific, while the antagonism of $GABA_A$Rs with the α_5 subunit evoked differences between the *ACh*$^+$

and *ACh*$^-$ condition over a broader frequency spectrum. The other $GABA_AR$ modulators did not influence spectral power in a way that depended on the cholinergic status.

3.2.1.3 Interlaminar LFP- and intralaminar LFP-ifr correlations especially differed between cholinergic conditions during modulation of $\alpha_{1,2,3}$ and -α_5 subunit-containing $GABA_ARs$

One described characteristic of ACh is its decorrelating effect (Goard and Dan, 2009). Thus, the question arose whether the correlation of LFP signals between supra- and infragranular layers were differentially affected by the cholinergic status in combination with different $GABA_AR$ modulators. In figure 20A, a raw data sample is given for *ACh*$^+$ and zolpidem (1.0 µM). At first sight, the raw signal from the supragranular layer seemed to change in a similar manner as the signal from the infragranular layers across substance conditions in terms of burst amplitude and burst length. However, how individual frequency bands were affected at the two different recording sites by the drug conditions was not clear. Thus, raw data traces from both recording sites were split up via digital filtering into signal components in the five frequency bands stated above (see example of theta signals in Figure 20Ab). Signals thus filtered from infra- and supragranular layers in the *ACh*$^+$ or *ACh*$^-$ condition and the subsequent $GABA_AR$ modulator condition were cross-correlated with each other (Figure 20Ac). The cross-correlation peak amplitude values of the $GABA_AR$ conditions were normalized to the ACh conditions (as for previous experiments, Figure 20B) and compared to each other with a Wilcoxon ranksum test and auroc (supplementary material Table S8, Figure 20C).

For zolpidem (1.0 µM), the theta (Figure 20B, C) and the high gamma frequency bands (Figure 20C) were each stronger decorrelated between layers in the *ACh*$^+$ than in the *ACh*$^-$ condition. Zolpidem (0.2 µM) showed stronger decorrelating effects under *ACh*$^+$ in the delta and theta frequency bands (supplementary material Table S8). For diazepam in the α_1 knock-in mutant, the high gamma frequency range was more strongly affected by *ACh*$^+$ than by *ACh*$^-$.

Cross-correlations for L-655,708 between the cholinergic conditions also differed. However, results indicated that this substance caused higher correlations in the delta, theta and beta frequency range under the *ACh*$^+$ than the *ACh*$^-$ condition. Thus, the analysis demonstrated that especially zolpidem induced differences between the cholinergic conditions by decreasing synchrony in interlaminar communication more in combination with *ACh*$^+$ than with *ACh*$^-$ while L-655,708 increased synchrony in the *ACh*$^+$ condition compared to *ACh*$^-$.

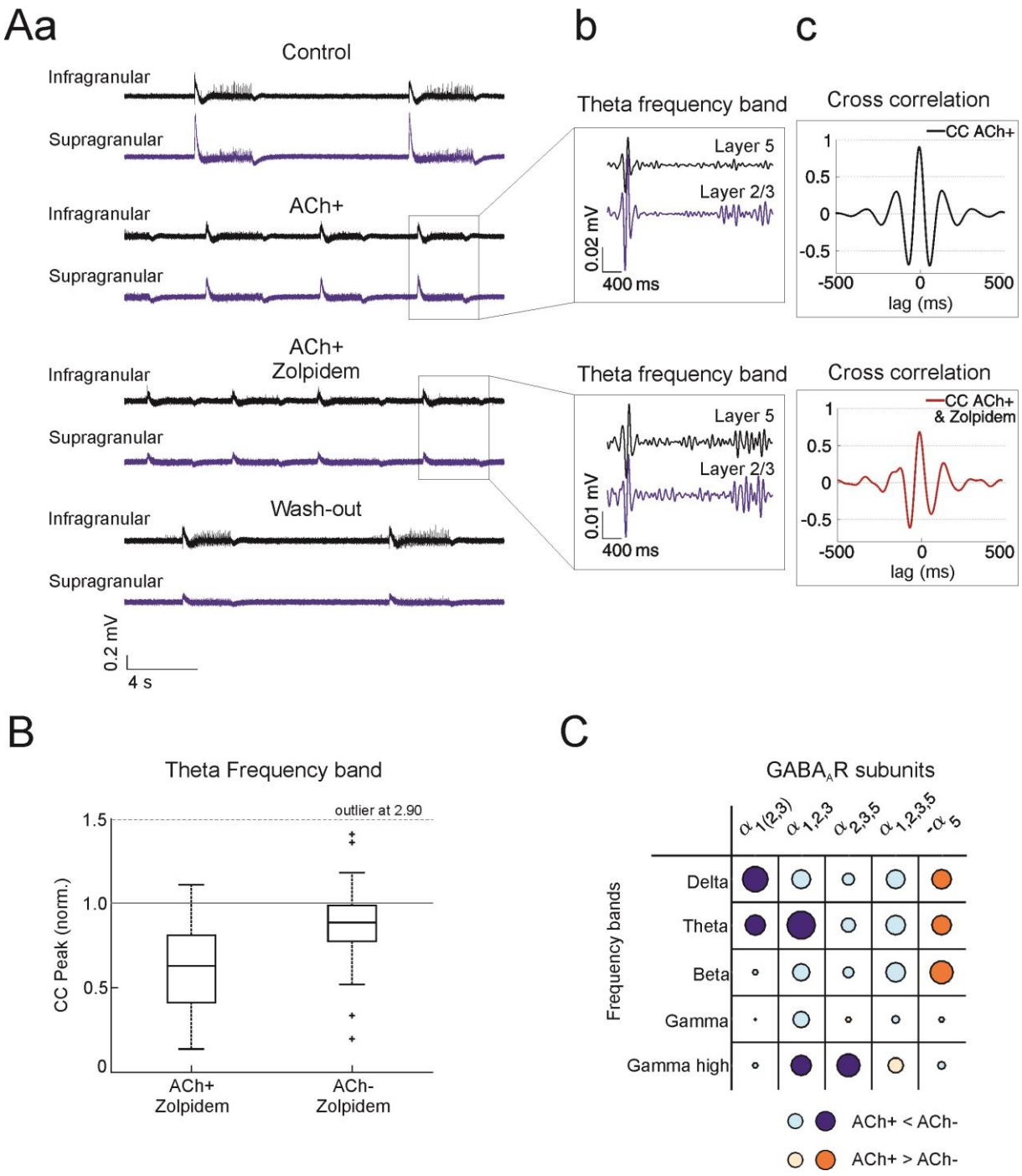

FIGURE 20: CROSS-CORRELATION OF LFP SIGNALS BETWEEN CORTICAL LAYERS AND ITS MODULATION BY THE ALPHA$_1$ SUBUNIT-PREFERRING GABA$_A$R MODULATOR ZOLPIDEM. ***Aa.*** Example of an extracellular recording from infra- and supragranular layers in control (drug-free), *ACh*$^+$, [*ACh*$^+$ & zolpidem (1 µM)], and wash-out. ***Ab.*** Excerpts of the data traces shown in a, bandpass filtered in the theta frequency band (6-12 Hz). ***Ac.*** Cross-correlation between infra- and supragranular layers of theta bandpass-filtered data traces. Note reduced peak correlation in [*ACh*$^+$ & zolpidem (1 µM)] condition. ***B.*** Summary data from all experiments of the effects of zolpidem (1 µM) on the cross-correlation between theta signals from supra-and infragranular layers. The peak cross-correlation values from the [ACh & GABA$_A$R] conditions were normalized to those of the preceding ACh conditions. Then, for each GABA$_A$R modulator, the difference between the *ACh*$^+$ and *ACh*$^-$ condition was analyzed. The example shows that layers did not correlate as well in the [*ACh*$^+$ & zopidem] condition compared to the [*ACh*$^-$ & zolpidem] condition. ***C.*** Summary of cross correlation analysis for all GABA$_A$R modulators (columns) and frequency bands (rows). See Figure 17 for detailed explanation of circle size and color. Light blue: auroc < 0.5; dark blue: auroc < 0.5 and significant at 0.05 level. Light orange: auroc > 0.5; dark orange: auroc > 0.5 and significant at 0.05 level.

Next, intra-electrode coupling of APs to LFP signals in the different frequency bands was studied. To illustrate this analysis, examples from the L-655,708 experimental series were chosen (Figure 21). A raw data example is given in Figure 21Aa and Ba showing the effects of L-655,708 in combination with ACh^+ or ACh^-, respectively. In Figure 21Ab and Bb, the raw signals were filtered according to the five frequency bands stated above and additionally with a lowpass filter with a cutoff of 200 Hz ('wide band'), which was chosen to represent the entire LFP frequency spectrum. Additionally, action potentials as detected by the threshold algorithm described before were converted into a continuous signal termed 'instantaneous firing rate', abbreviated ifr (see Methods, Figure 21Ab & Bb third trace from top). Finally, the ifr was correlated with LFP signals in the delta, theta, beta, gamma, high gamma and wide band range, and the envelope of the correlation was computed in order to obtain a measure of the strength of spike-LFP coupling independent of phase. The normalized peak amplitude of the cross correlation envelope was compared for different $GABA_AR$ modulators between the ACh^+ and ACh^- condition (Figure 21Ac and 21Bc).

Again, the strongest decorrelating effect was found with zolpidem (1.0 µM) and ACh^+ especially in the infragranular layers across all frequency bands (Figure 22B). In the supragranular layers, the correlation was especially decreased between the ifr and signals in the beta and high gamma range (Figure 22A). Equivalent to the attenuation of interlaminar signal correlations in the delta range, zolpidem (0.2 µM) in combination with ACh^+ had a decorrelating effect between ifr and the signal in the delta and wide band frequency ranges in both layers (Figure 22A & B). Additionally, diazepam in the α_1 knock-in in combination with ACh^+ had a decorrelating effect in the infragranular layer (delta frequency range). Evoking a similar effect with zolpidem (0.2 µM) and diazepam in the α_1 knock-in is rather counterintuitive. While results found with zolpidem (0.2 µM) were likely to be α_1-dependent (since zolpidem is supposed to highly prefer $GABA_AR$ containing the α_1 subunit when applied in low concentrations), they must be independent of $GABA_AR$ containing the α_1 subunit for diazepam in the α_1 knock-in as this subunit could not be modulated in the mutant. It is speculated that the same decorrelating effect was reached via different mechanistic routes, which will be elaborated on further in the discussion. Diazepam applied in wild-type had a tendency to decrease the correlation in the presence of ACh^+ especially in the infragranular layers in the wide band frequency range. As for interlaminar correlation analysis, L-655,708 acted contrarily to the other $GABA_AR$ modulators and improved the correlation of ifr in the theta and beta frequency band in the presence of ACh^+ in comparison to ACh^- (Figure 22B, supplementary material Table S9).

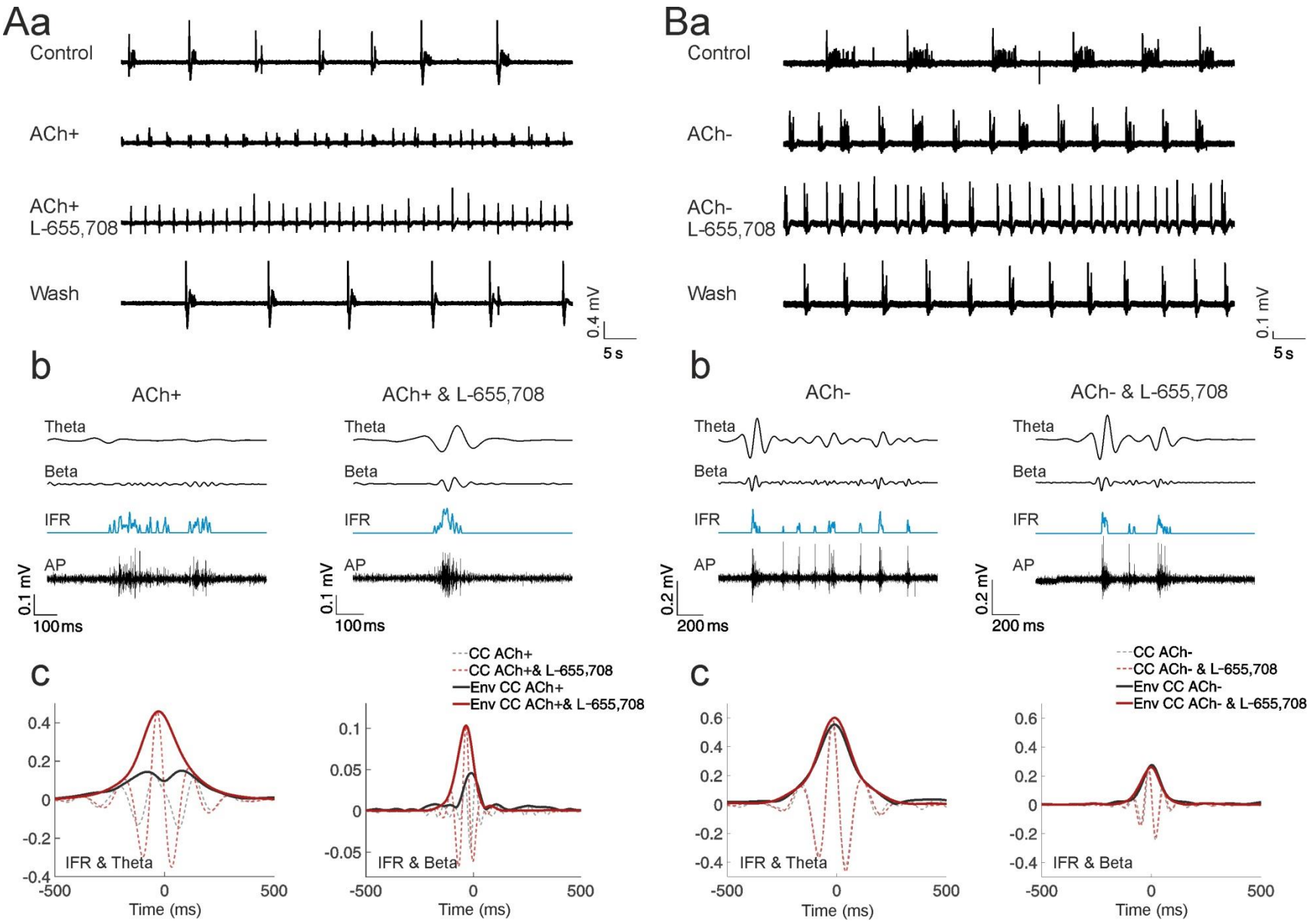
Aa
Control
ACh+
ACh+
L-655,708
Wash
0.4 mV
5 s
Ba
Control
ACh-
ACh-
L-655,708
Wash
0.1 mV
5 s
b
ACh+
ACh+ & L-655,708
Theta
Beta
IFR
AP
0.1 mV
100 ms
b
ACh-
ACh- & L-655,708
0.2 mV
200 ms
c
CC ACh+
CC ACh+& L-655,708
Env CC ACh+
Env CC ACh+& L-655,708
IFR & Theta
IFR & Beta
Time (ms)
CC ACh-
CC ACh- & L-655,708
Env CC ACh-
Env CC ACh- & L-655,708

FIGURE 21: INTRA-ELECTRODE CROSS-CORRELATION OF INSTANTANEOUS FIRING RATE (IFR) WITH LFP AND ITS ALTERATION BY AN ALPHA$_5$ SUBUNIT-SPECIFIC GABA$_A$R MODULATOR. ***Aa and Ba.*** Raw data examples of extracellular activity in the presence of ACh *(A)* or cholinergic antagonists *(B)* and L-655,708. ***Ab.*** Excerpts of data shown in ***Aa*** from one channel, filtered in different frequency bands as indicated (top two traces), and ifr (blue trace), derived from AP activity on the same channel (bottom trace). Note that in the presence of L-655,708, especially signals in the θ and β frequency range become more prominent again in comparison to *ACh*$^+$. ***Ac.*** Cross-correlation between ifr and θ signals (left) and ifr and β signals (right) for *ACh*$^+$ alone (black traces) and [*ACh*$^+$ & L-655,708] (red traces). Thin dotted curves show the cross correlations; continuous lines are the envelopes of the correlations from which the peak values were extracted for comparison between conditions. ***Bb.*** Excerpts of exemplary raw data shown in ***Ba***. ***Bc.*** Cross-correlations in the presence of cholinergic antagonists and L-655,708. Same conventions as in ***Ac*** apply.

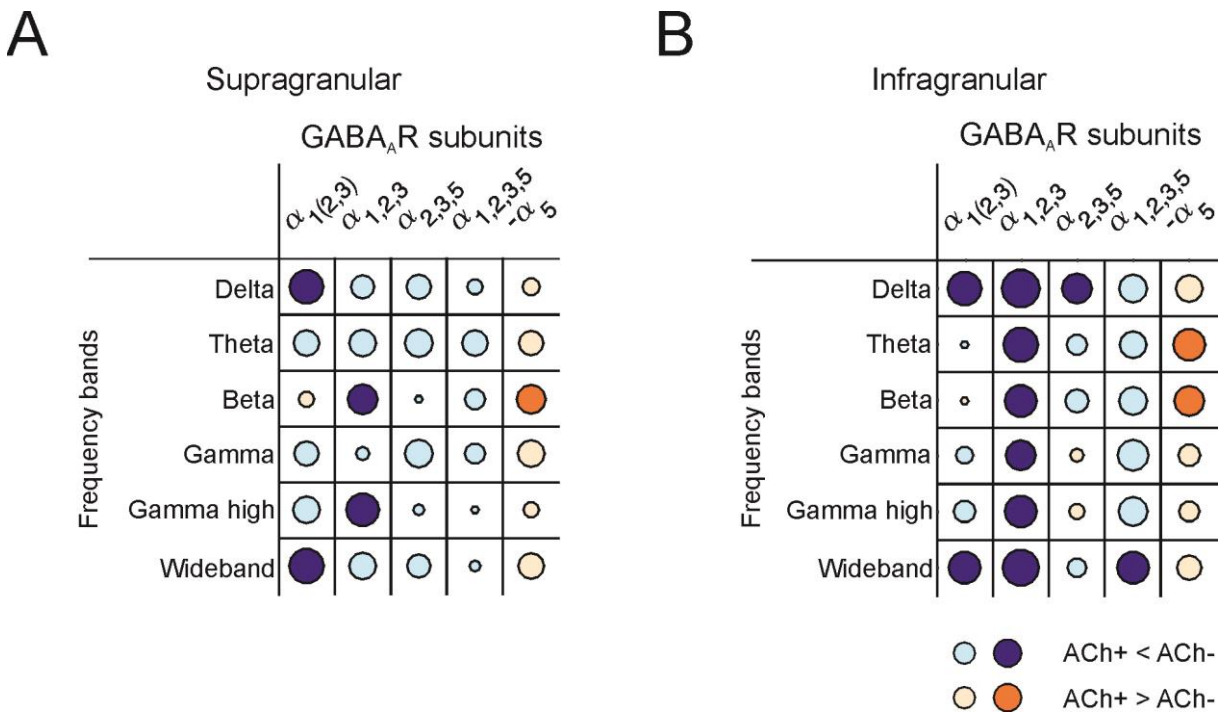

FIGURE 22. SUMMARY OF INTRA-ELECTRODE CROSS-CORRELATION ANALYSES (IFR WITH LFP IN DIFFERENT FREQUENCY BANDS). The plots show all comparisons between *ACh*$^+$ and *ACh*$^-$ conditions for all tested GABA$_A$R modulators. Results for supra- and infragranular layers are shown left and right, respectively. Refer to figure 17 for detailed description of GABA$_A$R subunits and auroc effect sizes.

In summary, cross-correlation analyses between both layers and ifr and LFP revealed the largest difference by far between the *ACh*$^+$ and *ACh*$^-$ conditions when zolpidem (1.0 µM) was applied. Zolpidem caused a strong decorrelation in combination with *ACh*$^+$ supposedly by enhancing currents through GABA$_A$R containing the $\alpha_{1,2,3}$ subunits. Contrastingly, but consistent with its action as a negative allosteric modulator, L-655,708 increased correlation in the presence of *ACh*$^+$ more than in the presence of *ACh*$^-$. Thus, the effects of positive and negative GABAergic modulators on spike-LFP coupling again demonstrated the strong recruitment of GABAergic inhibition during cholinergic stimulation.

3.2.2 Effects of $GABA_AR$ modulators on IPSCs under different cholinergic conditions

The analysis of the extracellular data set provided evidence that the cholinergic status indeed affected the action of $GABA_AR$ modulators with specific subunit affinities differentially. While the effect of diazepam seemed to be less impacted by the cholinergic status, the effect of zolpidem especially in the higher concentration changed in the presence of ACh. This finding supported the hypothesis that ACh modulates specific elements of the GABAergic system, by possibly exciting certain groups of INs but not others. To specifically investigate the effect of cholinergic modulation in combination with $GABA_AR$ modulators on the inhibitory power of the network, inhibitory postsynaptic currents (IPSCs) were recorded. Glutamatergic transmission was blocked with AP5 and CNQX. Recordings of IPSCs were performed from cortical layer V cells visually identified as pyramidal cells. For these experiments, first IPSCs were recorded under the ACh^+ condition alone as control. Then, the $GABA_AR$ modulators zolpidem (1 µM or 0.2 µM) or diazepam (1.0 µM) were applied during the ACh^+ condition, followed by the ACh^- condition plus modulator (Table 12). Thus, by design, the ACh^+ and ACh^- conditions were present within one experiment. Due to a large variability of IPSC parameters between cells, a within-subjects (repeated measures) design of the experiments with higher statistical power (in comparison to a between-subjects design) was chosen to detect differences between the cholinergic conditions. In order to control for experimental time and for effects of the cholinergic condition per se (see section 3.1.3), a sham experimental series was conducted independent of the effects of $GABA_AR$ modulators (Table 12).

Condition	**Drug application order**			
I **Sham**	ACh^+ (control)	***ACh*$^+$**	***ACh*$^-$**	ACh^+ (Wash-out)
II **ACh+ & ACh-**	ACh^+ (control)	***ACh*$^+$ &** **$GABA_AR$ modulator**	***ACh*$^-$ &** **$GABA_AR$ modulator**	ACh^+ Wash-out

TABLE 12: DRUG-APPLICATION DESIGN FOR IPSC EXPERIMENTS.

Raw data examples are shown in figure 23A. Identical to extracellular experiments, zolpidem was applied in two different concentrations where the low concentration was suited to predominantly enhance currents through $GABA_AR$ containing the α_1 receptor subunit while the high concentration additionally targeted receptors with α_2 and α_3 subunits (Munakata et al., 1998).

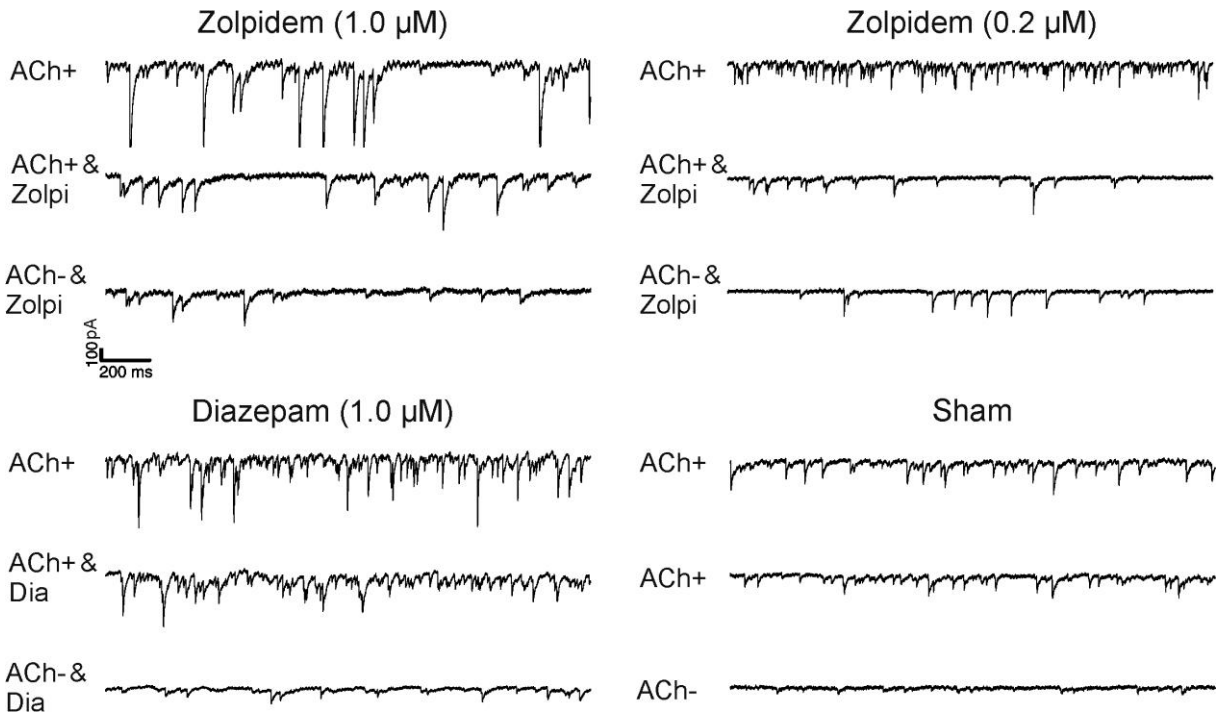

FIGURE 23: ALTERATION OF INHIBITORY POSTSYNAPTIC CURRENTS BY GABAERGIC MODULATORS UNDER THE ACH+ AND ACH- CONDITIONS. ***A.*** Exemplary current traces from cortical cells in culture obtained in voltage clamp, shown for the four different drug application series including sham. In all cases, ACh+ was the baseline condition (top trace), followed by [ACh+ & $GABA_AR$ modulator| sham] (middle trace, and [ACh- & $GABA_AR$ modulator| sham] (bottom trace).

As for previous IPSC recordings, four parameters were analyzed: decay time τ, frequency of IPSCs, peak IPSC amplitude and the total phasic current. All data and their respective medians and 25th and 75th quantiles are shown in figure 24 (see also supplementary material Table S10). When the control data (*ACh*$^+$ condition: first condition in each experimental series) was compared across the $GABA_AR$ modulator and sham conditions, the variability between cultures was noticeable. For example, the zolpidem (1 µM) data set had a median IPSC frequency of around 20 Hz under the *ACh*$^+$ condition, whereas the zolpidem (0.2 µM) data set started from a median IPSC frequency of around 50 Hz. Since the baseline IPSC activity was not comparable across experimental sets, all data sets were normalized to their respective *ACh*$^+$ control condition.

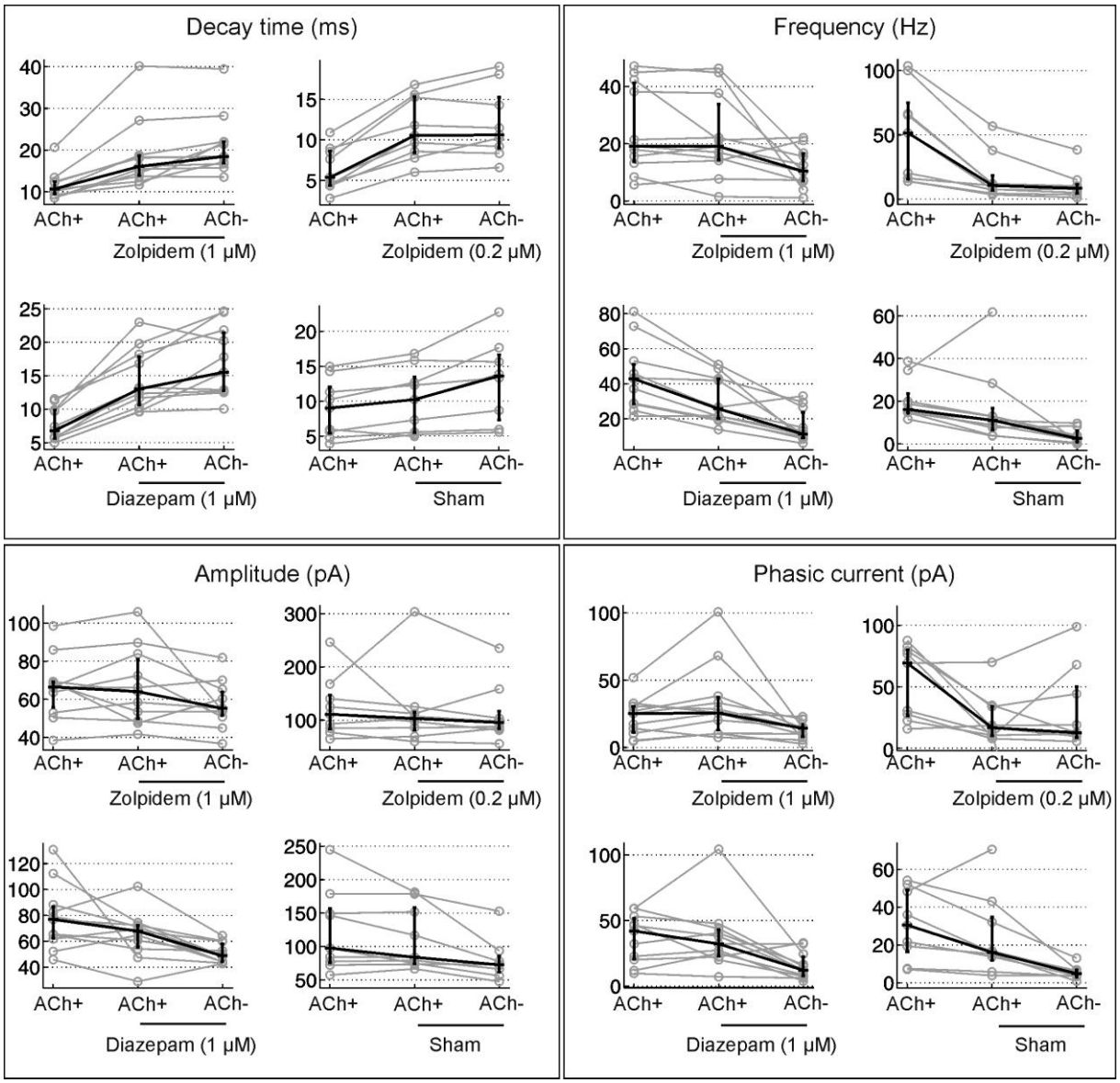

FIGURE 24: SUMMARY PLOTS OF IPSC PARAMETERS FOR ALL EXPERIMENTS FOR THE THREE $GABA_AR$ MODULATORS STUDIED AND SHAM APPLICATION. Grey lines are individual experiments, black lines are medians and 25th and 75th quantile. Bonferroni correction: $p < 0.02$; CI 0.983.

To show the effect of $GABA_AR$ modulators alone independent of the cholinergic status, data for each $GABA_AR$ modulator was pooled across the *ACh*$^+$ and *ACh*$^-$ conditions. For the sham condition, *ACh*$^+$ and *ACh*$^-$ data were also pooled. Since these pooled data sets were independent from one another, a Kruskal-Wallis test was applied to compare them. Then, three post-hoc comparisons were made between zolpidem (1 µM), zolpidem (0.2 µM) and diazepam each with sham (Figure 25). All three $GABA_AR$ modulators caused significantly longer IPSC decay times in comparison to sham. Since the main characteristic of positive allosteric $GABA_AR$ modulators consists of the prolongation of channel open times and thus, an increase of IPSC decay times (Rudolph and Antkowiak, 2004), this finding was expected and confirmed the efficacy of $GABA_AR$ modulators in the chosen model system.

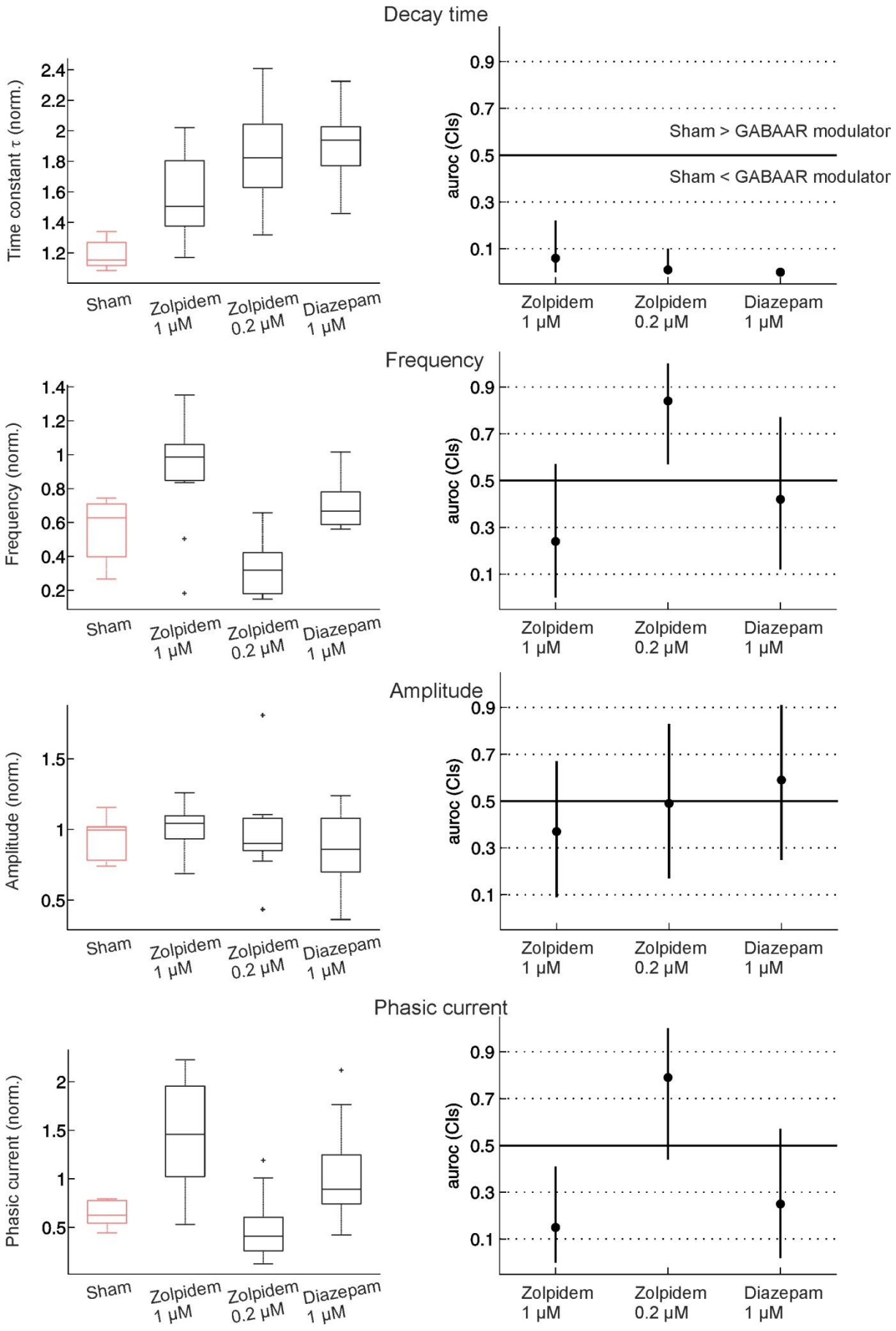
Decay time
Time constant τ (norm.)
2.4
2.2
2
1.8
1.6
1.4
1.2
Sham
Zolpidem 1 µM
Zolpidem 0.2 µM
Diazepam 1 µM
auroc (CIs)
0.9
0.7
0.5
0.3
0.1
Sham > GABAAR modulator
Sham < GABAAR modulator
Zolpidem 1 µM
Zolpidem 0.2 µM
Diazepam 1 µM
Frequency
Frequency (norm.)
1.4
1.2
1
0.8
0.6
0.4
0.2
Amplitude
Amplitude (norm.)
1.5
1
0.5
Phasic current
Phasic current (norm.)
2
1.5
1
0.5

FIGURE 25: EFFECTS OF $GABA_AR$ MODULATORS COMPARED TO SHAM CONDITION ON (FROM TOP TO BOTTOM) IPSC PARAMETERS DECAY TIME, FREQUENCY, AND AMPLITUDE, AND THE TOTAL PHASIC CURRENT. In this figure data were averaged across the ACh+ and ACh- conditions to illustrate the effects of the $GABA_AR$ modulators independent of the cholinergic status. Left column, box plots of the IPSC parameters normalized to control (ACh+ condition). Sham condition is in rosé. Right, Auroc effect sizes and CIs are shown to evaluate the difference between sham and $GABA_AR$ modulators.

In terms of IPSC frequency, only zolpidem (0.2 μM) differed substantially from the sham condition (auroc = 0.76). The IPSC peak amplitude was not affected by $GABA_AR$ modulators; there was no indication of a difference between all four conditions (X^2= 5.82, p = 0.12). The phasic current differed most between zolpidem (1 μM) and sham (auroc = 0.85), although application of diazepam also resulted in a slightly larger phasic current compared to sham (auroc = 0.72). In summary, all three $GABA_AR$ modulators differed substantially from the sham condition in decay time. When considering the overall inhibitory current, zolpidem (1 μM) and diazepam differed from sham, whereas the extraordinarily strong depression of IPSC frequency in zolpidem (0.2 μM) resulted in a net inhibition which was even lower than that in the sham condition.

Next, the effect of each $GABA_AR$ modulator was compared between the ACh^+ and ACh^- conditions. In figure 26, left column, normalized medians for all $GABA_AR$ conditions during the ACh^+ and ACh^- drug condition and sham were plotted per parameter. In order to answer the question if the ACh condition impacted the effect of $GABA_AR$ modulators, data from [$GABA_AR$ modulator & ACh^+] and [$GABA_AR$ modulator & ACh^-] (second and third recorded condition of each experimental series, respectively) were compared statistically (auroc). Results for each parameter are displayed in the right column of figure 26.

In the sham condition, the change of IPSC parameters from the ACh^+ to the ACh^- condition was quantified in the absence of $GABA_AR$ modulators. Although the decay time was significantly shorter in the ACh^+ condition, the overall phasic current was larger in the ACh^+ than in the ACh^- condition accompanied by a significantly higher IPSC frequency and larger IPSC peak amplitudes (Figure 26, supplementary material Table S11). In summary, the inhibitory current was larger in the ACh^+ than in the ACh^- condition, confirming previous results (section 3.1.3).

The main part of the analysis consisted of the comparison of different $GABA_AR$ modulators under both ACh conditions. For zolpidem (1 μM), the decay time was shorter under the ACh^+ than the ACh^- condition (auroc = 0.3), and IPSC frequency, amplitude and total phasic current were larger under the ACh^+ than the ACh^- condition (Figure 26). Similarly, diazepam had a shorter decay time under the ACh^+ than the ACh^- condition (auroc = 0.21), and IPSC frequency, amplitude and total phasic current were larger under the ACh^+ than the ACh^- condition. When comparing results for these $GABA_AR$

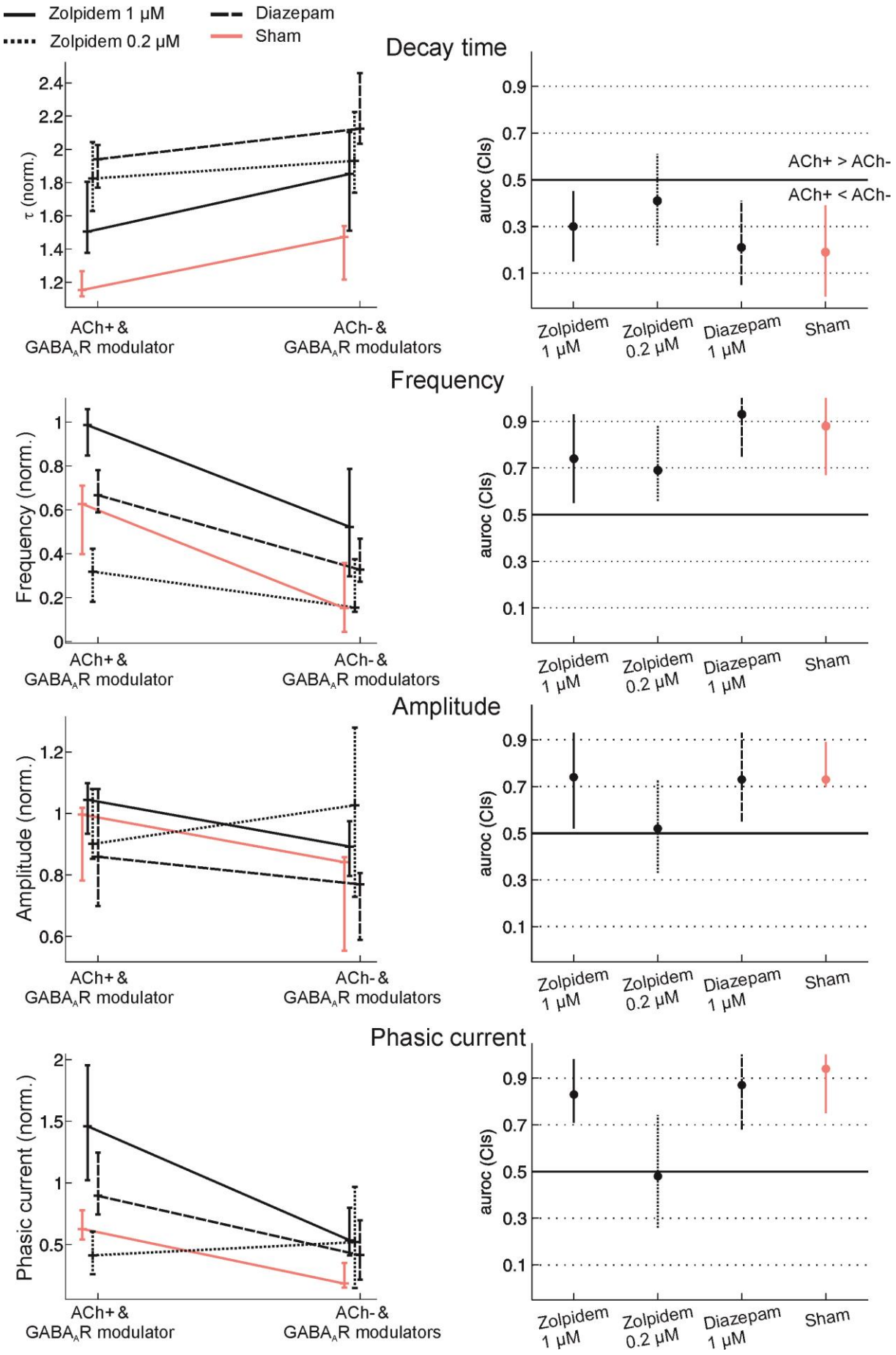
Zolpidem 1 µM
Zolpidem 0.2 µM
Diazepam
Sham
Decay time
τ (norm.)
ACh+ &
GABA$_A$R modulator
ACh- &
GABA$_A$R modulators
auroc (CIs)
ACh+ > ACh-
ACh+ < ACh-
Zolpidem
1 µM
Zolpidem
0.2 µM
Diazepam
1 µM
Sham
Frequency
Frequency (norm.)
Amplitude
Amplitude (norm.)
Phasic current
Phasic current (norm.)

FIGURE 26: COMPARISON OF THE EFFECTS OF $GABA_AR$ MODULATORS UNDER THE TWO DIFFERENT ACH CONDITIONS. On the left, normalized data (to ACh+ condition) is shown for all GABAAR modulators under ACh+ and ACh- conditions. Line styles encode different $GABA_AR$ modulators (see legend). On the right, auroc values with CIs are displayed for the differences between the ACh+ and ACh- condition for each $GABA_AR$ modulator.

modulators to the sham condition, it became apparent that all parameters changed qualitatively in the same way with an effect of similar size.

Zolpidem (0.2 µM) differed from zolpidem (1 µM) and diazepam as it remained mostly unaffected by the presence or absence of ACh since the effect was close to 0.5 for all four parameters (supplementary material Table S11). As mentioned before, an effect of 0.5 or crossing of confidence intervals of the 0.5 line indicates no effect (no difference between distributions; see Methods section on auroc). Only for IPSC frequency, about 70% of the data points (auroc = 0.69 [0.56 0.88]) under the [zolpidem (0.2 µM) & ACh^+] condition had higher frequencies than in the [zolpidem (0.2 µM) & ACh^-] condition, meaning that the IPSC frequency for zolpidem (0.2 µM) was significantly higher in the ACh^+ than in the ACh^- condition. Otherwise, the effect of zolpidem (0.2 µM) was independent of the ACh condition.

In conclusion, IPSC analysis showed that all $GABA_AR$ modulators alone prolonged the decay time independently of the ACh status. When effects of zolpidem (0.2 µM) were compared under the ACh^+ and ACh^- condition, IPSC parameters were unaffected by the ACh status. Zolpidem (1 µM) and diazepam had a shorter decay time in the presence of ACh^+, but higher IPSC frequencies, larger IPSC peak amplitudes and a larger phasic current qualitatively similar to the sham condition.

4 Discussion

The neuromodulator ACh is an essential component of sensory stimulus processing in the cortex. As ACh reduces intracortical communication and, at the same time, strengthens afferent thalamic input into cortex, newly perceived stimuli can pass through to cortex (Bloem et al., 2014; Eggermann et al., 2014; Kruglikov and Rudy, 2008; Wester and Contreras, 2013). How is this gating of information processing accomplished? Increasingly it appears that the neocortical GABAergic system takes on a central role in combination with ACh: numerous, diverse classes of GABAergic INs with differential sensitivities to ACh control cortical activity and sensory processing, including neuronal oscillations, synchrony and receptive field properties (Chen et al., 2015). Based on *in vitro* electrophysiology, the present thesis project was designed to illuminate how ACh alters qualitative and quantitative aspects of neocortical GABAergic inhibition. Specifically, the modulation of different $GABA_AR$ subtypes was contrasted between the ACh^+ condition, in which external ACh was applied, and the ACh^- condition, in which the cholinergic receptor system was antagonized. Two major results can be reported: 1) ACh increased inhibition by exciting parts of the interneuronal system. 2) ACh differentially affected $GABA_AR$ subunit modulation. In the following, these main results will be elaborated on, followed by a more detailed discussion of the various experimental approaches pursued in this thesis.

Since experiments with $GABA_AR$ modulators were based on an alteration of the cholinergic status via externally supplied ACh, first, the action of ACh in organotypic cultures was investigated alone. Current clamp recordings from neocortical cells revealed two sides of the ACh effect: on the one hand, ACh induced increases in average firing rate and burst rate, which seems to point to an excitation of the networks. On the other hand, the length of bursts, burst afterhyperpolarizations and in-burst peak depolarizations decreased – observations compatible with increased inhibition. Although on the behavioral level this neuromodulator is associated with wakefulness and attention which may imply general excitation of the network (Hasselmo and Sarter, 2011), findings from the current project support the notion that ACh at least partly increases inhibition. Since the focus of the thesis was on the interaction between ACh and the GABAergic system, further investigation of the inhibitory component of ACh was carried out by recording IPSCs from cortical PYs in the presence and absence of cholinergic activity. Results from this experimental series showed a dramatic increase in IPSC frequency as well as amplitude. Thus, it was concluded that at least parts of the GABAergic IN system were directly activated by ACh. Especially SOM^+ INs were suspected to be a major component of the GABAergic inhibition evoked through ACh since they had been shown before to depolarize in the presence of the neuromodulator (Kawaguchi, 1997). Paired recordings from Martinotti cells, a subgroup of SOM^+ INs, intracellulary and cortex extracellulary were conducted. Although the overall

firing rate of Martinotti cells did not increase during ACh application as might have been expected, their firing pattern became more tonic and independent of network activity. It is likely that the role of this IN class within the cortical network was altered by the change in firing pattern, which may be one key component of the ACh effect.

The main part of the project was concerned with the question whether or not the action of ACh on GABAergic inhibition depended on specific $GABA_AR$ subunits. It was hypothesized that inhibition mediated via receptors containing the α_5 subunit postsynaptic to SOM^+ INs would depend on the cholinergic status, since SOM^+ cells were shown to be ACh-sensitive. On the other hand, inhibition mediated via receptors containing the α_1 subunit postsynaptic to PV^+ INs, which are most likely not directly affected by ACh, should not be affected by the cholinergic status. To investigate this hypothesis, the action of different $GABA_AR$ modulators on extracellulary recorded network activity was compared between the presence and absence of ACh. This approach yielded a wealth of information which confirmed the general hypothesis of an ACh-dependent change in the recruitment of $GABA_AR$ subtypes, albeit in unexpected ways.

First, conventional burst and action potential parameters were compared to characterize the effect on the activity pattern. This analysis revealed that the burst rate was the most consistently affected parameter across all drug conditions. Especially in the infragranular layer, positive modulation of receptors containing the $\alpha_{1\ (2,\ 3)}$ (zolpidem 0.2 µM), $\alpha_{2,\ 3,\ 5}$ (diazepam in α_1 mutant) and $\alpha_{1,\ 2,\ 3,\ 5}$ (diazepam in WT) subunits caused significantly lower burst rates in the presence of ACh than in its absence. Differences between cholinergic conditions for GABAergic modulation involving the $\alpha_{1,\ 2,\ 3}$ subunits (zolpidem 1.0 µM) were similar but smaller. Intriguingly, the presence of α_5 among the positively modulated subunits determined the effect of $GABA_AR$ modulators on the amount of network activity: whereas modulation of $GABA_ARs$ containing the $\alpha_{1\ (2,\ 3)}$/ $\alpha_{1,\ 2,\ 3}$ subunits in reduced network activity in the presence of ACh in comparison to its absence, modulation of $GABA_ARs$ containing the $\alpha_{2,\ 3,\ 5}$/ $\alpha_{1,\ 2,\ 3,\ 5}$ subunits did not cholinergic-dependently change the amount of network activity despite the reduction in burst rate. The decrease in burst rate was compensated for by an increase in burst length in the presence of ACh. Thus, the overall amount of network activity stayed constant. Overall, modulation of $\alpha_{1\ (2,\ 3)}$/ $\alpha_{1,\ 2,\ 3}$-containing receptors reduced the network activity in the presence of ACh while modulation of $\alpha_{2,\ 3,\ 5}$/ $\alpha_{1,\ 2,\ 3,\ 5}$ -containing receptors changed the pattern of network activity without decreasing it in the presence of ACh. Fittingly, antagonism of the $GABA_ARs$ with the α_5 subunit (L-655,708) increased network activity in the presence of ACh comparatively to its absence, which underscores the essential role of this subunit for the ACh effect.

Second, power spectral analysis revealed that receptor modulation with the $\alpha_{1,\ 2,\ 3}$ subunits decreased the delta frequency band in the presence and absence of ACh; however, the effect was stronger in its

presence and only found in the infragranular layer. Antagonism of the $GABA_ARs$ containing the α_5 subunit evoked ACh-dependent changes across a wider frequency spectrum.

Third, cross-correlations of LFP signals from the infragranular and supragranular layers were calculated. While receptor modulation containing the $\alpha_{1\ (2,\ 3)}$/ $\alpha_{1,\ 2,\ 3}$ subunits had stronger decorrelating effects in the presence of ACh than in its absence in some frequency bands, modulation of the $\alpha_{2,\ 3,\ 5}$/ $\alpha_{1,\ 2,\ 3,\ 5}$ subunit-containing receptors depended clearly less on the cholinergic status. Antagonism of the α_5 subunit-containing receptors enhanced the correlation in the presence of ACh. Lastly, cross-correlations between the instantaneous firing rate and LFP signals showed the strongest difference between the presence and absence of ACh for modulation of receptors with the $\alpha_{1,\ 2,\ 3}$ subunits in the infragranular layers.

Overall, the project showed that ACh increased inhibition, which was at least in parts mediated via Martinotti cells, and that the cholinergic status differently impacts GABAergic inhibition depending on specific α-subunit modulation. Differences between the presence and absence of ACh were most reliable and explicit across different analyses when the $\alpha_{1,\ 2,\ 3}$ or the α_5 subunits were modulated or antagonized, respectively. Moreover, the modulation of $\alpha_{1,\ 2,\ 3,\ 5}$ subunits led to the least differences between cholinergic conditions. It is speculated that specifically α_1 and α_5 may act as opposing forced to balance inhibition. Further on, results will be discussed in more detail.

4.1 Methodological considerations

For the main part of the current thesis project, organotypic cortical cultures were used. In some respects, the organotypic culture model system bridges the gap between the *in vitro* acute slice system and *in vivo* experiments on animals. Cultures are maintained *in vitro* for at least two weeks before experiments are conducted so that recovery of neuronal pathways and further development after the slicing process is possible. It has been shown that axonal connections that have been cut during the preparation reform to create a cortical network that resembles *in vivo* conditions (De Simoni et al., 2003; Drexler et al., 2010; Gähwiler et al., 1997). This network architecture enables a high degree of spontaneous network activity. For experiments relying on this kind of activity cultures thus provide a clear advantage over cortical acute slices, in which rates of spontaneous network bursts are roughly an order of magnitude less. Although organotypic cultures were used as the primary model system in the current project for the reasons named above, they have their own limitations. Despite being morphologically and structurally *in vivo*-like, firing patterns of organotypic cultures do not resemble *in vivo* waking. While organotypic cultures produce distinct states of high and low network activity causing a slow-frequency rhythm as described in the introduction (section 1.4), the awake state *in vivo* is characterized by tonic, higher frequency activity (Steriade et al., 2001). However, slow-frequency activity can also be found *in vivo*, where it corresponds to slow-wave sleep

or anesthesia (Sanchez-Vives and McCormick, 2000; Steriade et al., 1993). Thus, results discussed further on should not be compared to *in vivo* waking. It should be kept in mind that organotypic cultures, although *in vivo*-like in terms of synaptic connectivity and other respects, are merely a model system which provided ideal conditions to develop a general idea about the interaction of the cholinergic and GABAergic transmitter systems in cortex.

The second consideration concerns the zolpidem concentrations chosen for the project. Zolpidem was used at 0.2 µM and 1.0 µM to create two relatively distinct $GABA_AR$ subunit modulating conditions. While zolpidem has the highest affinity for α_1 subunit-containing receptors, it also binds to receptors with the α_2 and α_3 subunit, but has negligible effects on receptors with the α_5 subunit (Engelhardt et al., 2007; Munakata et al., 1998; Puia et al., 1991; Sanna et al., 2002). The idea behind using the lower concentration of zolpidem was to potentiate the effect transmitted via the α_1 subunit-containing receptors and at the same time attenuate α_2- and α_3-mediated effects. It can be argued that for both concentrations, the α_1 subunit is dominating over the other two subunits since these concentrations fall relatively close together. However, a concentration-response curve measured as the increase of the GABA current in oocytes suggested that zolpidem evoked stronger current potentiation via the α_1 than the α_3 subunit at lower concentrations (< 1 µM) (Wafford et al., 1993). At 1 µM zolpidem, potentiation via the α_1 subunit seemed to reach a plateau, whereas potentiation via the α_3 subunit still increased with increasing concentration (Wafford et al., 1993). These results are in accordance with Puia et al. (1991), by tendency showing higher potentiation via the α_3 than the α_1 subunit for 10 µM zolpidem. Thus, for the current study, 1 µM was considered less selective for the α_1 subunit than 0.2 µM zolpidem. It also needs to be considered that zolpidem (1.0 µM) in the presence of ACh in some cultures had such a strong decreasing effect on network activity that no signals were detectable during this condition. Further increase of the zolpidem concentration (to increase the effect on α_2/ α_3) most likely would have led to more experiments with unquantifiable responses.

4.2 ACh increased inhibition in organotypic cortical cultures

4.2.1 Alterations of spontaneous firing patterns by ACh

Acetylcholine is a widely investigated neuromodulator whose impact on different cell types in the cortex has been studied in detail (Hasselmo and Sarter, 2011; Picciotto et al., 2012). Many conclusions are based on work with acute slices and relatively high ACh or carbachol (cholinergic receptor agonist) concentrations (Buhl et al., 1998; Kondo and Kawaguchi, 2001; Kuczewski et al., 2005). Less is known about the action of ACh on spontaneously active networks as they exist in organotypic slice cultures. Since neocortex contains cholinergic INs (Engelhardt et al., 2007) it was

plausible to ask whether or not notable amounts of ACh were released by these neurons and affected network activity. In acute slices, Engelhardt et al. (2007) found that these neurons did not exert direct postsynaptic effects on PYs but only modestly increased the number of spontaneous excitatory postsynaptic currents (EPSCs) by acting on nicotinic receptors on presynaptic glutamatergic terminals. It was concluded that intrinsic cholinergic INs were unable to modulate the cortical network in a notable manner. However, it was unclear whether the same would hold in spontaneously active slice cultures, the model system used here. Hence, extracellular experiments were carried out contrasting the effect of cholinergic receptor blockade (atropine and mecamylamine) subsequent to either no external ACh application (control) or application of 1 µM or 10 µM ACh in combination with the ACh-esterase inhibitor neostigmine, which was added to ensure a stable tonic ACh concentration. The logic behind this comparison was that network activity should not differ between aCSF alone and cholinergic receptor antagonism if no or little internal ACh was present. Only if amounts of ACh sufficient to shape network activity were released by cholinergic INs, receptor blockage was expected to show an effect. By contrast, effects of receptor antagonists were definitely anticipated subsequent to ACh application. Overall, cholinergic receptor blockage had little effect following the control condition. Only when blockers were applied subsequent to the application of either ACh concentration, two distinguishable activity patterns were evoked: while the ACh condition was characterized by higher burst rates with short bursts and less action potential firing during the initial phase of the burst, cholinergic receptor blockade decreased the burst rate, and increased burst length, amplitude and action potential firing during burst beginning.

Thus, two major conclusions could be drawn. First, the clear difference of cholinergic blocker effects in the control and ACh conditions revealed that the impact of intrinsic cholinergic neurons on the network, if present, did not match the impact of tonically present ACh at either of the chosen concentrations. Second, the lower of the tested concentrations of ACh (1 µM) had sufficiently clear effects on spontaneous activity. Therefore, this concentration in conjunction with 1 µM neostigmine was defined as the standard cholinergically activated (ACh^+) condition for all subsequent experiments, including those with $GABA_AR$ modulators. The findings reported above may be interpreted to mean that intrinsic cholinergic release in the cultures was null, so that the ACh^+ condition could have been contrasted with the control (drug-free condition). Although this may be the case on average, and in some series was done due to experimental considerations/limitations, it could not be excluded that putative intrinsic cholinergic release influenced activity in a small subset of cultures, or characteristics of activity that were not tested in this experimental series. Therefore, in order to exclude any influence of intrinsic cholinergic neurons a priori, in the majority of the subsequent experimental series, the ACh^+ condition was contrasted with the ACh^- condition (defined by the presence of cholinergic blockers as described above).

Although extracellular experiments discussed previously already provided some insight in the effect of ACh on network activity, firing pattern changes in the presence of 1 µM ACh in combination with neostigmine were investigated in more detail in current clamp experiments of somatosensory cortical cells in cultures. Spontaneous activity during the control condition consisted of synchronized, clearly separable network bursts and silent periods. Action potential firing occurred mainly during burst phases. The presence of ACh changed the firing pattern substantially. Bursts were shorter but more frequent, as in the extracellular recordings described above. Overall, more action potentials were triggered as the application of ACh led to a continuous, tonic action potential spiking which depended less on global network activity. At the same time, bursts and silent periods became less distinguishable from each other, which is an indicator of a more desynchronized activity pattern. *Desynchronization* is defined as a decrease in low-frequency spectral power and has been associated with the release of ACh before. For example, Tateno et al. (2005), who studied the effect of 10-50 µM carbachol on dissociated cortical cultures from rats, reported that carbachol transformed synchronous burst firing into a more asynchronous single-spike firing pattern just as has been shown in the current work. Another study by Metherate et al. (1992) found that ACh shifted originally large-amplitude, slow oscillation network bursts to low-amplitude, fast oscillations in the beta to low gamma frequency range. Thus, previously reported effects of ACh could be replicated in organotypic cultures and confirmed the usability of the chosen experimental conditions and model system.

In addition to the analysis of network bursts and action potential rates, the membrane potential before and during burst onset and after burst offset was analyzed. During the control condition, most of the cells were overexcited as the membrane potential went into a depolarization block after burst onset, during which no action potentials could be initialized. In the presence of ACh^+, the membrane potential was less depolarized and more full-scale action potentials occurred in this phase. The ACh-induced prevention of overexcitation could be explained by an increase in inhibitory currents. ACh has been shown to activate GABAergic INs (Alitto and Dan, 2013; Alkondon et al., 2000; Kawaguchi, 1997; Porter et al., 1999; Xiang et al., 1998) and increase inhibitory postsynaptic currents in pyramidal cells (Aracri et al., 2010; Xiao et al., 2009). In the current project, voltage clamp experiments were performed to further investigate the role of ACh on GABAergic inhibition, which will be discussed later on. Besides increasing GABAergic inhibition, ACh has been associated with a decrease in EPSP amplitude in cortical pyramidal neurons which may be due to the activation of presynaptically-located M_4 receptors (Gigout et al., 2012; Levy et al., 2006). The combination of increased inhibition and reduced excitation would lead to less excitatory input during burst beginning and thus to less depolarization.

Secondly, there was no considerable difference of the membrane potential prior and immediately following bursts unlike during the control condition, where notable afterhyperpolarizations (AHPs) existed. The reduction of AHP has been reported before for carbachol applied to neostriatal neurons (Pineda et al., 1995). Pineda et al. attributed the affected to M_1 muscarinic receptors, which are coupled to the phospholipase C cascade activating protein kinase C. Protein kinase C might lead to a reduction in Ca^{2+} influx which would cause a decrease in Ca^{2+}-activated K^+ currents contributing to AHPs. Additionally, the reduction in burst length might lead to a decrease in Na^+ and Ca^{2+} influx and thus a decrease in Na^+ and Ca^{2+}-activated K^+ currents (Sanchez-Vives et al., 2010).

Combining the results obtained from the analysis of firing patterns and changes in membrane potentials, the hypothesis that ACh emphasizes inhibition within the cortical network can be supported. First, the dampening of overexcitation during burst phases due to a less depolarized membrane potential of the cell hint at more inhibitory input received by the cell. Second, the shortening of burst phases also promotes the idea of more inhibition. Shorter, less fatiguing burst phases and reduced AHPs may be responsible for the cells increased capacity to quickly enter into the next burst phase as could be seen by an increase in burst and action potential rate. Thus, the increase of inhibition fundamentally changed the network firing pattern and ultimately led to an increase in cell activity.

4.2.2 Evidence of direct cholinergic excitation of INs in IPSC measurements

The hypothesis of an increase in inhibition by ACh was confirmed by voltage-clamp experiments which were performed to quantify inhibitory postsynaptic currents. In the presence of ACh in comparison to the control condition and cholinergic blockage, the overall inhibitory current increased almost five times and was action potential-dependent. Measurable changes in IPSC parameters were most likely resulting from somatic input, while dendritic IPSCs were probably underrepresented due to insufficient voltage clamp of the dendrites, a limitation inherent to the somatic voltage clamp method (Williams and Mitchell, 2008). Thus, two major IN classes which both project to the soma of PY cells in cortex may contribute to the increase in inhibition: PV^+ fast-spiking basket cells and CCK^+ irregular-spiking cells. Xiao et al. (2009) demonstrated the increase of spontaneous IPSC frequency and amplitude in cortical pyramidal cells of layer II/III due to the activation of the muscarinic M_3 receptor subtype. In addition, Rio et al. (2010) ascribed an increase in action potential firing frequency of CCK^+ INs in hippocampus, but not of PV^+ INs, to the activation of the M_3 receptor. PCR analyses revealed the presence of the M_1 as well as the M_3 receptor subtype on CCK^+ INs, whereas only the M_1 subunit was detected on PV^+ INs. CCK^+ INs in knock-out mice lacking the M_3 receptor failed to show an increase in firing frequency subsequent to ACh release. Taken

together, the direct activation of CCK^+ INs via M_3 receptors by ACh seems to be a plausible explanation for the IPSC increase in pyramidal cells observed in this work.

While early reports have already negated the direct cholinergic activation of PV^+ INs (Kawaguchi, 1997), some recent studies supported this view. For example, Alitto and Dan (2013) reported that PV^+ INs were exited in the presence of ACh, but could show that their increase in activity was only a secondary effect of ACh and stemmed from activation by PYs, which were directly excited by ACh and connected to PV^+ INs by a negative feedback loop. Moreover, this IN class has been shown to release less GABA in the presence of ACh due to inhibitory presynaptic $M_{2/4}$ receptors (Kruglikov and Rudy, 2008). Yet, there are studies providing evidence for a cholinergic excitability of these INs. For example, Rio et al. (2010) reported the activation of PV^+ INs via the M_1 receptor. In contrast to M_3 receptor-containing CCK^+ INs, a higher ACh concentration was needed for a notable increase in firing frequency. The authors speculated that M_1 receptors might be located in a less accessible location and thus, may only be activated during sustained ACh release. For cortex, Pafundo et al. (2013) found that ACh depolarized PV^+ INs but by far less than PYs and Yi et al. (2014) described a stronger depolarizing effects for hippocampal than for cortical PV^+ INs. In conclusion, ACh seems to directly recruit CCK^+ INs, while significant activation of PV^+ INs by ACh seems to be more dependent on corresponding PY activity. Therefore, in a network lacking excitatory transmission as was used for voltage clamp experiments, CCK^+ cells are proposed to be more likely to contribute large somatic IPSCs measured from pyramidal cells in the presence of ACh.

Combined results from extracellular, current clamp, and voltage clamp experiments suggest that ACh increased inhibitory signaling in cortex. One of the possible mechanisms explaining the effect of ACh may be an increase in direct inhibitory input to PY cells most likely by activating somatically-projecting CCK-positive INs, amongst other mechanisms (the role of dendritic-projecting SOM-positive INs will be discussed later on). Presumably as a consequence of this enhanced inhibition, the in-burst membrane potential was not driven into a depolarization block, which resulted in more regular action potential firing during the initial phase of the bursts. It is proposed that less excessive depolarization and shorter burst durations may be the reason for the absence of the strong AHPs as seen under control conditions, which allows for quicker development of a new burst phase. In its extreme form, when positive $GABA_AR$ modulators come into play (see section 4.3), this modulatory mechanism may by a major cause of a shift from phasic activity, which displays as separable burst phases and silent periods, to more tonic continuous activity.

4.2.3 Basal forebrain-neocortical co-cultures were not affected by cholinergic receptor antagonism

The extracellular experimental series with cholinergic receptor antagonists supported the hypothesis that intrinsic cholinergic INs did not hold a dominant role in shaping spontaneous network activity. Thus, ACh had to be supplied to the network from an external source. In morphological studies it has been shown that neocortex receives prominent cholinergic projection afferents from basal forebrain (Woolf, 1991). Therefore, a co-culture system between basal forebrain and neocortex was created in an attempt to release ACh in a more physiological way instead of bath-applying it via the perfusion system. These co-cultures have been described before, but they were exclusively used for morphological studies (Baratta et al., 1996; Distler and Robertson, 1992; Gähwiler and Hefti, 1984). For this thesis project, electrophysiological recordings from these co-cultures were obtained for the first time. Basal forebrain slices were acquired from genetically modified mice with GFP-labelled cholinergic cells. Thus, it was possible to record intracellularly from a basal forebrain cholinergic cell, while the network activity of the cortex was monitored with an extracellular electrode.

Electrophysiological characteristics of cholinergic cells in basal forebrain have been reported for acute slices (Arrigoni et al., 2006; Griffith and Matthews, 1986; Unal et al., 2012). The comparison between these three studies with the results from co-cultures prepared for the current project revealed a large divergence in cell resistances. Whereas the cells recorded here had a cell resistance of ~ 107 MΩ, Griffith and Matthews (1986), who recorded from cholinergic basal forebrain cells in guinea pig brain slices, reported a slightly lower membrane resistance, while Arrigoni et al. (2006) and Unal et al. (2012), who worked with the same mutant mouse strain as used in the current project, measured a three and six times greater membrane resistance and time constant than was reported here, respectively. One possible explanation for the marked difference may have been the culture system used here in comparison to acute slices employed by Arrigoni et al. and Unal et al. Cells in organotypic cultures are known to be highly interconnected with each other (Debanne et al., 1995; Drexler et al., 2010). Thus, neurons receive a multiple of the excitatory input neurons in acute slices experience. The depolarization block reported above (see cortical current clamp experiments in section 4.2.1) is one indicator of high levels of excitatory synaptic input. In order to compensate for this intense input, neurons grown in culture may reduce their membrane resistance significantly in comparison to cells in acute slices, a phenomenon known as 'homeostatic plasticity' (Desai et al., 1999).

As in cortical mono-cultures, the presence of cholinergic effects on network activity was tested by the application of cholinergic receptor blockers (which should reverse any ACh effects) and the choline-esterase inhibitor neostigmine (which should enhance ACh effects). If ACh had been released

in substantial amounts, clear differences in network activity between these two conditions should have surfaced. However, neither drug treatment had a consistent modulatory effect, which can be attributed to a number of factors. First of all, the connectivity between neocortex and basal forebrain was not systematically studied. Although it could be shown that cholinergic neurons fired well attuned to cortical bursts, implying connectivity from cortex to basal forebrain, the connectivity from basal forebrain to cortex has only been visually verified. In all preparations, axons could be traced from basal forebrain to neocortex spanning the gap between tissues. However, their distribution within cortex remains unclear. Taking earlier studies into account, it can be assumed that the connectivity between basal forebrain and cortex should develop easily in culture. For example, Gähwiler and Hefti (1984) showed that cholinergic neurons readily grew into target tissue independently of the original anatomical predetermined connectivity. Distler and Robertson (1992, 1993) reported rapid ingrowth of cholinergic fibers into cortex after the first week *in vitro*. Therefore, connectivity between the tissues is the less likely problem.

The other, more serious issue may be the attunement of cholinergic neurons to the cortical burst firing rhythm. For ACh to have a dominant effect on cortical network activity, it appears essential that cholinergic neurons fire independently and specifically prior to cortical burst beginnings. However, membrane potential comparison and cross-correlational analysis revealed that cortical bursts were the initiator of basal forebrain activity in most of the recorded cultures. Thus, cholinergic neurons were merely following the cortical rhythm. Another point to consider may be the amounts of ACh released. Cholinergic fibers have been shown to form classical synapses (Turrini et al., 2001). However, another body of evidence exists supporting the volume transmission hypothesis of ACh, which states that ACh is released into the extracellular space (Sarter et al., 2014). In agreement with the volume-transmission hypothesis, the previously discussed muscarinic M1 receptor is not directly contacted by cholinergic varicosities (Yamasaki et al., 2010) but proposed to be activated by ambient ACh. In order to exert an effect on network activity under these circumstances, ACh would have to be released over a longer period of time in order to accumulate to a receptor-activating concentration. It is possible that cortical burst frequency was not sufficiently high and silent periods between bursts were too long to drive cholinergic afferents sufficiently to release enough ACh in cortex for a notable effect on network activity.

In order to study the effects of ACh released by basal forebrain afferents independently of spontaneous activity, stimulation of cholinergic cells would be necessary, which would best be achieved with the optogenetic approach. The cholinergic cell population could then be stimulated independent of cortical activity and amounts of ACh released would be better controllable.

4.2.4 Cholinergic excitation of Martinotti cells

While IPSC recordings from cortical PYs indirectly disclosed the effect of ACh on somatic and perisomatic INs, the effect of ACh on dendritically projecting Martinotti cells could not be evaluated by this experimental series. By using a genetically modified mouse strain, in which Martinotti cells expressed GFP and could thus be visually identified, current clamp recordings were made from these cells to evaluate their response to ACh application. As previously discussed for basal forebrain cholinergic cells, Martinotti INs showed an about six times smaller membrane resistance in culture as compared to acute slices. This finding supports the notion that differences in membrane resistance between culture and acute slices are not cell type- or mouse strain-specific but rather a general difference between cultures and acute slices. It supports the idea that spontaneous activity in cultures and high network interconnectivity causes an increased amount of synaptic input received by cells, which is compensated for by a lower membrane resistance as prevention from overexcitation.

The action of ACh on Martinotti cells has only been sparsely studied thus far. Distinctions between studied INs were often made based on firing properties (Yamamoto et al., 2010) or molecular markers (Chen et al., 2015; Porter et al., 1999: PV^+ vs. SOM^+). However, SOM+ INs can be further subdivided by their morphology as Ma et al. (2006) showed. In this study, three different genetically modified mouse lines were investigated, in which SOM^+ neurons were labeled with GFP. SOM^+ INs in the X98 mouse line used in the current project perfectly resemble the structural properties of 'classical' Martinotti INs as their axons project to layer 1, where they branch extensively and span multiple columns. SOM^+ INs in the X94 strain were mainly detected in layer 4 and projected within the same layer. SOM^+ INs from the third examined mouse line called Gin does share properties of Martinotti cells as they project to layer 1; however their somas were located in layer 2/3. Based on distinct electrophysiological and chemical characteristics additionally to different morphology, Ma et al. (2006) concluded that in these three mouse lines, three non-overlapping SOM^+ groups were labelled. Nonetheless, the terms "SOM^+" and "Martinotti cell" are used almost interchangeably in the literature. For example, Fanselow et al. (2008) used the Gin line and claimed to study the effects of carbachol and muscarine on Martinotti cells. To the knowledge of the author, this is the closest study to investigate the action of ACh on Martinotti cells. Therefore, the investigation of cholinergic effects on layer 5 Martinotti cells in the X98 mouse line was necessary.

In the current work, the presence of ACh caused a strong depolarization and heightened excitability in Martinotti cells, which is in agreement with results reported by Fanselow et al. (2008), where carbachol caused a persistent action potential discharge in layer 2/3 SOM^+ INs. Especially interesting was the change in firing pattern observed here: driven by spontaneous network activity in cultures,

Martinotti cells fired during network burst phases under control condition. With the application of ACh, some cells switched into a tonic firing mode independent of burst phases. Recent work on IN connectivity has shown that Martinotti cells are connected to the entire IN types- spectrum and to PYs, with slightly stronger connection probability to the former (Jiang et al., 2015; Pfeffer et al., 2013). The only connection they do not form is onto themselves (Jiang et al., 2015; Pfeffer et al., 2013). Thus, their impact especially on the inhibitory network activity is supposedly powerful. Their change in activity pattern as achieved by ACh may influence the activity pattern of the entire network. In fact, Chen et al. (2015) could demonstrate that the activation of SOM^+ INs alone by ACh was sufficient to evoke desynchronization and decorrelation, while VIP INs were not involved in these processes. The authors argued that SOM^+ IN activity might not be the only source of desynchronization and decorrelation, but they play a most central role.

4.3 ACh changed the mode of action of $GABA_AR$ modulators

After the effects of ACh had been extensively investigated, the groundwork was laid to tackle the main question of the thesis project: Do $GABA_AR$ modulators differ in their effect in the presence of ACh? Research has suggested that IN classes are differentially modulated by ACh (Alitto and Dan, 2013; Chen et al., 2015; Kawaguchi, 1997; Porter et al., 1999). Thus, it was hypothesized that $GABA_AR$ modulators depend in their effect on network activity on the cholinergic status. Additionally, IN classes form synapses with specific $GABA_AR$ subunits (Ali and Thomson, 2008; Freund, 2003; Klausberger et al., 2002; Nyíri et al., 2001; Thomson et al., 2000). Combining both findings, the hypothesis can be formulated that the action of $GABA_AR$ modulators with different $GABA_AR$ subunit affinities will be differentially altered by the presence of ACh. Five $GABA_AR$ subunit combinations were investigated in the ACh^+ and ACh^- condition: Zolpidem (0.2 µM) with preference for $GABA_ARs$ with the $\alpha_{1\ (2,\ 3)}$ subunit; Zolpidem (1.0 µM) with preference for $\alpha_{1,\ 2,\ 3}$; Diazepam (1.0 µM) with preference for $\alpha_{1,\ 2,\ 3,\ 5}$, Diazepam (1.0 µM) in the α_1-knock-in mutant with preference for $\alpha_{2,\ 3,\ 5}$, and L-655,708 with preference for the α_5 subunit.

4.3.1 Differences in burst parameters

4.3.1.1 During the presence of ACh, network activity decreased when α_1 subunit-containing $GABA_ARs$ were modulated, and increased when α_5 subunit-containing $GABA_ARs$ were blocked

First, results from action potential and bust parameter analyses were consulted to describe the mode of activity of $GABA_AR$ modulators in the presence and absence of ACh. For zolpidem in both concentrations, differences between ACh conditions were largest for the time spent in bursts. Especially in infragranular layers, cultures spent less time in bursts when zolpidem was applied together with ACh instead of cholinergic receptor antagonists. The fact that both zolpidem (1.0 µM)

and zolpidem (0.2 µM) achieved the same effect on the network activity suggests that the α_1 subunit played an essential role, since it is the dominant subunit target for both concentrations tested.

For once, this result is surprising since the effect is more pronounced in the infragranular than in the supragranular layer. $GABA_A$Rs containing the α_1 subunit have been shown to be postsynaptic to PV^+ INs. Both, the α_1 subunit and PV^+ INs were localized in layers one to six (Fritschy and Mohler, 1995; Kawaguchi and Kondo, 2002). Since PV^+ INs are located near PY somata to exert local inhibition, their presence would be expected in layers two/three and five corresponding to PY somata distribution; thus equal results would have been expected for both layers. Taking a closer look at the results reveals almost equally large effect size values for supra- and infragranular layers, although supragranular effects were not significant. It is likely that random variation caused the discrepancy between layers. Here, more experiments might have helped to clarify whether or not results would also be significant for the supragranular layers. Another explanation may be developmental changes. Experiments with organotypic cultures used for this project were performed between 14 and 36 days *in vitro*. A study by Lecea et al. (1995) showed that PV^+ INs were almost exclusively present in layer five during early development (up to postnatal day 12). At postnatal day 14, they started to be also present in layers two and three, however, there were still twice as many cells detected in layer five. Only later in development, layers two to six encompass about equal amounts of PV^+ INs. Thus, it is possible that younger cultures used for the experiments might not show an effect in supragranular layers, while older cultures would show the effect.

The second surprising factor for this experimental set was that the action of zolpidem on spontaneous network activity was affected by the presence of ACh. As has already been stated in the introduction, PV^+ INs are likely not directly activated by ACh. Their GABA release may even be reduced in the presence of ACh by presynaptic inhibitory muscarinic M_2 receptors and inhibition by ACh-activated SOM^+ INs (Chen et al., 2015; Kruglikov and Rudy, 2008; Salgado et al., 2007). Reduced PV^+ activity might become apparent by shortened burst periods, as has been shown for UP states *in vivo* (Kuki et al., 2015). However, in the current project, there were no differences between ACh conditions in burst length and thus, no evidence of reduced PV^+ IN activity. An explanation for the differential effect of zolpidem during different cholinergic conditions could be found through the tight reciprocal coupling between PV^+ INs and PYs and the activation of PYs by ACh. When ACh was applied, PY neurons were excited, which then activated nearby PV^+ cells regulating the output of PY cells and preventing overexcitation. It is assumed that the addition of zolpidem increased the inhibitory power at the α_1 subunit postsynaptic to PV^+ INs. This increase of somatic PY inhibition led to stronger hyperpolarization of PYs, which ultimately led to less network activity. By antagonizing

ACh receptors, PV^+ INs were not activated by heightened PY activity and thus, the effect of zolpidem under this condition differed.

Interestingly, only zolpidem (0.2 µM) but not zolpidem (1.0 µM) caused a distinctly lower burst rate in the presence of ACh than in its absence for the infragranular layer. It is plausible that with the higher concentration and the enhanced modulation of $GABA_A$Rs with the $\alpha_{2,3}$ subunits, PV^+ neuron activity was itself inhibited and thus, less inhibition was present. Overall, these results underline the complexity of the cortical network and its many distinct set screws. Although this project was based on the hypotheses of direct effects of ACh on the GABAergic IN system, zolpidem results provide evidence that secondary actions of ACh also shape network activity fundamentally.

In order to gain more insight in the role of the α_5 subunit during different cholinergic conditions, L-655,708, a functional antagonist at α_5 subunit-containing receptors, was used. In this case, $GABA_A$Rs containing the $\alpha_{1,2,3}$ subunits were still functional, but not positively modulated as with zolpidem or diazepam. Thus, it is difficult to make predictions about the effects of L-655,708 based on results with these substances.

First of all, differences between the two ACh conditions and L-655,708 could only be observed for the supragranular layers. This finding is plausible since the α_5 subunit is located on PY dendrites reaching the upper layers, but not on their soma as the α_1 subunit or axon initial segment as the $\alpha_{2,3}$ subunits, respectively (Freund and Katona, 2007; Serwanski et al., 2006). Secondly, blocking α_5 resulted in more time spent in bursts during the presence of ACh than during its absence. Hence, network activity was increased more in the presence of ACh than in its absence. It can be assumed that the application of ACh evoked an increase of SOM^+ IN-mediated inhibition transmitted via $GABA_A$Rs with the α_5 subunit. When these receptors were antagonized, SOM^+ inhibition was disrupted resulting in an overall increase of network activity. The inhibitory impact of the remaining active receptors with the α_1 and $\alpha_{2,3}$ subunits may not have been strong enough to maintain the inhibitory component of the ACh effect. This finding points to the powerful role of α_5 subunit-containing $GABA_A$Rs for the ACh effect. Additionally, the blockage of the α_5 subunit-containing receptor led to a higher burst amplitude in the presence of ACh than during its absence. The burst amplitude is an indirect measure of the firing synchrony of neurons (provided other relevant factors are constant). Large burst amplitudes indicate that more cells fired simultaneously at burst onset while small burst amplitudes indicate a more tonic firing pattern and less neurons firing, respectively. Higher burst amplitudes during the combined application of ACh and L-655,708 indicate that synchrony was larger when the α_5 subunit-containing receptors were blocked. This result supports findings by Chen et al. (2015), who concluded that SOM^+ activity alone was the source of ACh-induced desynchronization. Overall,

results from the current project underline the role of $GABA_A$Rs with the α_5 subunit and consequently of presynaptic SOM^+ INs for the ACh effect on network activity.

4.3.1.2 Change of activity pattern via $GABA_A$Rs containing the $\alpha_{2,3,5}$ subunit in the absence of ACh

Diazepam applied in WT and in the α_1-knock-in mutant both showed differences across ACh conditions for burst rate and burst length. The application of diazepam in the presence of ACh caused fewer but longer bursts relative to the absence of ACh. These changes were found in both examined cortical layers. In contrast to zolpidem, which decreased the overall time spent in bursts, diazepam had no effect on the total time spent in bursts since the increase in burst length nullified the decrease of burst rate. Thus, diazepam changed the bursting pattern; however the overall amount of bursting activity stayed the same. PV^+ cells have been reported recently to maintain UP states (Kuki et al., 2015) and could be a possible reason to explain longer bursts seen here. However, since the effects were so similar between WT and knock-in, it is assumed that the α_1 subunit postsynaptic to PV^+ INs was not involved but that changes were evoked via $\alpha_{2,3,5}$-containing $GABA_A$ receptors. It was originally hypothesized that ACh would enhance diazepam effects strongly since INs presynaptic to $\alpha_{2,3}$ and α_5 subunits are excited by ACh. Thus, a combination of increased GABA release and prolonged channel open times at the same synapse should lead to more inhibition than in the absence of ACh when INs where not especially activated. First of all, a difference was found between the two ACh conditions for diazepam. However, when considering the raw data it becomes clear that the difference can mainly be reduced to effects of diazepam when ACh was absent. In the presence of ACh, diazepam had no major impact. This finding suggests that ACh sufficiently modulated the inhibitory network to such a degree that the addition of diazepam could not further enhance the ACh effect. CCK^+ INs presynaptic to $\alpha_{2,3}$ subunits and SOM^+ INs presynaptic to the α_5 subunit are both directly activated by ACh. ACh may increase GABA release significantly that prolongation of the postsynaptic channel open times via diazepam had no further effects on the network activity. Only when these IN classes were not previously activated by ACh was diazepam able to evoke notable changes. Another possible explanation may be that ACh modulates the network in such a way that diazepam effects at different $GABA_A$Rs cancel each other out.

In summary, burst parameter analysis revealed that $GABA_A$R modulators acted differently in the presence and absence of ACh. Furthermore, ACh in combination with an α_1 modulator and an α_5 antagonist had an effect on the total amount of network activity, while the pattern of activity was affected by $\alpha_{2,3,5}$ modulation only in the absence of ACh.

4.3.2 ACh-evoked LFP desynchronization in low frequency ranges mediated via the $\alpha_{1,2,3}$ subunit and in low and high frequency ranges via the α_5 subunit

Beyond affecting burst parameters, ACh and GABAergic INs have been proposed to influence neuronal activity in specific frequency bands. ACh for example is known to reduce power in the low frequency range (< 10 Hz) but to enhance power in higher frequency ranges (Chen et al., 2015; Kalmbach and Waters, 2014; Metherate et al., 1992; Roopun et al., 2010). For GABAergic INs, the activation and synchronization of PV^+ firing has been associated with the origin of gamma rhythms (Cardin et al., 2009; Kuki et al., 2015; Sohal et al., 2009; Suffczynski et al., 2014; Whittington et al., 1995). For SOM^+ INs, little is known about their effect on frequency bands. Kuki et al. (2015) demonstrated an increase in delta frequencies in the absence of SOM^+ activity. Thus, it was of interest to analyze the power spectrum of the $GABA_AR$ modulators under both ACh conditions. A second motivation for spectral analysis was the fact that ACh sometimes changed the activity pattern in such a way that clearly separable bursts and silent periods gave way to continuous ongoing activity or oscillations. Traditional burst analysis was not suited to analyze these patterns. Therefore, spectral power analysis of LFP signals with an emphasis on five different frequency bands (delta, theta, beta, low gamma and high gamma) was employed. Of all $GABA_AR$ modulators tested, only zolpidem (1.0 µM) and L-655,708 modulated the power of frequency bands in a manner that depended on the ACh status. In both ACh conditions, zolpidem caused a strong decrease in the delta frequency band. This finding is supported by clinical studies measuring brain activity with EEG (Arbon et al., 2015; Brunner et al., 1991). However, it is novel that additional ACh application can even strengthen this effect as data from the current project suggest. Since ACh alone decreased power in the lower frequency ranges as stated above and zolpidem had the same effect, effects of both modulators seem to have added together. Equivalent to results from burst parameter analysis (section 4.3.1), it was surprising to find a difference between cholinergic conditions and zolpidem since α_1 subunits – the main target of zolpidem – are postsynaptic to PV^+ INs not directly activated by ACh. Since this effect was not observed for zolpidem at the lower concentration (0.2 µM), it needs to be assumed that it is not α_1-specific, but also depends on the $\alpha_{2,3}$ subunits. It is possible that ACh-activated CCK^+ INs presynaptic to these subunits were responsible for the particularly strong decrease in the delta frequency band. To the knowledge of the author, the role of CCK^+ INs in shaping the frequency spectrum of cortical LFP activity have not been investigated thus far. Future research should focus on attributing spectral changes to specific IN activity.

Antagonizing $GABA_AR$s with the α_5 subunit with L-655,708 increased power in the theta frequency band, but decreased power in low and high gamma frequency bands in the presence of ACh compared to its absence. These results are in accordance with Chen et al. (2015). That study

demonstrated that the activation of SOM^+ INs (which are presumably presynaptic to α_5) caused the ACh-typical desynchronization by reducing low frequency power (< 10 Hz) and increasing high frequency power (10-100 Hz). When the receptors with the α_5 subunit were blocked in the current experiments, this SOM^+ IN-mediated effect could not be evoked, hence low frequencies increased while higher frequencies decreased. In the absence of ACh, SOM^+ INs were not especially activated and thus the blockade of the α_5 subunit did not lead to a change in spectral power.

For diazepam in WT or the α_1 knock-in mutant, no difference between cholinergic conditions was observed although $GABA_A$Rs containing the $\alpha_{2,3}$ were also facilitated. It is possible that the additional facilitation of α_5 subunit-containing receptors under the diazepam treatment counteracted the $\alpha_{2,3}$–effect, e.g. via some as yet unknown disinhibitory mechanism.

Again, these results accentuate the central role of SOM^+ INs and the α_5 subunit for the ACh effect. Moreover, CCK^+ INs and the $\alpha_{2,3}$ subunit may distinctly affect the lower frequency ranges during the presence of ACh.

4.3.3 Differences in LFP cross-correlations were strongest with ACh and $\alpha_{1,2,3}$-containing $GABA_A$R modulation

The action of ACh on network activity is not only characterized by a power shift from low to high frequencies, but also by decorrelation of neuronal firing (Chen et al., 2015; Goard and Dan, 2009). As local field potentials mostly reflect synaptic input into the local pool of neurons in the vicinity of the recording electrode, and there were no extracortical sources of synaptic input in the investigated slice cultures, a decorrelation of neuronal firing should be visible in a decorrelation of the field potential. Specifically, the burst parameter and spectral analysis hinted at the possibility of differences between the supra- and infragranular layers in terms of the interaction of ACh and $GABA_A$ receptor modulation. Hence, cross-correlations between signals filtered at the five different frequency bands mentioned above between the supra- and infragranular layers were analyzed. Cross-correlation can be understood as a measure of the similarity between two signals. For example, a decrease in correlation can be interpreted as more autonomic action of layers. Differences between both ACh conditions were detected for zolpidem at both concentrations, diazepam in the α_1 knock-in mutant, and L-655,708. ACh induced a decorrelation between layers together with zolpidem (0.2 µM) in the delta and theta frequency range and with zolpidem (1.0 µM) in the theta frequency range. For zolpidem, previous analyses revealed stronger differences between cholinergic conditions in the infragranular layers. Especially the decorrelation in the theta frequency band for zolpidem (1.0 µM) may be ascribed to the reduction of theta spectral power in the infragranular layer but not in the supragranular layer discussed above. As already pointed previously

and supported by these findings, effects of zolpidem (1.0 µM) are layer-dependent. Zolpidem (0.2 µM) decorrelations in the presence of ACh cannot be explained as intuitively. The delta and theta frequency band are the signature frequencies of LFP bursts while activity in higher frequency ranges may also be found outside of bursts. It is plausible that the larger reduction in burst rate by zolpidem (0.2 µM) in the infragranular layer (see burst parameter analysis) is responsible for the decorrelation seen between layers in the lower frequency bands.

By contrast, L-655,708 caused an ACh-dependent increase in correlations in the delta, theta and beta frequency bands suggesting that at least some of ACh's decorrelation action is mediated via $GABA_A$Rs containing the α_5 subunit. This finding is in agreement with Chen et al. (2015) who demonstrated that the cholinergic activation of SOM^+ INs – presynaptic to this receptor subunit – seems to be the major contributor to decorrelations. Interestingly, diazepam in WT did not alter correlations depending on the cholinergic status. This result suggests that the additional modulation of receptors with the $\alpha_{1,2,3}$ subunits counteracts the modulation of the α_5 subunit-containing receptors.

Overall, these findings illustrate that decorrelating effects of ACh rely on subtype-specific $GABA_A$R modulation. Moreover, decorrelation results provide evidence of layer-specific actions of ACh. Due to the specific activation of certain IN classes and postsynaptic receptor subunits with differential expression across layers, ACh affects different layers.

Additionally to analyzing the cross-correlation between LFP signals of the two layers, the 'instantaneous firing rate' (ifr) synthesized from action potential activity was correlated with LFP signals filtered in the five frequency bands as above for each layer separately. Especially in infragranular layers, differences were detected between the two ACh conditions. Zolpidem (1.0 µM) evoked strong decorrelations between the ifr and all frequency bands in the presence of ACh. Zolpidem (0.2 µM), on the other hand, only showed differences in the correlation between the ifr and the delta frequency. Hence, the modulation of the α_1 subunit-containing receptors together with the $\alpha_{2,3}$ subunit-containing receptors led to the most extended differences between cholinergic conditions. Presumably, the combined activation of PV^+ INs via PY neurons and CCK^+ INs may lead to more independent firing of these IN classes but also of PY neurons. This finding highlights the involvement of INs and according subunits other than SOM^+ cells with the corresponding α_5 subunit for decorrelation. The modulation of the $\alpha_{1,2,3,5}$ subunit-containing receptors (diazepam in WT) was not significantly affected by the presence or absence of ACh, similar to the results from the cross-correlational analysis between layers. However for the infragranular layer, effects were similar to $\alpha_{1,2,3}$ subunit-containing receptor modulations, only toned down. Again, the possibility that α_5 counteracts $\alpha_{1,2,3}$ activation to some degree in the presence of ACh seems supported. Firstly, Jiang et al. (2015) showed that Martinotti cells form connections to all other IN classes and PYs. Hence,

inhibition of PV^+ and CCK^+ activity may be the reason for smaller effects with diazepam than zolpidem. Secondly, the inhibition of PY cells by SOM^+ INs may down-regulate the PY-PV^+ feedback loop, which would decrease the effects of α_1 modulation. Similar to results from the LFP cross-correlation analysis, L-655,708 increased correlations in combination with ACh in comparison to the absence of ACh in the theta and beta frequency band. Again, evidence for the involvement of α_5 subunit for ACh-evoked decorrelation is provided.

To sum up, correlational differences for the two cholinergic conditions where especially pronounced with the modulation of the $\alpha_{1,2,3}$ subunit-containing receptors but weakened when $GABA_A$Rs with the α_5 subunit were additionally facilitated. This suggests that in the presence of ACh, α_5 subunit-containing $GABA_A$R at least partially counteract the action of $\alpha_{1,2,3}$-containing $GABA_A$R. Moreover, a blockade of α_5-mediated inhibition also caused differences between cholinergic conditions. However, in this case, the correlation was improved with ACh, indicating that α_5 is a main mediator of ACh-induced decorrelation of network activity as suggested by Chen et al. (2015).

4.3.4 ACh enhanced inhibitory efficacy of $\alpha_{1,2,3}$- and $\alpha_{1,2,3,5}$ $GABA_A$R modulator, but not of α_1 $GABA_A$R modulator

To understand the extracellular results on a cellular level, IPSCs were recorded from cortical pyramidal cells. The modulation of three different $GABA_A$R subunit combinations was tested in the presence and absence of ACh**:** $\alpha_{1\,(2,\,3)}$ (zolpidem 0.2 µm), $\alpha_{1,\,2,\,3}$ (zolpidem 1.0 µm), and $\alpha_{1,\,2,\,3,\,5}$ (diazepam 1.0 µm).

Across all four parameters analyzed (decay time, IPSC frequency, amplitude and total phasic current), $\alpha_{1,\,2,\,3}$ and $\alpha_{1,\,2,\,3,\,5}$ modulation was affected by the cholinergic status. While the decay time was shorter in the presence of ACh than in its absence when these subunits were modulated, frequency, amplitude and phasic current were larger in comparison to the absence of ACh. This finding points to an overall increase in inhibition when ACh is present. Since ACh alone already increased the inhibitory current as has been shown in the current project, it is not surprising that the additional modulation of $GABA_A$R subunits enhanced this effect. In contrast to results from extracellular burst parameter and cross-correlation analyses, effects of $\alpha_{1,\,2,\,3,\,5}$ and $\alpha_{1,\,2,\,3}$ subunit-containing receptor modulation on IPSCs were equally influenced by ACh. Thus, the IPSC data do not support the notion that α_5 counteracts $\alpha_{1,\,2,\,3}$ in the presence of ACh. This discrepancy may result from the experimentally required pharmacological blockade of the excitatory subnetwork during voltage clamp experiments. It is possible that excitatory input, which was present during extracellular recordings, is necessary to evoke the counterplay between $\alpha_{1,\,2,\,3}$ and α_5. Especially the PY input to PV^+ INs may be the key factor missing in this experimental condition. Without increased PY activity by ACh during voltage clamp

experiments, PV^+ INs may not be active and hence, modulation of the α_1 subunit might have no impact. To confirm this hypothesis, experiments are needed specifically investigating the interrelationship between α_1 and α_5 modulation.

A further indication of the importance of full network activity for unravelling the interaction between ACh and the GABAergic system is the fact that $\alpha_{1\,(2,\,3)}$ modulation was only affected by the ACh status in terms of IPSC frequency. Modulating $\alpha_{1\,(2,\,3)}$ in the presence of ACh increased IPSC frequency in comparison to the absence of ACh. In contrast to extracellular recordings where effects of $\alpha_{1\,(2,\,3)}$ modulation were enhanced on a number of parameters, IPSC results rather suggest an insensitivity of this subunit modulation to the cholinergic status. As stated above, network effects are very likely causal for differences between voltage clamp and extracellular results. As PV^+ INs presynaptic to α_1–containing receptors are likely not directly activated by ACh, a difference between the two ACh conditions is not expected. Differences detected in the extracellular data set most likely resulted from the activation of PY neurons by ACh, which in turn increase the activity of nearby PV^+ neurons. Hence, α_1 modulation in an intact network seems to indeed dependent on the cholinergic status. IPSC results underline the limitations of studying complex interactions like ACh and $GABA_AR$ subunit modulation on isolated subnetworks.

4.4 Summary

The current project was designed to investigate the effects of the cholinergic status on $GABA_AR$ modulation. Due to differential modulation of IN classes by ACh and specific IN-$GABA_AR$ coupling, it was hypothesized that $GABA_AR$ modulators should have different effects in the presence or absence of ACh. First, ACh alone was investigated on a range of experiments. Direct evidence for an increase in inhibition by ACh was provided in voltage clamp results by an increase in IPSC frequency and amplitude. Increased firing and burst rates in current clamp experiments indicated the more complex effects ACh had on a spontaneously active network.

Secondly, the effects of $GABA_AR$ modulators on the extracellular network were investigated in the presence and absence of ACh. Experiments involving L-655,708 and ACh supported the role of the α_5 subunit and consequently of SOM^+ INs in ACh´s desynchronizing and decorrelating effect as already reported by Chen et al. (2015). Additionally, data from zolpidem (1.0 µM) experiments suggest the involvement of CCK^+ INs as well. Here, further research is needed to confirm their role for the ACh effects. The lack of effects across different parameters investigated when diazepam was applied in the presence and absence of ACh implies that the α_1 and the α_5 subunit may counteract each other's effects when modulated together.

5 References

Ali, A.B., and Thomson, A.M. (2008). Synaptic alpha5 Subunit-Containing GABAA Receptors Mediate IPSPs Elicited by Dendrite-Preferring Cells in Rat Neocortex. Cereb Cortex *18*, 1260–1271.

Alitto, H.J., and Dan, Y. (2013). Cell-type-specific modulation of neocortical activity by basal forebrain input. Front. Syst. Neurosci. *6*, 79.

Alkondon, M., Pereira, E.F.R., Eisenberg, H.M., and Albuquerque, E.X. (2000). Nicotinic Receptor Activation in Human Cerebral Cortical Interneurons: a Mechanism for Inhibition and Disinhibition of Neuronal Networks. J Neurosci *20*, 66–75.

Amar, M., Lucas-Meunier, E., Baux, G., and Fossier, P. (2010). Blockade of different muscarinic receptor subtypes changes the equilibrium between excitation and inhibition in rat visual cortex. Neuroscience *169*, 1610–1620.

Antkowiak, B. (1999). Different Actions of General Anesthetics on the Firing Patterns of Neocortical Neurons Mediated by the GABAAReceptor. J. Am. Soc. Anesthesiol. *91*, 500–511.

Antkowiak, B., and Helfrich-Forster, C. (1998). Effects of Small Concentrations of Volatile Anesthetics on Action Potential Firing of Neocortical Neurons In Vitro. J. Am. Soc. Anesthesiol. *88*, 1592–1605.

Aracri, P., Consonni, S., Morini, R., Perrella, M., Rodighiero, S., Amadeo, A., and Becchetti, A. (2010). Tonic Modulation of GABA Release by Nicotinic Acetylcholine Receptors in Layer V of the Murine Prefrontal Cortex. Cereb Cortex *20*, 1539–1555.

Arbon, E.L., Knurowska, M., and Dijk, D.-J. (2015). Randomised clinical trial of the effects of prolonged-release melatonin, temazepam and zolpidem on slow-wave activity during sleep in healthy people. J. Psychopharmacol. (Oxf.) *29*, 764–776.

Armstrong, C., and Soltesz, I. (2012). Basket cell dichotomy in microcircuit function. J. Physiol. *590*, 683–694.

Arrigoni, E., Chamberlin, N.L., Saper, C.B., and McCarley, R.W. (2006). Adenosine inhibits basal forebrain cholinergic and noncholinergic neurons in vitro. Neuroscience *140*, 403–413.

Arroyo, S., Bennett, C., Aziz, D., Brown, S.P., and Hestrin, S. (2012). Prolonged Disynaptic Inhibition in the Cortex Mediated by Slow, Non-A7 Nicotinic Excitation of a Specific Subset of Cortical Interneurons. J. Neurosci. *32*, 3859–3864.

Ascoli, G.A., Alonso-Nanclares, L., Anderson, S.A., Barrionuevo, G., Benavides-Piccione, R., Burkhalter, A., Buzsáki, G., Cauli, B., DeFelipe, J., Fairén, A., et al. (2008). Petilla terminology: nomenclature of features of GABAergic interneurons of the cerebral cortex. Nat. Rev. Neurosci. *9*, 557–568.

Bacci, A., and Huguenard, J.R. (2006). Enhancement of Spike-Timing Precision by Autaptic Transmission in Neocortical Inhibitory Interneurons. Neuron *49*, 119–130.

Bacci, A., Huguenard, J.R., and Prince, D.A. (2003). Functional Autaptic Neurotransmission in Fast-Spiking Interneurons: A Novel Form of Feedback Inhibition in the Neocortex. J. Neurosci. *23*, 859–866.

Bacci, A., Huguenard, J.R., and Prince, D.A. (2005). Modulation of neocortical interneurons: extrinsic influences and exercises in self-control. Trends Neurosci. *28*, 602–610.

Banks, M.I., White, J.A., and Pearce, R.A. (2000). Interactions between distinct GABA(A) circuits in hippocampus. Neuron *25*, 449–457.

Baratta, J., Ha, D.H., Weiss, J.H., Yu, J., and Robertson, R.T. (1996). Cholinergic neurons from different subdivisions of the basal forebrain lack connectional specificity for cerebral cortical target sites in vitro. Dev. Brain Res. *97*, 143–147.

Beierlein, M., Gibson, J.R., and Connors, B.W. (2003). Two Dynamically Distinct Inhibitory Networks in Layer 4 of the Neocortex. J. Neurophysiol. *90*, 2987–3000.

Berger, T.K., Silberberg, G., Perin, R., and Markram, H. (2010). Brief Bursts Self-Inhibit and Correlate the Pyramidal Network. PLoS Biol *8*, e1000473.

Blatow, M., Rozov, A., Katona, I., Hormuzdi, S.G., Meyer, A.H., Whittington, M.A., Caputi, A., and Monyer, H. (2003). A Novel Network of Multipolar Bursting Interneurons Generates Theta Frequency Oscillations in Neocortex. Neuron *38*, 805–817.

Bloem, B., Poorthuis, R.B., and Mansvelder, H.D. (2014). Cholinergic modulation of the medial prefrontal cortex: the role of nicotinic receptors in attention and regulation of neuronal activity. Front. Neural Circuits *8*, 17.

Broussard, J.I., Karelina, K., Sarter, M., and Givens, B. (2009). Cholinergic optimization of cue-evoked parietal activity during challenged attentional performance. Eur. J. Neurosci. *29*, 1711–1722.

Brown, C.D., and Davis, H.T. (2006). Receiver operating characteristics curves and related decision measures: A tutorial. Chemom. Intell. Lab. Syst. *80*, 24–38.

Brunner, D.P., Dijk, D.-J., Münch, M., and Borbély, A.A. (1991). Effect of zolpidem on sleep and sleep EEG spectra in healthy young men. Psychopharmacology (Berl.) *104*, 1–5.

Buhl, E.H., Tamás, G., and Fisahn, A. (1998). Cholinergic activation and tonic excitation induce persistent gamma oscillations in mouse somatosensory cortex *in vitro*. J. Physiol. *513*, 117–126.

Cape, E.G., Manns, I.D., Alonso, A., Beaudet, A., and Jones, B.E. (2000). Neurotensin-Induced Bursting of Cholinergic Basal Forebrain Neurons Promotes gamma and theta Cortical Activity Together with Waking and Paradoxical Sleep. J Neurosci *20*, 8452–8461.

Caraiscos, V.B., Newell, J.G., You-Ten, K.E., Elliott, E.M., Rosahl, T.W., Wafford, K.A., MacDonald, J.F., and Orser, B.A. (2004). Selective Enhancement of Tonic GABAergic Inhibition in Murine Hippocampal Neurons by Low Concentrations of the Volatile Anesthetic Isoflurane. J Neurosci *24*, 8454–8458.

Cardin, J.A., Carlen, M., Meletis, K., Knoblich, U., Zhang, F., Deisseroth, K., Tsai, L.-H., and Moore, C.I. (2009). Driving fast-spiking cells induces gamma rhythm and controls sensory responses. Nature *459*, 663–667.

Carruthers, S.P., Gurvich, C.T., and Rossell, S.L. (2015). The muscarinic system, cognition and schizophrenia. Neurosci. Biobehav. Rev. *55*, 393–402.

Castro-Alamancos, M.A., and Gulati, T. (2014). Neuromodulators Produce Distinct Activated States in Neocortex. J. Neurosci. *34*, 12353–12367.

Chen, N., Sugihara, H., and Sur, M. (2015). An acetylcholine-activated microcircuit drives temporal dynamics of cortical activity. Nat. Neurosci. *18*, 892–902.

Consonni, S., Leone, S., Becchetti, A., and Amadeo, A. (2009). Developmental and neurochemical features of cholinergic neurons in the murine cerebral cortex. BMC Neurosci. *10*, 18.

Constantinople, C.M., and Bruno, R.M. (2013). Deep Cortical Layers Are Activated Directly by Thalamus. Science *340*, 1591–1594.

Cruikshank, S.J., Lewis, T.J., and Connors, B.W. (2007). Synaptic basis for intense thalamocortical activation of feedforward inhibitory cells in neocortex. Nat. Neurosci. *10*, 462–468.

Cumming, G., Fidler, F., and Vaux, D.L. (2007). Error bars in experimental biology. J. Cell Biol. *177*, 7–11.

Czarnecki, A., Tscherter, A., and Streit, J. (2012). Network activity and spike discharge oscillations in cortical slice cultures from neonatal rat. Eur. J. Neurosci. *35*, 375–388.

De Simoni, A., Griesinger, C.B., and Edwards, F.A. (2003). Development of Rat CA1 Neurones in Acute Versus Organotypic Slices: Role of Experience in Synaptic Morphology and Activity. J. Physiol. *550*, 135–147.

Debanne, D., Guerineau, N.C., Gahwiler, B.H., and Thompson, S.M. (1995). Physiology and pharmacology of unitary synaptic connections between pairs of cells in areas CA3 and CA1 of rat hippocampal slice cultures. J. Neurophysiol. *73*, 1282–1294.

DeFelipe, J., López-Cruz, P.L., Benavides-Piccione, R., Bielza, C., Larrañaga, P., Anderson, S., Burkhalter, A., Cauli, B., Fairén, A., Feldmeyer, D., et al. (2013). New insights into the classification and nomenclature of cortical GABAergic interneurons. Nat. Rev. Neurosci. *14*, 202–216.

Desai, N.S., Rutherford, L.C., and Turrigiano, G.G. (1999). Plasticity in the intrinsic excitability of cortical pyramidal neurons. Nat. Neurosci. *2*, 515–520.

Descarries, L. (1998). The hypothesis of an ambient level of acetylcholine in the central nervous system. J. Physiol.-Paris *92*, 215–220.

Destexhe, A., and Paré, D. (1999). Impact of network activity on the integrative properties of neocortical pyramidal neurons in vivo. J. Neurophysiol. *81*, 1531–1547.

Destexhe, A., Rudolph, M., and Paré, D. (2003). The high-conductance state of neocortical neurons in vivo. Nat. Rev. Neurosci. *4*, 739–751.

Disney, A.A., and Aoki, C. (2008). Muscarinic acetylcholine receptors in macaque V1 are most frequently expressed by parvalbumin-immunoreactive neurons. J. Comp. Neurol. *507*, 1748–1762.

Distler, P.G., and Robertson, R.T. (1992). Development of AChE-positive neuronal projections from basal forebrain to cerebral cortex in organotypic tissue slice cultures. Brain Res. Dev. Brain Res. *67*, 181–196.

Distler, P.G., and Robertson, R.T. (1993). Formation of synapses between basal forebrain afferents and cerebral cortex neurons: an electron microscopic study in organotypic slice cultures. J. Neurocytol. *22*, 627–643.

Drexler, B., Jurd, R., Rudolph, U., and Antkowiak, B. (2009). Distinct actions of etomidate and propofol at β3-containing γ-aminobutyric acid type A receptors. Neuropharmacology *57*, 446–455.

Drexler, B., Hentschke, H., Antkowiak, B., and Grasshoff, C. (2010). Organotypic Cultures as Tools for Testing Neuroactive Drugs – Link Between In-Vitro and In-Vivo Experiments. Curr. Med. Chem. *17*, 4538–4550.

Eckenstein, F.P., Baughman, R.W., and Quinn, J. (1988). An anatomical study of cholinergic innervation in rat cerebral cortex. Neuroscience *25*, 457–474.

Eggermann, E., Kremer, Y., Crochet, S., and Petersen, C.C.H. (2014). Cholinergic Signals in Mouse Barrel Cortex during Active Whisker Sensing. Cell Rep. *9*, 1654–1660.

Engelhardt, J. von, Eliava, M., Meyer, A.H., Rozov, A., and Monyer, H. (2007). Functional Characterization of Intrinsic Cholinergic Interneurons in the Cortex. J. Neurosci. *27*, 5633–5642.

Erceg-Hurn, D.M., and Mirosevich, V.M. (2008). Modern robust statistical methods: An easy way to maximize the accuracy and power of your research. Am. Psychol. *63*, 591–601.

Fanselow, E.E., and Connors, B.W. (2010). The Roles of Somatostatin-Expressing (GIN) and Fast-Spiking Inhibitory Interneurons in up-down States of Mouse Neocortex. J. Neurophysiol. *104*, 596–606.

Fanselow, E.E., Richardson, K.A., and Connors, B.W. (2008). Selective, State-Dependent Activation of Somatostatin-Expressing Inhibitory Interneurons in Mouse Neocortex. J Neurophysiol *100*, 2640–2652.

Fino, E., Packer, A.M., and Yuste, R. (2013). The Logic of Inhibitory Connectivity in the Neocortex. The Neuroscientist *19*, 228–237.

Freund, T.F. (2003). Interneuron Diversity series: Rhythm and mood in perisomatic inhibition. Trends Neurosci. *26*, 489–495.

Freund, T.F., and Katona, I. (2007). Perisomatic Inhibition. Neuron *56*, 33–42.

Fries, P., Nikolić, D., and Singer, W. (2007). The gamma cycle. Trends Neurosci. *30*, 309–316.

Fritschy, J.-M., and Mohler, H. (1995). GABAA-receptor heterogeneity in the adult rat brain: Differential regional and cellular distribution of seven major subunits. J. Comp. Neurol. *359*, 154–194.

Fritschy, J.-M., and Panzanelli, P. (2014). GABAA receptors and plasticity of inhibitory neurotransmission in the central nervous system. Eur. J. Neurosci. *39*, 1845–1865.

Gähwiler, B.H., and Hefti, F. (1984). Guidance of acetylcholinesterase-containing fibres by target tissue in co-cultured brain slices. Neuroscience *13*, 681–689.

Gähwiler, B.H., Capogna, M., Debanne, D., McKinney, R.A., and Thompson, S.M. (1997). Organotypic slice cultures: a technique has come of age. Trends Neurosci. *20*, 471–477.

Gentet, L.J., Kremer, Y., Taniguchi, H., Huang, Z.J., Staiger, J.F., and Petersen, C.C.H. (2012). Unique functional properties of somatostatin-expressing GABAergic neurons in mouse barrel cortex. Nat. Neurosci. *15*, 607–612.

Gibson, J.R., Beierlein, M., and Connors, B.W. (1999). Two networks of electrically coupled inhibitory neurons in neocortex. Nature *402*, 75–79.

Gigout, S., Jones, G.A., Wierschke, S., Davies, C.H., Watson, J.M., and Deisz, R.A. (2012). Distinct muscarinic acetylcholine receptor subtypes mediate pre- and postsynaptic effects in rat neocortex. BMC Neurosci. *13*, 42.

Glykys, J., and Mody, I. (2007). The main source of ambient GABA responsible for tonic inhibition in the mouse hippocampus. J. Physiol. *582*, 1163–1178.

Goard, M., and Dan, Y. (2009). Basal forebrain activation enhances cortical coding of natural scenes. Nat. Neurosci. *12*, 1444–1449.

Gonzalez-Burgos, G., and Lewis, D.A. (2008). GABA Neurons and the Mechanisms of Network Oscillations: Implications for Understanding Cortical Dysfunction in Schizophrenia. Schizophr. Bull. *34*, 944–961.

Gould, R.W., Dencker, D., Grannan, M., Bubser, M., Zhan, X., Wess, J., Xiang, Z., Locuson, C., Lindsley, C.W., Conn, P.J., et al. (2015). Role for the M1 Muscarinic Acetylcholine Receptor in Top-Down Cognitive Processing Using a Touchscreen Visual Discrimination Task in Mice. ACS Chem. Neurosci. *6*, 1683–1695.

Griffith, W.H., and Matthews, R.T. (1986). Electrophysiology of AChE-positive neurons in basal forebrain slices. Neurosci. Lett. *71*, 169–174.

Grissom, R.J. (1994). Probability of the Superior Outcome of One Treatment Over Another. J. Appl. Psychol. *79*, 314.

Grissom, R.J., and Kim, J.J. (2012). Effect Sizes for Research (New York, NY, US: Routledge).

Gulledge, A.T., and Stuart, G.J. (2005). Cholinergic Inhibition of Neocortical Pyramidal Neurons. J Neurosci *25*, 10308–10320.

Gulledge, A.T., Park, S.B., Kawaguchi, Y., and Stuart, G.J. (2007). Heterogeneity of Phasic Cholinergic Signaling in Neocortical Neurons. J Neurophysiol *97*, 2215–2229.

Gulledge, A.T., Bucci, D.J., Zhang, S.S., Matsui, M., and Yeh, H.H. (2009). M1 Receptors Mediate Cholinergic Modulation of Excitability in Neocortical Pyramidal Neurons. J Neurosci *29*, 9888–9902.

Gupta, A., Wang, Y., and Markram, H. (2000). Organizing Principles for a Diversity of GABAergic Interneurons and Synapses in the Neocortex. Science *287*, 273–278.

Ha, D.H., Robertson, R.T., Roshanaei, M., and Weiss, J.H. (1999). Enhanced survival and morphological features of basal forebrain cholinergic neurons in vitro: Role of neurotrophins and other potential cortically derived cholinergic trophic factors. J. Comp. Neurol. *406*, 156–170.

Haider, B., and McCormick, D.A. (2009). Rapid Neocortical Dynamics: Cellular and Network Mechanisms. Neuron *62*, 171–189.

Hájos, N., Papp, E.C., Acsády, L., Levey, A.I., and Freund, T.F. (1997). Distinct interneuron types express m2 muscarinic receptor immunoreactivity on their dendrites or axon terminals in the hippocampus. Neuroscience *82*, 355–376.

Hasenstaub, A., Shu, Y., Haider, B., Kraushaar, U., Duque, A., and McCormick, D.A. (2005). Inhibitory Postsynaptic Potentials Carry Synchronized Frequency Information in Active Cortical Networks. Neuron *47*, 423–435.

Hasselmo, M.E., and McGaughy, J. (2004). High acetylcholine levels set circuit dynamics for attention and encoding and low acetylcholine levels set dynamics for consolidation. Prog. Brain Res. *145*, 207–231.

Hasselmo, M.E., and Sarter, M. (2011). Modes and Models of Forebrain Cholinergic Neuromodulation of Cognition. Neuropsychopharmacology *36*, 52–73.

Hedrick, T., and Waters, J. (2015). Acetylcholine excites neocortical pyramidal neurons via nicotinic receptors. J. Neurophysiol. *113*, 2195–2209.

Hentschke, H., and Stüttgen, M.C. (2011). Computation of measures of effect size for neuroscience data sets. Eur. J. Neurosci. *34*, 1887–1894.

Hodgkins, P.S., and Schwarcz, R. (1998). Interference with cellular energy metabolism reduces kynurenic acid formation in rat brain slices: reversal by lactate and pyruvate. Eur. J. Neurosci. *10*, 1986–1994.

Holmgren, C.D., Mukhtarov, M., Malkov, A.E., Popova, I.Y., Bregestovski, P., and Zilberter, Y. (2010). Energy substrate availability as a determinant of neuronal resting potential, GABA signaling and spontaneous network activity in the neonatal cortex in vitro. J. Neurochem. *112*, 900–912.

Hu, H., Gan, J., and Jonas, P. (2014). Fast-spiking, parvalbumin+ GABAergic interneurons: From cellular design to microcircuit function. Science *345*, 1255263.

Isaacson, J.S., and Scanziani, M. (2011). How Inhibition Shapes Cortical Activity. Neuron *72*, 231–243.

Jiang, M., Zhu, J., Liu, Y., Yang, M., Tian, C., Jiang, S., Wang, Y., Guo, H., Wang, K., and Shu, Y. (2012). Enhancement of Asynchronous Release from Fast-Spiking Interneuron in Human and Rat Epileptic Neocortex. PLoS Biol *10*, e1001324.

Jiang, X., Shen, S., Cadwell, C.R., Berens, P., Sinz, F., Ecker, A.S., Patel, S., and Tolias, A.S. (2015). Principles of connectivity among morphologically defined cell types in adult neocortex. Science *350*, aac9462.

Jiménez-Capdeville, M.E., and Dykes, R.W. (1996). Changes in cortical acetylcholine release in the rat during day and night: differences between motor and sensory areas. Neuroscience *71*, 567–579.

Johnson, H.A., and Buonomano, D.V. (2007). Development and Plasticity of Spontaneous Activity and Up States in Cortical Organotypic Slices. J. Neurosci. *27*, 5915–5925.

Kalmbach, A., and Waters, J. (2014). Modulation of high- and low-frequency components of the cortical local field potential via nicotinic and muscarinic acetylcholine receptors in anesthetized mice. J. Neurophysiol. *111*, 258–272.

Kawaguchi, Y. (1993). Groupings of nonpyramidal and pyramidal cells with specific physiological and morphological characteristics in rat frontal cortex. J. Neurophysiol. *69*, 416–431.

Kawaguchi, Y. (1995). Physiological subgroups of nonpyramidal cells with specific morphological characteristics in layer II/III of rat frontal cortex. J. Neurosci. *15*, 2638–2655.

Kawaguchi, Y. (1997). Selective Cholinergic Modulation of Cortical GABAergic Cell Subtypes. J Neurophysiol *78*, 1743–1747.

Kawaguchi, Y., and Kondo, S. (2002). Parvalbumin, somatostatin and cholecystokinin as chemical markers for specific GABAergic interneuron types in the rat frontal cortex. J. Neurocytol. *31*, 277–287.

Kawaguchi, Y., and Kubota, Y. (1996). Physiological and morphological identification of somatostatin- or vasoactive intestinal polypeptide-containing cells among GABAergic cell subtypes in rat frontal cortex. J. Neurosci. Off. J. Soc. Neurosci. *16*, 2701–2715.

Kawaguchi, Y., and Kubota, Y. (1997). GABAergic cell subtypes and their synaptic connections in rat frontal cortex. Cereb. Cortex N. Y. N 1991 *7*, 476–486.

Kawaguchi, Y., and Kubota, Y. (1998). Neurochemical features and synaptic connections of large physiologically-identified GABAergic cells in the rat frontal cortex. Neuroscience *85*, 677–701.

Kepecs, A., and Fishell, G. (2014). Interneuron cell types are fit to function. Nature *505*, 318–326.

Kim, J., Matney, C.J., Blankenship, A., Hestrin, S., and Brown, S.P. (2014). Layer 6 Corticothalamic Neurons Activate a Cortical Output Layer, Layer 5a. J. Neurosci. *34*, 9656–9664.

Kimura, F. (2000). Cholinergic modulation of cortical function: A hypothetical role in shifting the dynamics in cortical network. Neurosci. Res. *38*, 19–26.

Klausberger, T., Roberts, J.D.B., and Somogyi, P. (2002). Cell Type- and Input-Specific Differences in the Number and Subtypes of Synaptic GABAA Receptors in the Hippocampus. J Neurosci *22*, 2513–2521.

Klostermann, O., and Wahle, P. (1999). Patterns of spontaneous activity and morphology of interneuron types in organotypic cortex and thalamus–cortex cultures. Neuroscience *92*, 1243–1259.

Kondo, S., and Kawaguchi, Y. (2001). Slow synchronized bursts of inhibitory postsynaptic currents (0.1-0.3 Hz) by cholinergic stimulation in the rat frontal cortex in vitro. Neuroscience *107*, 551–560.

Korpi, E.R., and Sinkkonen, S.T. (2006). GABAA receptor subtypes as targets for neuropsychiatric drug development. Pharmacol. Ther. *109*, 12–32.

Krause, B.M., Raz, A., Uhlrich, D.J., Smith, P.H., and Banks, M.I. (2014). Spiking in auditory cortex following thalamic stimulation is dominated by cortical network activity. Front. Syst. Neurosci. *8*, 170.

Krishnamurthy, P., Silberberg, G., and Lansner, A. (2012). A Cortical Attractor Network with Martinotti Cells Driven by Facilitating Synapses. PLoS ONE *7*, e30752.

Kruglikov, I., and Rudy, B. (2008). Perisomatic GABA Release and Thalamocortical Integration onto Neocortical Excitatory Cells Are Regulated by Neuromodulators. Neuron *58*, 911–924.

Kuczewski, N., Aztiria, E., Gautam, D., Wess, J., and Domenici, L. (2005). Acetylcholine modulates cortical synaptic transmission via different muscarinic receptors, as studied with receptor knockout mice. J. Physiol. *566*, 907–919.

Kuki, T., Fujihara, K., Miwa, H., Tamamaki, N., Yanagawa, Y., and Mushiake, H. (2015). Contribution of parvalbumin and somatostatin-expressing GABAergic neurons to slow oscillations and the balance in beta-gamma oscillations across cortical layers. Front. Neural Circuits *9*, 6.

Lecea, L. de, del Ri´o, J., and Soriano, E. (1995). Developmental expression of parvalbumin mRNA in the cerebral cortex and hippocampus of the rat. Mol. Brain Res. *32*, 1–13.

Levitt, P., Eagleson, K.L., and Powell, E.M. (2004). Regulation of neocortical interneuron development and the implications for neurodevelopmental disorders. Trends Neurosci. *27*, 400–406.

Levy, R.B., Reyes, A.D., and Aoki, C. (2006). Nicotinic and Muscarinic Reduction of Unitary Excitatory Postsynaptic Potentials in Sensory Cortex; Dual Intracellular Recording In Vitro. J Neurophysiol *95*, 2155–2166.

de Lima, A.D., and Morrison, J.H. (1989). Ultrastructural analysis of somatostatin-immunoreactive neurons and synapses in the temporal and occipital cortex of the macaque monkey. J. Comp. Neurol. *283*, 212–227.

Lucas-Meunier, E., Monier, C., Amar, M., Baux, G., Frégnac, Y., and Fossier, P. (2009). Involvement of Nicotinic and Muscarinic Receptors in the Endogenous Cholinergic Modulation of the Balance between Excitation and Inhibition in the Young Rat Visual Cortex. Cereb. Cortex *19*, 2411–2427.

Ma, Y., Hu, H., Berrebi, A.S., Mathers, P.H., and Agmon, A. (2006). Distinct Subtypes of Somatostatin-Containing Neocortical Interneurons Revealed in Transgenic Mice. J. Neurosci. *26*, 5069–5082.

Mann, E.O., Kohl, M.M., and Paulsen, O. (2009). Distinct Roles of GABAA and GABAB Receptors in Balancing and Terminating Persistent Cortical Activity. J. Neurosci. *29*, 7513–7518.

Manns, I.D., Alonso, A., and Jones, B.E. (2000). Discharge Properties of Juxtacellularly Labeled and Immunohistochemically Identified Cholinergic Basal Forebrain Neurons Recorded in Association with the Electroencephalogram in Anesthetized Rats. J. Neurosci. *20*, 1505–1518.

Markram, H., Toledo-Rodriguez, M., Wang, Y., Gupta, A., Silberberg, G., and Wu, C. (2004). Interneurons of the neocortical inhibitory system. Nat Rev Neurosci *5*, 793–807.

Marlin, J.J., and Carter, A.G. (2014). GABA-A Receptor Inhibition of Local Calcium Signaling in Spines and Dendrites. J. Neurosci. *34*, 15898–15911.

Marrosu, F., Portas, C., Mascia, M.S., Casu, M.A., Fà, M., Giagheddu, M., Imperato, A., and Gessa, G.L. (1995). Microdialysis measurement of cortical and hippocampal acetylcholine release during sleep-wake cycle in freely moving cats. Brain Res. *671*, 329–332.

McCormick, D.A., Connors, B.W., Lighthall, J.W., and Prince, D.A. (1985). Comparative electrophysiology of pyramidal and sparsely spiny stellate neurons of the neocortex. J. Neurophysiol. *54*, 782–806.

Metherate, R., Cox, C.L., and Ashe, J.H. (1992). Cellular bases of neocortical activation: modulation of neural oscillations by the nucleus basalis and endogenous acetylcholine. J. Neurosci. *12*, 4701–4711.

Mobley, W.C., Rutkowski, J.L., Tennekoon, G.I., Gemski, J., Buchanan, K., and Johnston, M.V. (1986). Nerve growth factor increases choline acetyltransferase activity in developing basal forebrain neurons. Mol. Brain Res. *1*, 53–62.

Munakata, M., Jin, Y.-H., Akaike, N., and Nielsen, M. (1998). Temperature-dependent effect of zolpidem on the GABAA receptor-mediated response at recombinant human GABAA receptor subtypes. Brain Res. *807*, 199–202.

Murayama, M., Pérez-Garci, E., Nevian, T., Bock, T., Senn, W., and Larkum, M.E. (2009). Dendritic encoding of sensory stimuli controlled by deep cortical interneurons. Nature *457*, 1137–1141.

Nassar, M., Simonnet, J., Lofredi, R., Cohen, I., Savary, E., Yanagawa, Y., Miles, R., and Fricker, D. (2015). Diversity and overlap of parvalbumin and somatostatin expressing interneurons in mouse presubiculum. Front. Neural Circuits 20.

Nawrot, M., Aertsen, A., and Rotter, S. (1999). Single-trial estimation of neuronal firing rates: From single-neuron spike trains to population activity. J. Neurosci. Methods *94*, 81–92.

Neske, G.T., Patrick, S.L., and Connors, B.W. (2015). Contributions of Diverse Excitatory and Inhibitory Neurons to Recurrent Network Activity in Cerebral Cortex. J. Neurosci. *35*, 1089–1105.

Nyíri, G., Freund, T.F., and Somogyi, P. (2001). Input-dependent synaptic targeting of alpha2-subunit-containing GABA(A) receptors in synapses of hippocampal pyramidal cells of the rat. Eur. J. Neurosci. *13*, 428–442.

Okun, M., and Lampl, I. (2008). Instantaneous correlation of excitation and inhibition during ongoing and sensory-evoked activities. Nat. Neurosci. *11*, 535–537.

Oldford, E., and Castro-Alamancos, M.A. (2003). Input-specific effects of acetylcholine on sensory and intracortical evoked responses in the “barrel cortex” in vivo. Neuroscience *117*, 769–778.

Olsen, R.W., and Sieghart, W. (2009). GABAA receptors: Subtypes provide diversity of function and pharmacology. Neuropharmacology *56*, 141–148.

Otsuka, T., and Kawaguchi, Y. (2008). Firing-Pattern-Dependent Specificity of Cortical Excitatory Feed-Forward Subnetworks. J. Neurosci. *28*, 11186–11195.

Otsuka, T., and Kawaguchi, Y. (2009). Cortical Inhibitory Cell Types Differentially Form Intralaminar and Interlaminar Subnetworks withExcitatory Neurons. J Neurosci *29*, 10533–10540.

Öztuna, D., Elhan, A.H., and Tüccar, E. (2006). Investigation of Four Different Normality Tests in Terms of Type 1 Error Rate and Power under Different Distributions. Turk. J. Med. Sci. *36*, 171–176.

Pafundo, D.E., Miyamae, T., Lewis, D.A., and Gonzalez-Burgos, G. (2013). Cholinergic modulation of neuronal excitability and recurrent excitation-inhibition in prefrontal cortex circuits: implications for gamma oscillations. J. Physiol. *591*, 4725–4748.

Parikh, V., Kozak, R., Martinez, V., and Sarter, M. (2007). Prefrontal acetylcholine release controls cue detection on multiple time scales. Neuron *56*, 141–154.

Parikh, V., Man, K., Decker, M.W., and Sarter, M. (2008). Glutamatergic Contributions to Nicotinic Acetylcholine Receptor Agonist-Evoked Cholinergic Transients in the Prefrontal Cortex. J. Neurosci. *28*, 3769–3780.

Pfeffer, C.K., Xue, M., He, M., Huang, Z.J., and Scanziani, M. (2013). Inhibition of inhibition in visual cortex: the logic of connections between molecularly distinct interneurons. Nat. Neurosci. *16*, 1068–1076.

Picciotto, M.R., Higley, M.J., and Mineur, Y.S. (2012). Acetylcholine as a Neuromodulator: Cholinergic Signaling Shapes Nervous System Function and Behavior. Neuron *76*, 116–129.

Pineda, J.C., Bargas, J., Flores-Hernández, J., and Galarraga, E. (1995). Muscarinic receptors modulate the afterhyperpolarizing potential in neostriatal neurons. Eur. J. Pharmacol. *281*, 271–277.

Porter, J.T., Cauli, B., Tsuzuki, K., Lambolez, B., Rossier, J., and Audinat, E. (1999). Selective Excitation of Subtypes of Neocortical Interneurons by Nicotinic Receptors. J Neurosci *19*, 5228–5235.

Puia, G., Vicini, S., Seeburg, P., and Costa, E. (1991). Influence of Recombinant gamma-Aminobutyric Acid(a)-Receptor Subunit Composition on the Action of Allosteric Modulators of gamma-Aminobutyric Acid-Gated Cl Currents. Mol Pharmacol *39*, 691–696.

Puig, M.V., Ushimaru, M., and Kawaguchi, Y. (2008). Two distinct activity patterns of fast-spiking interneurons during neocortical UP states. Proc. Natl. Acad. Sci. *105*, 8428–8433.

Quirk, K., Blurton, P., Fletcher, S., Leeson, P., Tang, F., Mellilo, D., Ragan, C.I., and McKernan, R.M. (1996). [3H]L-655,708, a novel ligand selective for the benzodiazepine site of GABAA receptors which contain the alpha 5 subunit. Neuropharmacology *35*, 1331–1335.

Razali, N.M., and Wah, Y.B. (2011). Power comparisons of Shapiro-Wilk, Kolmogorov-Smirnov, Lilliefors and Anderson-Darling tests. J. Stat. Model. Anal. *2*, 21–33.

Razik, D.S., Hawellek, D.J., Antkowiak, B., and Hentschke, H. (2013). Impairment of GABA transporter GAT-1 terminates cortical recurrent network activity via enhanced phasic inhibition. Front. Neural Circuits *7*, 141.

Reyes, A., Lujan, R., Rozov, A., Burnashev, N., Somogyi, P., and Sakmann, B. (1998). Target-cell-specific facilitation and depression in neocortical circuits. Nat. Neurosci. *1*, 279–285.

Rio, C.A.C., Lawrence, J.J., Tricoire, L., Erdelyi, F., Szabo, G., and McBain, C.J. (2010). M3 Muscarinic Acetylcholine Receptor Expression Confers Differential Cholinergic Modulation to Neurochemically Distinct Hippocampal Basket Cell Subtypes. J. Neurosci. *30*, 6011–6024.

Roopun, A.K., LeBeau, F.E.N., Rammell, J., Cunningham, M.O., Traub, R.D., and Whittington, M.A. (2010). Cholinergic Neuromodulation Controls Directed Temporal Communication in Neocortex in Vitro. Front Neural Circuits *4*.

Rossignol, E., Kruglikov, I., van den Maagdenberg, A.M.J.M., Rudy, B., and Fishell, G. (2013). CaV 2.1 ablation in cortical interneurons selectively impairs fast-spiking basket cells and causes generalized seizures. Ann. Neurol. *74*, 209–222.

Rotaru, D.C., Barrionuevo, G., and Sesack, S.R. (2005). Mediodorsal thalamic afferents to layer III of the rat prefrontal cortex: Synaptic relationships to subclasses of interneurons. J. Comp. Neurol. *490*, 220–238.

Rudolph, U., and Antkowiak, B. (2004). Molecular and neuronal substrates for general anaesthetics. Nat Rev Neurosci *5*, 709–720.

Rudolph, U., and Möhler, H. (2014). GABAA Receptor Subtypes: Therapeutic Potential in Down Syndrome, Affective Disorders, Schizophrenia, and Autism. Annu. Rev. Pharmacol. Toxicol. *54*, 483–507.

Rudy, B., Fishell, G., Lee, S., and Hjerling-Leffler, J. (2011). Three groups of interneurons account for nearly 100% of neocortical GABAergic neurons. Dev. Neurobiol. *71*, 45–61.

Runfeldt, M.J., Sadovsky, A.J., and MacLean, J.N. (2014). Acetylcholine functionally reorganizes neocortical microcircuits. J. Neurophysiol. *112*, 1205–1216.

Salgado, H., Bellay, T., Nichols, J.A., Bose, M., Martinolich, L., Perrotti, L., and Atzori, M. (2007). Muscarinic M2 and M1 receptors reduce GABA release by Ca2+ channel modulation through activation of PI3K/Ca2+ -independent and PLC/Ca2+ -dependent PKC. J. Neurophysiol. *98*, 952–965.

Sanchez-Vives, M.V., and McCormick, D.A. (2000). Cellular and network mechanisms of rhythmic recurrent activity in neocortex. Nat. Neurosci. *3*, 1027–1034.

Sanchez-Vives, M.V., Mattia, M., Compte, A., Perez-Zabalza, M., Winograd, M., Descalzo, V.F., and Reig, R. (2010). Inhibitory Modulation of Cortical Up States. J. Neurophysiol. *104*, 1314–1324.

Sanna, E., Busonero, F., Talani, G., Carta, M., Massa, F., Peis, M., Maciocco, E., and Biggio, G. (2002). Comparison of the effects of zaleplon, zolpidem, and triazolam at various GABAA receptor subtypes. Eur. J. Pharmacol. *451*, 103–110.

Sarter, M., Parikh, V., and Howe, W.M. (2009). Phasic acetylcholine release and the volume transmission hypothesis: time to move on. Nat Rev Neurosci *10*, 383–390.

Sarter, M., Lustig, C., Howe, W.M., Gritton, H., and Berry, A.S. (2014). Deterministic functions of cortical acetylcholine. Eur. J. Neurosci. *39*, 1912–1920.

Scheffzük, C., Kukushka, V.I., Vyssotski, A.L., Draguhn, A., Tort, A.B.L., and Brankačk, J. (2013). Global slowing of network oscillations in mouse neocortex by diazepam. Neuropharmacology *65*, 123–133.

Schüz, A., and Miller, R. (2002). Cortical Areas: Unity and Diversity (London: Taylor & Francis).

Selden, N.R., Gitelman, D.R., Salamon-Murayama, N., Parrish, T.B., and Mesulam, M.M. (1998). Trajectories of cholinergic pathways within the cerebral hemispheres of the human brain. Brain *121*, 2249–2257.

Serwanski, D.R., Miralles, C.P., Christie, S.B., Mehta, A.K., Li, X., and De Blas, A.L. (2006). Synaptic and nonsynaptic localization of GABAA receptors containing the α5 subunit in the rat brain. J. Comp. Neurol. *499*, 458–470.

Sigel, E., and Buhr, A. (1997). The benzodiazepine binding site of GABAA receptors. Trends Pharmacol. Sci. *18*, 425–429.

Silberberg, G., and Markram, H. (2007). Disynaptic Inhibition between Neocortical Pyramidal Cells Mediated by Martinotti Cells. Neuron *53*, 735–746.

Sohal, V.S., Zhang, F., Yizhar, O., and Deisseroth, K. (2009). Parvalbumin neurons and gamma rhythms enhance cortical circuit performance. Nature *459*, 698–702.

Steriade, M., Nunez, A., and Amzica, F. (1993). A novel slow (< 1 Hz) oscillation of neocortical neurons in vivo: depolarizing and hyperpolarizing components. J. Neurosci. *13*, 3252–3265.

Steriade, M., Contreras, D., Amzica, F., and Timofeev, I. (1996). Synchronization of fast (30-40 Hz) spontaneous oscillations in intrathalamic and thalamocortical networks. J. Neurosci. *16*, 2788–2808.

Steriade, M., Timofeev, I., and Grenier, F. (2001). Natural Waking and Sleep States: A View From Inside Neocortical Neurons. J. Neurophysiol. *85*, 1969–1985.

Suffczynski, P., Crone, N.E., and Franaszczuk, P.J. (2014). Afferent inputs to cortical fast-spiking interneurons organize pyramidal cell network oscillations at high-gamma frequencies (60–200 Hz). J. Neurophysiol. *112*, 3001–3011.

Szűcs, A. (1998). Applications of the spike density function in analysis of neuronal firing patterns. J. Neurosci. Methods *81*, 159–167.

Tai, C., Abe, Y., Westenbroek, R.E., Scheuer, T., and Catterall, W.A. (2014). Impaired excitability of somatostatin- and parvalbumin-expressing cortical interneurons in a mouse model of Dravet syndrome. Proc. Natl. Acad. Sci. *111*, E3139–E3148.

Tateno, T., Jimbo, Y., and Robinson, H.P.C. (2005). Spatio-temporal cholinergic modulation in cultured networks of rat cortical neurons: Spontaneous activity. Neuroscience *134*, 425–437.

Thomson, A.M., and Jovanovic, J.N. (2010). Mechanisms underlying synapse-specific clustering of GABAA receptors. Eur. J. Neurosci. *31*, 2193–2203.

Thomson, A.M., Bannister, A.P., Hughes, D.I., and Pawelzik, H. (2000). Differential sensitivity to Zolpidem of IPSPs activated by morphologically identified CA1 interneurons in slices of rat hippocampus. Eur. J. Neurosci. *12*, 425–436.

Tian, M.K., Bailey, C.D.C., and Lambe, E.K. (2014). Cholinergic excitation in mouse primary vs. associative cortex: region-specific magnitude and receptor balance. Eur. J. Neurosci. n/a-n/a.

Turrini, P., Casu, M.A., Wong, T.P., De Koninck, Y., Ribeiro-da-Silva, A., and Cuello, A.C. (2001). Cholinergic nerve terminals establish classical synapses in the rat cerebral cortex: synaptic pattern and age-related atrophy. Neuroscience *105*, 277–285.

Unal, C.T., Golowasch, J.P., and Zaborszky, L. (2012). Adult mouse basal forebrain harbors two distinct cholinergic populations defined by their electrophysiology. Front. Behav. Neurosci. *6*, 21.

Vidal, C., and Changeux, J.-P. (1993). Nicotinic and muscarinic modulations of excitatory synaptic transmission in the rat prefrontal cortexin vitro. Neuroscience *56*, 23–32.

Wafford, K.A., Whiting, P.J., and Kemp, J.A. (1993). Differences in affinity and efficacy of benzodiazepine receptor ligands at recombinant gamma-aminobutyric acidA receptor subtypes. Mol. Pharmacol. *43*, 240–244.

Wang, Y., Toledo-Rodriguez, M., Gupta, A., Wu, C., Silberberg, G., Luo, J., and Markram, H. (2004). Anatomical, physiological and molecular properties of Martinotti cells in the somatosensory cortex of the juvenile rat. J. Physiol. *561*, 65–90.

Wester, J.C., and Contreras, D. (2013). Differential Modulation of Spontaneous and Evoked Thalamocortical Network Activity by Acetylcholine Level In Vitro. J. Neurosci. *33*, 17951–17966.

Whittington, M.A., Traub, R.D., and Jefferys, J.G.R. (1995). Synchronized oscillations in interneuron networks driven by metabotropic glutamate receptor activation. Nature *373*, 612–615.

Williams, S.R., and Mitchell, S.J. (2008). Direct measurement of somatic voltage clamp errors in central neurons. Nat. Neurosci. *11*, 790–798.

Winsky-Sommerer, R. (2009). Role of GABAA receptors in the physiology and pharmacology of sleep. Eur. J. Neurosci. *29*, 1779–1794.

Woolf, N.J. (1991). Cholinergic systems in mammalian brain and spinal cord. Prog. Neurobiol. *37*, 475–524.

Xiang, Z., Huguenard, J.R., and Prince, D.A. (1998). Cholinergic Switching Within Neocortical Inhibitory Networks. Science *281*, 985–988.

Xiao, Z., Deng, P.-Y., Yang, C., and Lei, S. (2009). Modulation of GABAergic Transmission by Muscarinic Receptors in the Entorhinal Cortex of Juvenile Rats. J. Neurophysiol. *102*, 659–669.

Xu, X., and Callaway, E.M. (2009). Laminar Specificity of Functional Input to Distinct Types of Inhibitory Cortical Neurons. J Neurosci *29*, 70–85.

Xue, M., Atallah, B.V., and Scanziani, M. (2014). Equalizing excitation-inhibition ratios across visual cortical neurons. Nature *511*, 596–600.

Yamada, J., Furukawa, T., Ueno, S., Yamamoto, S., and Fukuda, A. (2007). Molecular Basis for the GABAA Receptor-Mediated Tonic Inhibition in Rat Somatosensory Cortex. Cereb Cortex *17*, 1782–1787.

Yamamoto, K., Koyanagi, Y., Koshikawa, N., and Kobayashi, M. (2010). Postsynaptic Cell Type-Dependent Cholinergic Regulation of GABAergic Synaptic Transmission in Rat Insular Cortex. J Neurophysiol *104*, 1933–1945.

Yamasaki, M., Matsui, M., and Watanabe, M. (2010). Preferential Localization of Muscarinic M1 Receptor on Dendritic Shaft and Spine of Cortical Pyramidal Cells and Its Anatomical Evidence for Volume Transmission. J. Neurosci. *30*, 4408–4418.

Yi, F., Ball, J., Stoll, K.E., Satpute, V.C., Mitchell, S.M., Pauli, J.L., Holloway, B.B., Johnston, A.D., Nathanson, N.M., Deisseroth, K., et al. (2014). Direct excitation of parvalbumin-positive interneurons by M1 muscarinic acetylcholine receptors: roles in cellular excitability, inhibitory transmission and cognition. J. Physiol. *592*, 3463–3494.

Zaborszky, L., Csordas, A., Mosca, K., Kim, J., Gielow, M.R., Vadasz, C., and Nadasdy, Z. (2013). Neurons in the Basal Forebrain Project to the Cortex in a Complex Topographic Organization that Reflects Corticocortical Connectivity Patterns: An Experimental Study Based on Retrograde Tracing and 3D Reconstruction. Cereb. Cortex bht210.

Zaitsev, A.V., Povysheva, N.V., Lewis, D.A., and Krimer, L.S. (2007). P/Q-type, but not N-type, calcium channels mediate GABA release from fast-spiking interneurons to pyramidal cells in rat prefrontal cortex. J. Neurophysiol. *97*, 3567–3573.

Zassler, B., Dechant, G., and Humpel, C. (2005). Urea enhances the nerve growth factor-induced neuroprotective effect on cholinergic neurons in organotypic rat brain slices. Neuroscience *130*, 317–323.

6 Supplementary material

		Treatment			Test comparisons				
		I ACh- (norm. to Ctrl) n = 13	II ACh- (norm. to ACh+$_{1\mu m}$) n = 21	III ACh- (norm. to ACh+$_{10\mu m}$) n = 14	I & II & III	I & II	I & II	I & III	I & III
Parameter	**Layer**	*md* [25th & 75th quantile]	*md* [25th & 75thquantile]	*md* [25th & 75th quantile]	Kruskal-Wallis X^2, *p*	Wilcoxon ranksum *p*	auroc [CIs]	Wilcoxon ranksum *p*	auroc [CIs]
Action potential rate	Supra	0.81 [0.56 1.06]	0.75 [0.36 1.07]	0.68 [0.54 1.01]	0.31, 0.85	--	--	--	--
	Infra	0.51 [0.25 0.94]	0.59 [0.44 0.84]	0.88 [0.56 1.30]	4.32, 0.12	--	--	--	--
Fraction of active bins	Supra	0.75 [0.58 1.07]	0.63 [0.39 0.94]	0.51 [0.38 0.81]	2.03, 0.36	--	--	--	--
	Infra	0.51 [0.34 0.70]	0.53 [0.35 0.82]	0.64 [0.44 0.95]	1.64, 0.44	--	--	--	--
Burst rate	Supra	1.09 [0.90 1.57]	0.66 [0.28 0.89]	0.62 [0.32 0.79]	9.47, 0.009	0.01	0.77 [0.56 0.94]	0.005	0.82 [0.60 0.97]
	Infra	1.10 [0.93 1.61]	0.59 [0.28 0.81]	0.72 [0.31 0.83]	16.2, 0.0003	0.0002	0.88 [0.72 0.99]	0.0009	0.88 [0.70 1.00]
Relative time in burst	Supra	0.71 [0.55 1.03]	0.81 [0.58 0.93]	0.64 [0.54 0.77]	2.18, 0.34	--	--	--	--
	Infra	0.81 [0.65 0.96]	0.68 [0.56 0.89]	0.68 [0.58 0.87]	2.19, 0.33	--	--	--	--
Burst length	Supra	0.90 [0.55 1.01]	1.44 [1.04 1.99]	1.03 [0.79 1.26]	9.79, 0.008	0.0014	0.17 [0.04 0.35]	0.17	0.34 [0.12 0.59]
	Infra	0.73 [0.41 0.92]	1.20 [0.98 1.65]	1.00 [0.83 1.92]	11.99, 0.003	0.0007	0.14 [0.02 0.31]	0.02	0.24 [0.06 0.47]
Burst amplitude	Supra	0.96 [0.64 1.22]	1.66 [1.30 1.80]	1.46 [1.18 2.16]	14.22, 0.0008	0.0005	0.14 [0.03 0.3]	0.0024	0.15 [0.02 0.35]
	Infra	0.78 [0.69 0.95]	1.57 [1.06 2.44]	1.32 [1.18 2.04]	17.55, 0.0002	0.0003	0.12 [0.01 0.27]	0.0003	0.08 [0.0 0.23]

Table S1: Extracellular data comparing the effect of *ACh-* subsequent to different control conditions. *ACh-* normalized to aCSF (I), ACh 1 µM (II), and ACh 10 µM (III). Medians (md) [25th and 75th quantiles] are presented. All three groups were compared with a Kruskal-Wallis test for independent data. Post-hoc analysis was done with the Wilcoxon ranksum test. Effect size as auroc [95% confidence intervals]. Bonferroni correction: $p < 0.025$; CI 0.975.

	Treatment			Test comparisons				
	I Control	II ACh+	III Wash-out	I & II & III	I & II	I & II	II & III	II & III
Parameter	*md* [25th & 75th quantile]	*md* [25th & 75th quantile]	*md* [25th & 75th quantile]	Friedman's *X2, p*	Wilcoxon signrank *p*	auroc [CIs]	Wilcoxon signrank *p*	auroc [CIs]
Action potential rate (Hz)	3.06 [0.81 3.89]	4.33 [1.34 7.60]	2.66 [0.79 5.57]	8.67, 0.01	0.01	0.35 [0.22 0.44]	0.02	0.62 [0.49 0.77]
Fraction of active bins	0.09 [0.04 0.15]	0.17 [0.08 0.27]	0.07 [0.05 0.15]	6.17, 0.05	0.009	0.32 [0.15 0.48]	0.01	0.66 [0.49 0.83]
Burst rate (Hz)	0.08 [0.04 0.11]	0.14 [0.09 0.20]	0.05 [0.02 0.11]	15.27, 0.0005	0.003	0.30 [0.13 0.41]	0.001	0.75 [0.69 0.90]
Relative time in burst	0.24 [0.14 0.26]	0.23 [0.17 0.48]	0.17 [0.11 0.26]	7.09, 0.03	0.01	0.37 [0.25 0.49]	0.04	0.66 [0.55 0.80]
Burst length (ms)	1897 [1140 8101]	1559 [555 4631]	7001 [972 14710]	7.17, 0.03	0.12	0.60 [0.47 0.76]	0.02	0.33 [0.19 0.44]

Table S2: Analysis of current clamp *ACh+* data. Medians (md) with 25th and 75th quantile were calculated. Friedman's test for dependent data was applied to compare control, *ACh+*, and wash-out conditions, and Wilcoxon signed rank test and auroc with 95% confidence intervals (CIs) were used for post-hoc analyses.

	Treatment			Test comparisons				
	I Control	II ACh+	III ACh-	I & II & III	I & II	I & II	II & III	II & III
Parameter	*md* [25th & 75th quantile]	*md* [25th & 75th quantile]	*md* [25th & 75th quantile]	Friedman's *X2, p*	Wilcoxon signrank *p*	auroc [CIs]	Wilcoxon signrank *p*	auroc [CIs]
Time constant τ (ms)	7.78 [6.52 10.37]	7.75 [7.08 11.12]	9.24 [8.09 12.40]	4.00, 0.14	--	--	--	--
IPSC frequency (Hz)	6.51 [4.47 9.97]	21.88 [19.01 23.11]	5.15 [3.78 10.52]	12.25, 0.002	0.008	0.08 [0.0 0.19]	0.008	0.94 [0.81 1.00]
IPSC amplitude (pA)	43.57 [40.22 69.20]	55.30 [49.60 75.41]	40.59 [38.08 63.52]	13.00, 0.002	0.008	0.25 [0.03 0.55]	0.008	0.80 [0.53 1.00]
Phasic current (pA)	2.92 [1.71. 5.17]	12.65 [10.33 19.47]	3.63 [2.49 6.57]	12.25, 0.002	0.008	0.02 [0.00 0.09]	0.008	0.94 [0.78 1.00]

Table S3: IPSC parameters for comparison between control, ACh^+ and ACh^-. Friedman's test was calculated for the omnibus effect, Wilcoxon signed rank test was used as post hoc test for specific group comparisons. md = median; CI = confidence interval

	Treatment		Test comparisons	
	I ACh^+ (norm. to aCSF)	II TTX & ACh (norm. to TTX)	I & II	I & II
Parameter	*md* [25^{th} & 75^{th} quantile]	*md* [25^{th} & 75^{th} quantile]	Wilcoxon ranksum *p*	auroc [CIs]
Time constant τ	1.02 [0.93 1.08]	1.23 [1.09 1.28]	0.02	0.14 [0.00 0.39]
IPSC frequency	3.56 [2.24 4.67]	0.72 [0.50 1.04]	0.0003	1.00 [1.00 1.00]
IPSC amplitude	1.20 [1.10 1.34]	1.01 [0.93 1.04]	0.002	0.95 [0.80 1.00]
Phasic current	4.04 [3.78 4.92]	0.86 [0.63 0.95]	0.01	0.88 [0.63 1.00]

Table S4: Comparison between effects of ACh^+ and [TTX and ACh^+]. Data were normalized to preceding control condition. The two independent data sets were compared with a Wilcoxon ranksum test and effect sizes were determined with auroc.

		Treatment				Test comparisons				
		I Ctrl	II ACh+	III ACh-	IV Wash-out	I & II & III	I & II	I & II	I & III	I & III
Parameter	**Rec Type**	*md* [25th & 75th quantile]	*md* [25th & 75th quantile]	*md* [25th & 75th quantile]	*md* [25th & 75th quantile]	Friedman's *X2, p*	Wilcoxon signed rank *p*	auroc [CIs]	Wilcoxon signed rank *p*	auroc [CIs]
Action potential rate (Hz)	Extra	9.15 [5.29 12.10]	7.26 [4.79 10.07]	5.36 [1.98 13.55]	5.90 [2.57 12.14]	8.24, 0.04	0.08	0.63 [0.47 0.81]	0.74	0.56 [0.36 0.77]
	Intra	0.74 [0.28 1.20]	0.60 [0.08 1.13]	0.32 [0.05 0.77]	0.36 [0.04 0.82]	1.18, 0.76	--	--	--	--
Fraction of active bins	Extra	0.19 [0.09 0.21]	0.14 [0.08 0.18]	0.10 [0.05 0.19]	0.13 [0.08 0.15]	8.25, 0.04	0.15	0.63 [0.50 0.81]	0.55	0.57 [0.36 0.80]
	Intra	0.06 [0.03 0.09]	0.04 [0.01 0.10]	0.03 [0.01 0.07]	0.03 [0.00 0.05]	2.61, 0.46	--	--	--	--
Burst rate (Hz)	Extra	0.31 [0.21 0.41]	0.25 [0.17 0.41]	0.17 [0.12 0.35]	0.14 [0.13 0.20]	12.15, 0.007	0.74	0.53 [0.30 0.80]	0.38	0.59 [0.42 0.77]
Relative time in burst	Extra	0.14 [0.11 0.18]	0.12 [0.10 0.15]	0.13 [0.08 0.15]	0.13 [0.09 0.14]	8.55, 0.04	0.02	0.64 [0.53 0.80]	0.64	0.52 [0.34 0.69]
Burst length (ms)	Extra	419 [342 624]	336 [265 622]	513 [381 587]	577 [398 970]	1.95, 0.58	--	--	--	--
Burst amplitude (mV)	Extra	0.07 [0.05 0.11]	0.08 [0.05 0.11]	0.08 [0.05 0.10]	0.10 [0.05 0.12]	0.15, 1.00	--	--	--	--

Table S5: Comparison of Control (Ctrl), *ACh^{+}*, *ACh^{-}*, and wash condition for extra- and intracellular current clamp recordings in cortex-basal forebrain MIK co-cultures.

	Treatment			Test comparisons				
	I Control	II ACh+	III Wash-out	I & II & III	I & II	I & II	II & III	II & III
Parameter	*md* [25th & 75th quantile]	*md* [25th & 75th quantile]	*md* [25th & 75th quantile]	Friedman's *X2, p*	Wilcoxon signrank *p*	auroc [CIs]	Wilcoxon signrank *p*	auroc [CIs]
Resistance (MΩ)	52.92 [43.40 58.62]	58.43 [49.85 74.60]	53.70 [48.15 59.10]	1.4, 0.50	--	--	--	--
Em_{rest} (mV)	-76.49 [-80.28 -72.72]	-69.63 [-76.22 -64.51]	-74.30 [-82.89 -68.07]	12.2, 0.002†	0.01†	0.28 [0.11 0.42]	--	--
Em_{rest} fluct (mV)	0.80 [0.57 1.38]	1.70 [1.14 5.89]	0.83 [0.53 1.20]	7.8, 0.02	0.01	0.21 [0.05 0.38]	0.01	0.82 [0.66 0.97]
Em_{burst} (mV) (10-100 ms)	-66.22 [-69.70 -59.01]	-61.93 [-68.36 -59.84]	-63.92 [-66.90 -58.86]	4.2, 0.12	--	--	--	--
Action potential rate (Hz)	2.57 [0.79 6.51]	2.88 [1.24 3.52]	1.34 [0.52 2.77]	2.21, 0.33	--	--	--	--
Excitability (# SPX)	4.00 [3.19 5.09]	7.50 [6.08 8.58]	6.00 [4.67 7.17]	12.67, 0.002	0.004	0.10 [0.00 0.22]	0.02	0.70 [0.57 0.89]
Cross-correlation of SPX	0.66 [0.44 0.68]	0.41 [0.16 0.57]	0.54 [0.44 0.72]	6.75, 0.03	0.02	0.72 [0.53 0.91]	0.04	0.30 [0.09 0.47]

Table S6: Analysis of intracellular current clamp parameters of X98 data set of organotypic cultures. Data sets, where *p*-values were marked with † do not fulfill the requirement of equal variances.

		Treatment							
		Zolpidem 1 µM				Zolpidem 0.2 µM			
Parameter	**Layer**	*ACh+* *md* [25th & 75th quantile] (n = 37)	*ACh-* *md* [25th & 75th quantile] (n = 35)	Wilcoxon ranksum *p*	auroc [CIs]	*ACh+* *md* [25th & 75th quantile] (n = 49)	*ACh-* *md* [25th & 75th quantile] (n = 33)	Wilcoxon ranksum *p*	auroc [CIs]
Action potential rate	Supra	0.21 [0.04 1.01]	0.57 [0.27 0.78]	0.17	0.40 [0.26 0.55]	0.34 [0.16 0.86]	0.49 [0.29 0.71]	0.41	0.45 [0.32 0.57]
	Infra	0.49 [0.17 0.74]	0.51 [0.34 0.65]	1.00	0.50 [0.36 0.64]	0.75 [0.52 1.02]	0.73 [0.42 0.82]	0.38	0.56 [0.43 0.69]
Fraction of active bins	Supra	0.42 [0.06 1.14]	0.72 [0.49 1.09]	0.09	0.38 [0.24 0.52]	0.55 [0.29 1.06]	0.84 [0.60 1.11]	0.11†	0.40 [0.28 0.52]
	Infra	0.76 [0.41 1.13]	0.83 [0.48 1.06]	0.94†	0.49 [0.35 0.64]	1.01 [0.87 1.15]	0.92 [0.71 1.11]	0.26	0.58 [0.44 0.70]
Burst rate	Supra	0.80 [0.52 1.29]	1.05 [0.67 1.36]	0.27	0.42 [0.29 0.56]	0.50 [0.32 0.74]	0.78 [0.46 1.10]	0.07	0.37 [0.23 0.51]
	Infra	0.99 [0.73 1.39]	1.18 [0.67 1.42]	0.56	0.46 [0.32 0.60]	**0.52 [0.31 0.91]**	**0.84 [0.62 1.01]**	**0.01**	**0.32 [0.19 0.46]**
Relative time in burst	Supra	0.63 [0.17 1.04]	0.79 [0.53 1.12]	0.07	0.37 [0.24 0.51]	0.36 [0.17 0.80]	0.70 [0.29 0.84]	0.13	0.39 [0.25 0.53]
	Infra	**0.62 [0.30 1.18]**	**0.92 [0.65 1.23]**	**0.04**	**0.36 [0.23 0.50]**	**0.49 [0.12 0.86]**	**0.82 [0.60 0.97]**	**0.02**	**0.33 [0.20 0.47]**
Burst length	Supra	0.72 [0.28 1.07]	0.80 [0.39 1.40]	0.26	0.42 [0.29 0.56]	0.73 [0.19 1.08]	0.86 [0.51 1.08]	0.27	0.42 [0.29 0.56]
	Infra	0.60 [0.28 1.04]	0.84 [0.50 0.98]	0.18	0.41 [0.27 0.54]	1.01 [0.64 1.48]	0.97 [0.68 1.06]	0.33	0.57 [0.43 0.71]
Burst amplitude	Supra	0.51 [0.33 0.81]	0.55 [0.45 0.73]	0.72	0.47 [0.34 0.62]	0.63 [0.45 0.93]	0.71 [0.50 0.87]	0.64	0.47 [0.33 0.60]
	Infra	0.56 [0.41 0.79]	0.57 [0.44 0.72]	1.00	0.50 [0.36 0.64]	0.81 [0.53 0.99]	0.69 [0.62 0.87]	0.76	0.52 [0.38 0.67]

		Treatment							
		Diazepam				Diazepam in alpha 1			
Parameter	**Layer**	*ACh*$^{+}$ *md* [25th & 75th quantile] (n = 26)	*ACh-* *md* [25th & 75th quantile] (n = 22)	Wilcoxon ranksum *p*	auroc [CIs]	*ACh+* *md* [25th & 75th quantile] (n = 38)	*ACh-* *md* [25th & 75th quantile] (n = 36)	Wilcoxon ranksum *p*	auroc [CIs]
Action potential rate	Supra	0.42 [0.26 0.68]	0.40 [0.19 0.77]	0.72	0.53 [0.36 0.70]	0.72 [0.37 1.01]	0.79 [0.59 1.05]	0.36	0.44 [0.30 0.58]
	Infra	0.54 [0.32 1.08]	0.60 [0.44 0.95]	0.99	0.50 [0.32 0.67]	0.84 [0.51 1.13]	0.75 [0.59 1.04]	0.98	0.50 [0.36 0.65]
Fraction of active bins	Supra	0.86 [0.61 1.06]	0.77 [0.54 1.20]	0.89	0.49 [0.32 0.66]	0.90 [0.69 1.06]	1.08 [0.80 1.30]	0.06	0.37 [0.24 0.51]
	Infra	1.09 [0.49 1.40]	1.09 [0.92 1.63]	0.56	0.45 [0.28 0.62]	0.97 [0.75 1.18]	0.96 [0.86 1.24]	0.59	0.46 [0.32 0.61]
Burst rate	**Supra**	**0.88 [0.42 0.98]**	**1.41 [0.74 1.76]**	**0.01**	**0.29 [0.12 0.45]**	**0.84 [0.67 1.20]**	**1.15 [0.79 1.55]**	**0.01†**	**0.32 [0.20 0.45]**
	Infra	**0.82 [0.41 1.04]**	**1.32 [0.64 1.66]**	**0.03**	**0.31 [0.16 0.48]**	**0.87 [0.62 1.17]**	**1.21 [0.89 1.55]**	**0.005**	**0.29 [0.17 0.43]**
Relative time in burst	Supra	0.82 [0.58 1.15]	0.86 [0.59 1.14]	0.87	0.52 [0.34 0.68]	0.87 [0.71 1.10]	0.91 [0.64 1.16]	0.83	0.52 [0.38 0.65]
	Infra	0.85 [0.53 1.06]	0.86 [0.50 1.17]	1.00	0.50 [0.33 0.66]	0.83 [0.61 0.97]	0.85 [0.54 1.21]	0.31†	0.42 [0.28 0.57]
Burst length	**Supra**	**0.92 [0.81 1.05]**	**0.65 [0.25 0.84]**	**0.001**	**0.78 [0.63 0.91]**	**0.98 [0.81 1.18]**	**0.80 [0.51 0.92]**	**0.001**	**0.72 [0.60 0.84]**
	Infra	0.97 [0.64 1.12]	0.75 [0.29 0.91]	0.07	0.66 [0.49 0.81]	**0.95 [0.75 1.13]**	**0.79 [0.34 0.94]**	**0.04**	**0.65 [0.51 0.79]**
Burst amplitude	Supra	0.54 [0.44 0.75]	0.57 [0.47 0.74]	0.86	0.48 [0.32 0.65]	0.76 [0.63 0.87]	0.75 [0.58 0.83]	0.31	0.57 [0.43 0.70]
	Infra	0.57 [0.51 0.92]	0.57 [0.48 0.76]	0.42	0.57 [0.40 0.73]	**0.77 [0.63 0.86]**	**0.63 [0.55 0.76]**	**0.01**	**0.69 [0.55 0.82]**

		Treatment			
		L-655,708			
Parameter	**Layer**	*ACh+* *md* [25th & 75th quantile] (n = 54)	*ACh-* *md* [25th & 75th quantile] (n = 36)	Wilcoxon ranksum *p*	auroc [CIs]
Action potential rate	Supra	1.14 [0.64 1.40]	1.02 [0.83 1.35]	0.86	0.51 [0.39 0.63]
	Infra	0.98 [0.72 1.17]	1.08 [0.75 1.37]	0.36	0.44 [0.32 0.57]
Fraction of active bins	Supra	1.00 [0.70 1.24]	0.93 [0.75 1.06]	0.39	0.56 [0.43 0.68]
	Infra	0.95 [0.66 1.08]	0.89 [0.73 1.12]	0.91	0.49 [0.37 0.61]
Burst rate	Supra	1.25 [0.83 1.80]	1.12 [0.93 1.37]	0.67†	0.53 [0.40 0.65]
	Infra	1.29 [0.76 1.91]	1.20 [0.91 1.58]	0.71†	0.53 [0.40 0.65]
Relative time in burst	**Supra**	**1.23 [1.04 1.56]**	**1.02 [0.84 1.27]**	**0.01**	**0.67 [0.55 0.78]**
	Infra	1.07 [0.87 1.37]	1.00 [0.86 1.21]	0.49	0.55 [0.41 0.68]
Burst length	Supra	0.96 [0.75 1.20]	0.96 [0.71 1.10]	0.47	0.55 [0.42 0.67]
	Infra	0.90 [0.65 1.27]	0.93 [0.70 1.10]	0.65	0.53 [0.40 0.66]
Burst amplitude	**Supra**	**1.10 [0.92 1.45]**	**0.96 [0.87 1.11]**	**0.04†**	**0.64 [0.52 0.76]**
	Infra	0.97 [0.79 1.42]	1.01 [0.82 1.10]	0.35†	0.56 [0.43 0.68]

Table S7: Extracellular parameter analysis for all $GABA_AR$ modulators. Data sets were normalized to ACh^+ or ACh^- and then compared per $GABA_AR$ modulator for each layer separately.

	Treatment		Test comparisons	
	I *ACh*$^{+}$	II ACh^{-}	I & II	I & II
Frequency band **Drug condition**	*md* [25th & 75th quantile]	*md* [25th & 75th quantile]	Wilcoxon ranksum *p*	auroc [CIs]
Delta [2 5] Hz				
Zolpidem 1.0 µM	0.88 [0.52 0.98]	0.93 [0.81 0.98]	0.09	0.38 [0.25 0.52]
Zolpidem 0.2 µM	**0.77 [0.52 0.89]**	**0.95 [0.82 1.04]**	**0.0008**	**0.28 [0.17 0.40]**
Diazepam	0.87 [0.67 0.96]	0.94 [0.90 0.99]	0.16	0.38 [0.22 0.55]
Diazepam alpha 1	0.98 [0.90 0.99]	0.99 [0.91 1.02]	0.47	0.45 [0.31 0.59]
L-655.708	**1.02 [0.97 1.07]**	**0.99 [0.95 1.02]**	**0.04**	**0.63 [0.51 0.75]**
Theta [6 12] Hz				
Zolpidem 1.0 µM	**0.63 [0.41 0.81]**	**0.89 [0.78 0.99]**	**0.0001**	**0.23 [0.13 0.35]**
Zolpidem 0.2 µM	**0.73 [0.43 0.86]**	**0.85 [0.68 0.99]**	**0.03**	**0.36 [0.24 0.48]**
Diazepam	0.75 [0.57 0.92]	0.87 [0.76 0.95]	0.13†	0.37 [0.21 0.54]
Diazepam alpha 1	0.89 [0.71 0.97]	0.96 [0.82 1.00]	0.29	0.43 [0.29 0.57]
L-655,708	**1.05 [0.93 1.28]**	**0.99 [0.90 1.04]**	**0.04†**	**0.63 [0.51 0.74]**
Beta [15 30] Hz				
Zolpidem 1.0 µM	0.66 [0.42 0.88]	0.78 [0.58 0.91]	0.16	0.40 [0.27 0.54]
Zolpidem 0.2 µM	0.82 [0.69 1.00]	0.80 [0.62 1.11]	0.83	0.49 [0.35 0.62]
Diazepam	0.75 [0.53 0.93]	0.83 [0.70 1.03]	0.14	0.37 [0.22 0.54]
Diazepam alpha 1	0.90 [0.57 1.08]	0.90 [0.76 1.05]	0.54†	0.46 [0.32 0.60]
L-655,708	**1.10 [0.93 1.47]**	**0.95 [0.74 1.07]**	**0.003**	**0.68 [0.57 0.79]**
Gamma [30 50] Hz				
Zolpidem 1.0 µM	0.91 [0.64 1.07]	1.02 [0.71 1.46]	0.20	0.41 [0.28 0.55]
Zolpidem 0.2 µM	1.05 [0.91 1.15]	1.06 [0.79 1.36]	0.98†	0.50 [0.36 0.65]
Diazepam	0.92 [0.62 1.27]	0.87 [0.81 1.03]	0.86	0.48 [0.32 0.65]
Diazepam alpha 1	0.97 [0.70 1.30]	0.99 [0.78 1.16]	0.90	0.51 [0.37 0.65]
L-655,708	1.05 [0.90 1.34]	1.08 [0.83 1.30]	0.90	0.49 [0.37 0.61]
High gamma [50 80] Hz				
Zolpidem 1.0 µM	**0.90 [0.78 1.00]**	**1.04 [0.73 1.27]**	**0.04†**	**0.36 [0.23 0.50]**
Zolpidem 0.2 µM	1.00 [0.94 1.21]	1.06 [0.89 1.21]	0.87	0.49 [0.36 0.62]

Diazepam	0.99 [0.89 1.25]	0.95 [0.82 1.08]	0.33	0.58 [0.42 0.74]
Diazepam alpha 1	**0.90 [0.72 1.04]**	**1.02 [0.87 1.32]**	**0.009**	**0.32 [0.20 0.45]**
L-655,708	0.96 [0.81 1.11]	0.98 [0.85 1.10]	0.75	0.48 [0.36 0.60]

Table S8: Cross correlation between signals from supra- and infragranular layers for given frequency band and substance.

	Treatment		Test comparisons	
	I *ACh*$^{+}$	II ACh^{-}	I & II	I & II
Frequency band **Drug condition/ Layer**	*md* [25th & 75th quantile]	*md* [25th & 75th quantile]	Wilcoxon ranksum *p*	auroc [CIs]
Delta [2 5] Hz				
Zolpidem 1.0 µM/ L2	0.70 [0.24 1.01]	0.77 [0.60 1.02]	0.19	0.41 [0.27 0.55]
Zolpidem 0.2 µM/ L2	**0.69 [0.48 0.79]**	**0.81 [0.71 0.90]**	**0.004**	**0.31 [0.20 0.43]**
Diazepam/ L2	0.77 [0.57 0.90]	0.81 [0.64 0.93]	0.67	0.46 [0.30 0.63]
Diazepam alpha 1/ L2	0.89 [0.76 1.04]	0.96 [0.88 1.03]	0.16	0.40 [0.27 0.54]
L-655,708/ L2	1.03 [0.94 1.29]	1.01 [0.97 1.06]	0.47	0.55 [0.43 0.67]
Theta [6 12] Hz				
Zolpidem 1.0 µM/ L2	0.74 [0.35 1.12]	0.96 [0.75 1.12]	0.09	0.38 [0.25 0.52]
Zolpidem 0.2 µM/ L2	0.72 [0.45 1.04]	0.83 [0.70 0.99]	0.11	0.39 [0.28 0.52]
Diazepam/ L2	0.79 [0.54 1.14]	0.89 [0.77 1.05]	0.19	0.39 [0.23 0.55]
Diazepam alpha 1/ L2	0.93 [0.67 1.02]	1.01 [0.90 1.07]	0.06	0.37 [0.24 0.50]
L-655,708/ L2	1.02 [0.96 1.45]	1.01 [0.92 1.08]	0.10†	0.60 [0.48 0.72]
Beta [15 30] Hz				
Zolpidem 1.0 µM/ L2	**0.78 [0.33 1.25]**	**1.02 [0.78 1.37]**	**0.04**	**0.35 [0.22 0.49]**
Zolpidem 0.2 µM/ L2	0.89 [0.59 1.25]	0.77 [0.64 1.13]	0.57	0.54 [0.41 0.67]
Diazepam/ L2	0.97 [0.52 1.43]	0.99 [0.77 1.56]	0.41	0.43 [0.27 0.60]
Diazepam alpha 1/ L2	0.97 [0.80 1.32]	1.00 [0.86 1.17]	0.86	0.49 [0.35 0.63]
L-655,708/ L2	**1.12 [0.89 1.46]**	**0.93 [0.77 1.22]**	**0.03**	**0.64 [0.52 0.76]**
Low gamma [30 50] Hz				
Zolpidem 1.0 µM/ L2	0.90 [0.49 1.26]	0.95 [0.76 1.06]	0.67†	0.47 [0.32 0.62]
Zolpidem 0.2 µM/ L2	0.79 [0.59 1.01]	0.93 [0.78 1.01]	0.11†	0.40 [0.28 0.52]
Diazepam/ L2	0.83 [0.72 0.98]	0.90 [0.79 1.00]	0.40	0.43 [0.26 0.59]
Diazepam alpha 1/ L2	0.89 [0.71 1.01]	0.97 [0.84 1.06]	0.07	0.37 [0.24 0.51]
L-655,708/ L2	1.06 [0.94 1.20]	0.98 [0.89 1.07]	0.06†	0.62 [0.50 0.73]
High gamma [50 80] Hz				
Zolpidem 1.0 µM/ L2	**0.69 [0.48 0.94]**	**1.01 [0.79 1.18]**	**0.01**	**0.32 [0.19 0.45]**
Zolpidem 0.2 µM/ L2	0.78 [0.49 0.98]	0.90 [0.82 0.98]	0.06†	0.38 [0.26 0.50]
Diazepam/ L2	0.88 [0.77 1.08]	0.94 [0.75 1.04]	0.94	0.49 [0.32 0.66]

Diazepam alpha 1/ L2	0.97 [0.70 1.13]	0.95 [0.88 1.04]	0.74†	0.48 [0.34 0.62]
L-655,708/ L2	1.03 [0.94 1.16]	1.00 [0.95 1.09]	0.53†	0.54 [0.42 0.66]
Wideband [0 200] Hz				
Zolpidem 1.0 µM/ L2	0.64 [0.22 1.00]	0.79 [0.57 0.98]	0.08	0.38 [0.25 0.52]
Zolpidem 0.2 µM/ L2	**0.67 [0.47 0.76]**	**0.81 [0.79 0.90]**	**0.002**	**0.30 [0.19 0.42]**
Diazepam/ L2	0.74 [0.56 1.04]	0.80 [0.71 0.88]	0.83	0.48 [0.31 0.65]
Diazepam alpha 1/ L2	0.90 [0.75 1.01]	0.93 [0.87 1.00]	0.20†	0.41 [0.27 0.55]
L-655,708/ L2	1.05 [0.97 1.28]	1.01 [0.91 1.06]	0.09	0.61 [0.49 0.72]

	Treatment		**Test comparisons**	
	I *ACh*$^{+}$	II ACh^{-}	I & II	I & II
Frequency band **Drug condition/ Layer**	*md* [25th & 75th quantile]	*md* [25th & 75th quantile]	Wilcoxon ranksum *p*	auroc [CIs]
Delta [2 5] Hz				
Zolpidem 1.0 µM/ L5	**0.59 [0.48 0.79]**	**0.89 [0.71 1.03]**	**0.0008**	**0.26 [0.15 0.39]**
Zolpidem 0.2 µM/ L5	**0.59 [0.51 0.84]**	**0.81 [0.68 0.96]**	**0.005**	**0.31 [0.20 0.44]**
Diazepam/ L5	0.69 [0.55 0.99]	0.92 [0.74 1.00]	0.12	0.37 [0.21 0.53]
Diazepam alpha 1/ L5	**0.82 [0.70 0.10]**	**0.95 [0.86 1.02]**	**0.03**	**0.35 [0.22 0.48]**
L-655,708	1.04 [0.99 1.34]	0.98 [0.91 1.10]	0.06	0.62 [0.49 0.74]
Theta [6 12] Hz				
Zolpidem 1.0 µM/ L5	**0.73 [0.49 0.97]**	**0.98 [0.81 1.38]**	**0.005**	**0.30 [0.18 0.43]**
Zolpidem 0.2 µM/ L5	0.83 [0.63 1.11]	0.87 [0.63 1.03]	0.94	0.49 [0.37 0.62]
Diazepam/ L5	0.85 [0.57 1.27]	1.05 [0.92 1.13]	0.15†	0.38 [0.21 0.55]
Diazepam alpha 1/ L5	0.87 [0.74 1.07]	0.98 [0.84 1.10]	0.35	0.43 [0.30 0.58]
L-655,708/ L5	**1.07 [0.96 1.42]**	**0.96 [0.85 1.09]**	**0.007†**	**0.67 [0.55 0.78]**
Beta [15 30] Hz				
Zolpidem 1.0 µM/ L5	**0.84 [0.64 1.09]**	**1.18 [0.96 1.49]**	**0.02**	**0.33 [0.20 0.47]**
Zolpidem 0.2 µM/ L5	0.98 [0.76 1.24]	1.01 [0.76 1.25]	0.86	0.51 [0.38 0.64]
Diazepam/ L5	1.05 [0.72 1.31]	1.19 [1.01 1.68]	0.13	0.37 [0.21 0.53]
Diazepam alpha 1/ L5	0.90 [0.76 1.15]	1.05 [0.87 1.22]	0.27	0.42 [0.29 0.56]
L-655,708/ L5	**1.16 [0.92 1.48]**	**0.92 [0.82 1.18]**	**0.02**	**0.65 [0.53 0.76]**

Low gamma [30 50] Hz				
Zolpidem 1.0 µM/ L5	**0.71 [0.57 1.02]**	**0.97 [0.73 1.11]**	**0.04**	**0.35 [0.22 0.49]**
Zolpidem 0.2 µM/ L5	0.88 [0.64 1.06]	0.91 [0.78 1.08]	0.48	0.45 [0.33 0.58]
Diazepam/ L5	0.83 [0.69 1.04]	0.99 [0.87 1.10]	0.08	0.34 [0.19 0.51]
Diazepam alpha 1/ L5	0.96 [0.85 1.08]	0.96 [0.83 1.05]	0.72	0.53 [0.38 0.67]
L-655,708/ L5	**0.99 [0.88 1.10]**	0.95 [0.85 1.03]	0.19	0.58 [0.46 0.70]
High gamma [50 80] Hz				
Zolpidem 1.0 µM/ L5	**0.71 [0.47 0.90]**	**0.95 [0.67 1.14]**	**0.02**	**0.33 [0.20 0.46]**
Zolpidem 0.2 µM/ L5	0.83 [0.70 0.99]	0.92 [0.79 1.01]	0.21	0.42 [0.29 0.54]
Diazepam/ L5	0.86 [0.62 1.07]	0.93 [0.83 1.21]	0.12	0.36 [0.21 0.53]
Diazepam alpha 1/ L5	0.97 [0.82 1.14]	0.93 [0.85 1.05]	0.56	0.54 [0.40 0.68]
L-655,708/ L5	1.01 [0.91 1.07]	0.97 [0.89 1.04]	0.24	0.57 [0.45 0.70]
Wideband [0 200] Hz				
Zolpidem 1.0 µM/ L5	**0.62 [0.48 0.84]**	**0.87 [0.76 1.10]**	**0.001**	**0.28 [0.16 0.40]**
Zolpidem 0.2 µM/ L5	**0.58 [0.47 0.83]**	**0.83 [0.73 0.91]**	**0.01**	**0.33 [0.21 0.45]**
Diazepam/ L5	**0.68 [0.53 0.77]**	**0.82 [0.62 0.94]**	**0.05**	**0.33 [0.17 0.49]**
Diazepam alpha 1/ L5	0.82 [0.72 1.00]	0.92 [0.81 0.99]	0.44	0.44 [0.30 0.59]
L-655,708/ L5	1.09 [0.96 1.25]	1.00 [0.90 1.12]	0.11	0.60 [0.48 0.71]

Table S9: Cross correlation of ifr with different frequency bands (gamma and high gamma envelop). Zolpidem (1.0 µM), zolpidem (0.2 µM), diazepam, diazepam in alpha 1 knock-in, and L655, 708 were analyzed for supragranular (L2) and infragranular (L5) layers for all frequency bands listed in the table. Data sets, where *p*-values were marked in red with † do not fulfill the requirement of equal variances.

	Treatment			
	I Zolpidem (1 µM)	II Zolpidem (0.2 µM)	III Diazepam	IV Sham
Parameter	*md* [25th & 75th quantile]	*md* [25th & 75th quantile]	*md* [25th & 75th quantile]	*md* [25th & 75th quantile]
Time constant τ	1.65 [1.48 1.95]	1.91 [1.71 2.16]	2.03 [1.87 2.26]	1.25 [1.13 1.47]
IPSC frequency	0.82 [0.38 1.03]	0.25 [0.15 0.38]	0.56 [0.33 0.67]	0.40 [0.15 0.65]
IPSC amplitude	0.96 [0.80 1.06]	0.95 [0.74 1.11]	0.80 [0.66 0.93]	0.85 [0.75 1.01]
Phasic current	0.88 [0.53 1.94]	0.43 [0.19 0.89]	0.73 [0.41 1.10]	0.49 [0.18 0.63]

	Treatment					
	I, II, III & IV	I & IV		II & IV		III & IV	
Parameter	Kruskal-Wallis X^2, *p*	Wilcoxon ranksum *p*	auroc [CIs]	Wilcoxon ranksum *p*	auroc [CIs]	Wilcoxon ranksum *p*	auroc [CIs]
Time constant τ	35.46, 0.0000001	0.0003	0.85 [0.68 0.97]	0.00001	0.94 [0.83 1.00]	0.0000005	0.99 [0.94 1.00]
IPSC frequency	18.76, 0.0003†	0.006	0.76 [0.55 0.92]	0.34	0.40 [0.16 0.66]	0.12	0.65 [0.41 0.86]
IPSC amplitude	8.03, 0.045	0.11	0.65 [0.42 0.86]	0.20	0.63 [0.39 0.85]	0.34	0.41 [0.19 0.63]
Phasic current	14.67, 0.002	0.002	0.80 [0.60 0.93]	0.50	0.50 [0.25 0.73]	0.03	0.71 [0.49 0.89]

Table S10: Comparison of zolpidem (1 µM), zolpidem (0.2 µM), and diazepam against sham for analysis of $GABA_AR$ modulator effect independent of ACh condition. For all four groups, ACh^+ and ACh^- data were pooled. Data were normalized to control condition. For post-hoc pairwise comparisons with Wilcoxon ranksum test, *p*-value was adjusted with Bonferroni correction: $p < 0.02$; CIs 0.983.

	Treatment							
	Zolpidem 1 µM (n = 11)				Zolpidem 0.2 µM (n = 9)			
Parameter	*ACh*$^{+}$ *md* [25th & 75th quantile]	*ACh*$^{-}$ *md* [25th & 75th quantile]	Wilcoxon signrank *p*	auroc [CIs]	*ACh*$^{+}$ *md* [25th & 75th quantile]	*ACh*$^{-}$ *md* [25th & 75th quantile]	Wilcoxon signrank *p*	auroc [CIs]
Time constant τ (ms)	1.50 [1.38 1.80]	1.85 [1.51 2.10]	0.02	0.30 [0.15 0.45]	1.82 [1.63 2.04]	1.93 [1.74 2.23]	0.36	0.41 [0.22 0.61]
IPSC frequency (Hz)	0.99 [0.85 1.06]	0.52 [0.30 0.79]	0.03	0.74 [0.55 0.93]	0.32 [0.18 0.42]	0.15 [0.13 0.38]	0.01	0.69 [0.56 0.88]
IPSC amplitude (pA)	1.05 [0.93 1.10]	0.89 [0.80 0.97]	0.05	0.74 [0.52 0.93]	0.90 [0.85 1.08]	1.03 [0.73 1.28]	0.50	0.52 [0.33 0.73]
Phasic current (pA)	1.46 [1.02 1.96]	0.54 [0.41 0.80]	0.001	0.83 [0.71 0.98]	0.41 [0.26 0.61]	0.52 [0.15 0.97]	1.00	0.48 [0.26 0.74]

	Treatment							
	Diazepam (n = 11)				Sham (n = 8)			
Parameter	*ACh*$^{+}$ *md* [25th & 75th quantile]	*ACh*$^{-}$ *md* [25th & 75th quantile]	Wilcoxon signrank *p*	auroc [CIs]	*ACh*$^{+}$ *md* [25th & 75th quantile]	*ACh*$^{-}$ *md* [25th & 75th quantile]	Wilcoxon signrank *p*	auroc [CIs]
Time constant τ (ms)	1.94 [1.77 2.03]	2.12 [2.03 2.46]	0.02	0.21 [0.05 0.41]	1.15 [1.12 1.27]	1.47 [1.22 1.54]	0.02	0.19 [0.00 0.39]
IPSC frequency (Hz)	0.67 [0.59 0.78]	0.33 [0.27 0.47]	0.002	0.93 [0.75 1.00]	0.63 [0.40 0.71]	0.15 [0.04 0.36]	0.02	0.88 [0.67 1.00]
IPSC amplitude (pA)	0.86 [0.70 1.08]	0.77 [0.59 0.81]	0.02	0.73 [0.55 0.93]	1.00 [0.79 1.02]	0.84 [0.55 0.86]	0.01	0.73 [0.70 0.89]
Phasic current (pA)	0.90 [0.74 1.25]	0.41 [0.22 0.70]	0.01	0.87 [0.68 1.00]	0.64 [0.55 0.79]	0.18 [0.15 0.35]	0.02	0.94 [0.75 1.00]

Table S11: IPSC analysis for zolpidem (1 µM), zolpidem (0.2 µM), diazepam and sham in the *ACh*$^{+}$ and *ACh*$^{-}$ condition.

7 Acknowledgement

My deepest gratitude belongs to my supervisor Dr. Harald Hentschke for his constructive and valuable suggestions during the planning, development and execution of this research project. His support and guidance throughout has been tremendous and helped to let me grow as a research scientist. His encouragements were much appreciated, especially during rougher patches. Endless scientific discussions at all hours are definitely some of the most memorable moments of the thesis process.

Advice and suggestions given by Prof. Bernd Antkowiak and Prof. Cornelius Schwarz as part of my advisory board has been great help in critically questioning and rethinking aspects of the thesis project and developing more profound work.

I would like to extend my thanks to Claudia Holt, Ina Pappe and Helga Garcia for their technical assistance around the laboratory and for their constructive input on presentations and the thesis.

I am also very grateful for the warm and friendly atmosphere which was provided by the entire group of the Experimental Anaesthesiology. It created an amazing environment to work in.

My special appreciation is entitled to all the people around me who supported me unconditionally throughout the entire process of researching, analyzing and writing the thesis.